https://theses.gla.ac.uk/

Theses Digitisation:

https://www.gla.ac.uk/myglasgow/research/enlighten/theses/digitisation/

This is a digitised version of the original print thesis.

Copyright and moral rights for this work are retained by the author

A copy can be downloaded for personal non-commercial research or study, without prior permission or charge

This work cannot be reproduced or quoted extensively from without first obtaining permission in writing from the author

The content must not be changed in any way or sold commercially in any format or medium without the formal permission of the author

When referring to this work, full bibliographic details including the author, title, awarding institution and date of the thesis must be given

Enlighten: Theses
https://theses.gla.ac.uk/
research-enlighten@glasgow.ac.uk

FORCED-CONVECTION HEAT AND MASS TRANSFER FROM HUMID AIR TO ROPED TUBES

A THESIS
SUBMITTED TO THE FACULTY OF ENGINEERING
FOR THE DEGREE OF
MASTER OF SCIENCE IN ENGINEERING

DEPARTMENT OF MECHANICAL ENGINEERING
UNIVERSITY OF GLASGOW

BY

ROBERTO PROSPERI
SEPTEMBER 1997

© ROBERTO PROSPERI, 1997

ProQuest Number: 10391168

All rights reserved

INFORMATION TO ALL USERS
The quality of this reproduction is dependent upon the quality of the copy submitted.

In the unlikely event that the author did not send a complete manuscript
and there are missing pages, these will be noted. Also, if material had to be removed,
a note will indicate the deletion.

ProQuest 10391168

Published by ProQuest LLC (2017). Copyright of the Dissertation is held by the Author.

All rights reserved.
This work is protected against unauthorized copying under Title 17, United States Code
Microform Edition © ProQuest LLC.

ProQuest LLC.
789 East Eisenhower Parkway
P.O. Box 1346
Ann Arbor, MI 48106 – 1346

GLASGOW UNIVERSITY
LIBRARY
11192 (copy 2)

GLASGOW
UNIVERSITY
LIBRARY

Abstract

The results of experimental measurements of forced-convection heat and mass transfer from hot, humid air to three spirally indented (roped) tubes are presented. Comparisons are also made with experimental results for an equivalent plain tube. An experimental rig was built which allowed for the varying of the two main experimental values of gas free-stream velocity and air humidity content. Filmwise condensation on the horizontally-mounted, 12 mm diameter tubes was studied at nominal air–vapour mixture Reynolds numbers of 1100, 2100 and 4600. Water vapour concentrations ranged from 0 to 24% by weight. Modest condensation enhancement was found for two of the roped tubes while the third tube showed little or no improvement relative to the plain tube. The gas-side enhancements found for the most-highly-grooved 2-start tube were similar to those for the 6-start tube at all three mixture velocities tested. The average enhancement over the vapour concentration range was between 7 and 15%, with the degree of enhancement increasing with increasing mixture velocity. The dual mechanisms of improved condensate drainage and increased boundary layer mixing are presented as factors which account for this enhancement. The experimental data suggests the predominance of the latter effect at the relatively low condensation rates seen here. Additionally, a computer program was developed to simulate the plain-tube condensing case under the same conditions considered in the experimental study. A very satisfactory comparison with the experimental results confirms the consistency of the theory as well as the suitability of the chosen simulation method. An example of the successful extension of the program to roped tubes is also provided.

Acknowledgements

I would like to thank my supervisor, Mr. J. Cunningham, for his invaluable guidance, support and encouragement throughout the course of this project. Many thanks also to Dr. S.K. Nisbet for his advice on temperature and humidity measurement, and to Mr. W. Hay, Mr. P. Smythe and Mr. G. Falconner for their help with the construction of the experimental rig.

Contents

Nomenclature

Symbol	Description	Units
A	Surface Area	m^2
C_p	Specific Heat Capacity	kJ/kg·K
d	Tube Diameter	m
D	Diffusion Coefficient	m^2/s
g	Gravitational Constant	9.80665 N/kg
h	Heat-Transfer Coefficient	$W/m^2 \cdot K$
h_D	Condensation Coefficient	m/s
H	Height	m
h_{fg}	Latent Heat of Vaporisation	kJ/kg
j	Colburn j-factor	–
j_h	Colburn mass transfer j-factor	–
k	Thermal Conductivity	W/m·K
L	Tube Length	m
m	Mass Flux	$kg/m^2 \cdot s$
$\dot{m}$	Mass Flow Rate	kg/s
M	Molar Mass	kg/kgmole
n	Number of Tube Elements	–
Nu	Nusselt Number	–
P	Pressure	Pa
Pr	Prandtl Number	–
q	Heat-Transfer Rate	W
Q	Heat Flux	W/m^2
Re	Reynolds Number	–
R_u	Universal Gas Constant	8314.4 J/kgmole·K
S	Sutherland Constant	K
Sc	Schmidt Number	–

Sh	Sherwood Number	–
t	Time	s
T	Temperature	°C
$U_{overall}$	Overall Heat Transfer Coefficient (OHTC)	$W/m^2 \cdot K$
V	Velocity	m/s
X	Mass Fraction	–
y	Molar Fraction	–

Greek Symbols:

ε	Accuracy in Eqn. (2.13)	W
ϕ	Relative humidity	%
	Viscosity Parameter in Eqn. (2.35)	–
ρ	Density	kg/m^3
μ	Dynamic Viscosity	$kg/m \cdot s$

Subscripts:

a	Air
atm	Atmospheric
c	Condensate
d	Diameter
f	Film
i	Inside
int	Interface
l	Latent
mix	Mixture of Air and Water Vapour
o	Outside
sat	Saturation Condition
tot	Total
w	Water, liquid
v	Water, vapour
∞	Free-Stream Condition

List of Tables

List of Figures

Chapter 1

General Introduction.

1.1 Introduction.

Heat exchangers play an important role in many process industries. In most cases, the effectiveness of heat exchange is a major factor in the overall performance of a particular thermodynamic cycle. With energy costs continuing to rise, significant savings in total costs can be made by using increasingly more efficient heat exchangers. With this as a major motivating factor, a great deal of research has gone into improving heat exchanger design, construction and operation. Of course, current efforts also include attempts to better understand the fundamental principles involved in the transfer of heat from one fluid to another. Basic research of this type is relevant to areas that are not restricted solely to one particular type of exchanger or application. The present study is intended to continue in that vein, with a relatively narrow focus on roped heat exchanger tubes having a generally wider potential application. With greatly-different heat transfer requirements being met with shell and tube type exchangers, knowledge gained in this field may prove of value in diverse situations. The following paragraphs provide an overview of the much more general field of heat transfer enhancement, and describe where the present study fits within this larger area.

Specific methods of improving heat exchanger performance are as varied as the conditions under which the different exchangers operate. A useful classification scheme that identifies the most common methods is provided by Bergles [1], in which augmentation techniques are placed into three general categories:

1) Passive Techniques.
    - Treated Surfaces
    - Rough Surfaces
    - Extended Surfaces
    - Enhanced Surfaces
    - Displaced Enhancement Devices
    - Swirl Flow Devices
    - Coiled Tubes
    - Surface Tension Devices
    - Additives for Liquids
    - Additives for Gases

2) Active Techniques.
    - Mechanical Aids
    - Surface Vibration
    - Fluid Vibration
    - Electric and/or Magnetic Fields, etc.

3) Compound Techniques – A combination of passive and active techniques.

Passive techniques are, by far, the most common class of augmentation techniques encountered. Roped tubes clearly fall into this general category. In most heat exchanger applications both the temperature difference and thermal load are fixed, and as such are not variables in the design of the exchanger. In these cases, two variables that influence heat transfer remain, namely the overall heat-transfer coefficient (OHTC) and the exposed surface area. The two are related insofar as any increase in one results in a corresponding decreased requirement for the other. Extended surfaces are an example of augmentation techniques which seek primarily to increase the surface area relative to traditional shell and tube heat exchangers. A

classic example is the familiar low- or high-finned tube. While local heat transfer coefficients may actually be lower for the extended surfaces than for plain tubes, the increase in surface area more than makes up for this in terms of heat transfer per unit shell volume.

On the other hand, techniques aimed at increasing the OHTC promise a smaller required surface area for a given set of design conditions. Roped tubes (alternately called "corrugated" or "spirally-indented" tubes) are an example of this goal directed towards the overall tube *geometry*, a sub-category which falls under the heading of enhanced surfaces. This type of tube is manufactured using a process which results in a tube of effectively the same size as the equivalent plain tube, both in terms of the outside diameter and surface area. The increase in OHTC relative to the plain tube results in a need for less tube length for a given heat load. The obvious benefit is the savings related to tube material costs. When used in large-scale condensers, for example, the cost of the heat transfer area can be a substantial portion of the start-up costs. In this case, the relatively small increased cost of manufacturing the roped tubes, estimated by Newson [2] at 5 to 10% greater than that of plain tubes, is more than offset by the requirement for less tube material. An additional benefit is the fact that the overall exchanger size is reduced, resulting in further capital cost savings. One disadvantage of the use of roped tubes is the increased pressure drop on the water side due to an increased friction factor relative to plain tubes. This translates into higher capital and operating costs associated with the greater pumping power requirement at equivalent flow rates, and must be factored into any cost analysis along with the benefits described above.

At this point, a general overview of the mechanism of OHTC enhancement for roped tubes is warranted. In condensing situations, the overall degree of enhancement is a combination of effects created by both the internal and external surface geometries of the tube. On the tube side, the aforementioned increased pressure drop is associated with the promotion of increased turbulence in the coolant flow. This is a consequence of the inside-surface helical ridges extending

the core turbulent flow farther into the laminar sub-layer as the fluid passes over them. The result is an increased tube-side convective heat-transfer coefficient. This effect has been widely established for a large range of other interior geometries, inserts and surface finishes, and is not unique to roped tubes.

The presence of a condensate film on the exterior tube surface is a source of thermal resistance due to the relatively low thermal conductivity across the film layer. With this in mind, Gregorig [3] first demonstrated the heat transfer augmentation effect of reducing the condensate thickness in filmwise condensation. The general approach, which he demonstrated with fluted tubes, is to create pressure gradients on the tube surface which result in condensate migration from high to low pressure zones. When applied to roped tubes, condensate surface tension creates a pressure gradient resulting in a very thin film in the vicinity of the corrugation crests. This benefit is somewhat offset by the thickening of the condensate film at the base of the groove. However, the net effect is an average heat-transfer resistance over the tube surface which is significantly lower than that of a plain tube.

The previous discussion of the benefits of roped tubes, for the most part, applies to a consideration of the roped tubes as replacements for plain tubes in condensers. Although the knowledge base for their use in these applications is nowhere near complete, this potential application has, quite rightly (and for the most part, profitably), been explored. Another class of potential applications for roped tubes, of which less is known, is their use as replacements for *extended* surface tubes. Extended surface tubes are often the first choice for applications which require the greatest space savings. For example, integral high-finned tubes are often chosen as the means of providing the heat transfer area in compact heat exchangers. Under many operating environments, their ability to provide a higher OHTC per unit tube length makes them a logical choice over plain tubes. However, certain types of operational issues preclude the use of extended surface tubes. Examples of this include issues related to fouling and the need for routine cleaning and maintenance. Also, a potential lack of durability under certain operating conditions

can exclude the choice of extended surface tubes. An example of this is the condensation of mildly corrosive mixtures for which surface treatment of extended surface tubes may not be effective in the long term. In these cases, roped tubes may not be the first choice from the point of view of efficiency, but may prove to be the only cost-effective method able to provide a workable solution.

Nothing immediately suggests that the condensate-thinning properties of roped tubes cannot be exploited in environments different from those found in pure vapour condensers. A relatively common subset of conditions for which extended surface tubes are used, is in heat recovery from air containing various concentrations of water vapour. The use of roped tubes in selected applications of this type may prove of considerable benefit. Examples of processes that fit this description include the recovery of latent heat from the products of combustion of hydrocarbons, as well as dehumidifying processes in HVAC installations. Irrespective of their final application, these processes share the fact that they are largely diffusion-regulated, that is, the condensation of the vapour is limited by its ability to migrate through the air vapour–mixture. In addition, the resistance to heat transfer provided by the condensate film remains as in all instances of filmwise condensation.

The condensing performance of roped tubes under this general set of conditions forms the basis for the present investigation. Attention is not directed towards any particular potential application, and as such, the range of parameters tested is left fairly wide. With a lack of previous data for their use under these conditions, it was felt that the most-immediately useful test program would consist of the examination of a single, horizontally-oriented, roped tube in cross-flow. The relatively low concentrations of water vapour relative to pure steam experiments suggested that experimental condensation rates would be proportionately smaller. The smaller anticipated gas-side heat-transfer coefficients imply that the gas-side resistance has the potential to be the major contributor to the overall heat-transfer resistance. Because of this, and in view of the substantial existing knowledge of

water-side enhancement for roped tubes, it was decided to concentrate efforts towards an examination of possible gas-side enhancements only.

Three different roped tubes were chosen based on their ability to cover a relatively wide range of groove geometry parameters. An equivalent plain tube was also selected in order to provide a basis for comparison with the roped tube results. It was felt that an examination of the influences of water vapour concentration and air–vapour velocity were equally important in the analysis of the performance of the roped tubes. This was suggested by the general form of existing correlations for humid-air condensation on other surfaces. A suitable experimental program was created to accomplish these goals. Computer simulations of condensation of pure vapours are relatively well-developed, with purposely-designed humid-air programs less widely available. For this reason, and in order to ensure the applicability of a computer simulation over the full range of experimental parameters tested here, a new air–steam specific computer program was written. Without sufficient prior knowledge of the performance of roped tubes under these circumstances, the initial computer code is designed for plain tubes only. Possible modifications to include roped tubes will depend on the results of the experimental investigation.

1.2 Literature Survey.

Organising the body of previous work of benefit to the present investigation is simplified by dividing it into two general categories. The first category consists of research which relates to investigations of the performance of plain and roped tubes in the presence of pure vapours, or vapour with a relatively small proportion of non-condensing gas. In most cases the shell-side fluid is pure steam. While the theory was not intended specifically for condensation of vapour from air, any description of the evolution of the theory of filmwise condensation is incomplete without a description of the initial analysis for pure vapours.

The second body of research includes investigations carried out for condensation in the presence of large concentrations of a non-condensing gas. In

most instances, this concerns studies of water vapour condensation out of air. The second collection of literature is not specific to roped tubes, dealing only with condensation on plain tubes.

1.2.1 Pure or Near-Pure Vapour.

A theoretical analysis of filmwise condensation was first performed by Nusselt [4]. His initial analysis was of a falling film on a vertical plate which he later extended to condensation on a horizontal tube. The basic assumptions include the following:

1) Fluid properties are constant across the film.
2) Undercooling of the condensate below its saturation temperature may be neglected.
3) The condensate film is turbulence-free.
4) The vapour is stationary, hence there is no shear force acting on the condensate surface.
5) Momentum changes across the film may be neglected.
6) A linear temperature distribution exists between the tube wall and vapour conditions.
7) The film thickness is small compared with the outside tube radius.

The final expression for the condensing heat-transfer coefficient based on the Nusselt analysis is:

$$h_f = 0.725\left[\frac{\rho_f\left(\rho_f-\rho_g\right)g\,k_f^3\,h_{fg}}{d_o\,\mu_f\left(T_v-T_o\right)}\right]^{1/4} \tag{1.1}$$

Many modifications to the Nusselt theory were subsequently made, each an attempt to address the original limiting assumptions. Rohsenow [5] extended Nusselt's analysis to take into account a non-linear temperature profile in the film, as well as subcooling of the condensate layer, effectively eliminating assumptions 2) and 6) above. Both effects are taken care of by replacing h_{fg} with:

$$h'_{fg} = h_{fg} + 0.68\, C_p\left(T_v - T_o\right) \qquad (1.2)$$

In practice, it has been found that ripples will routinely develop in the film even at low Reynolds numbers. Adams [6] suggests that a multiplier of 1.2 be used in conjunction with equations (1.1) and (1.2) to account for this effect. In general, there is good agreement between similarly-corrected correlations and experimental results for single horizontal plain tubes.

A mathematical analysis of condensation on roped tubes, similar to the plain-tube analysis of Nusselt and others, is made more difficult by the complex geometry created by the external grooving. Hydrodynamic and heat-transfer effects must be taken into account, with the role of surface tension given particular attention. A theoretical model and enhancement correlation that drew upon the previously-described plain tube analysis was developed by Baghernejad [7], extending the plain tube theory to roped tubes of arbitrary geometry. An experimental investigation by Ben Boudinar [8] found that the accuracy of the Baghernejad theory was less than adequate the more the tube geometry differed from that of a plain tube. However, the predictions made for selected geometries, for 2-start tubes in particular, were found to be reasonable. To the author's knowledge, no rigorous theoretical treatment for roped tubes has been reported which is able to predict the condensing performance for the full range of roped tube geometries.

A strategy based on semi-empirical correlations appears to offer the most-immediate promise for the development of a means to predict shell-side enhancement ratios. In response, a number of experimental investigations have been conducted into both the inside heat-transfer enhancement (usually including the related pressure drop), and the outside condensing enhancement. Rabas' [9] review of published data identifies six major test programs or groups of investigators whose research efforts were aimed at developing predictions for steam condensation on roped tubes. A short summary of the portion of the research

directed towards possible condensing-side enhancement is given in the following paragraphs.

Withers and Young [10] studied filmwise condensation on two roped tubes with approximate outside diameters of 16 and 25 mm. The tubes were mounted in a multitube test facility and the roped tube results were compared to equivalent plain-tube experimental condensing results. In all cases, including the plain-tube tests, the condensing heat-transfer coefficients were greater than those predicted by the Nusselt theory. While significant water-side enhancement was reported, no appreciable vapour-side enhancement was observed.

In tests carried out in the United Kingdom, Catchpole and Drew [11] examined five individually-mounted roped tubes of varying geometries. An equivalent plain tube was included for comparison. All roped tube OHTC's were greater than that of the plain tube. In contrast to the Withers and Young investigation, experimental condensing-side heat-transfer coefficients were higher than those for the plain tube. Typical steam-side enhancements were on the order of 25%. The investigators also reported that condensing-side enhancement was generally greater at lower helix angles, with very high helix angles tending to promote condensate retention on the tube surface. Cunningham and Milne [12] studied the influence of the helix angle and determined that, all other factors being equal, both heat transfer and pressure drop increase with decreasing helix angle. Their results suggest that most of the heat transfer augmentation is due to enhancement on the coolant side. Further experimental investigations at the University of Glasgow [8,13,14] explored the role of condensate inundation and vapour shear on roped tube condensation. Similar findings were reported with respect to the dominance of the internal enhancement over the steam-side enhancement. Cunningham and Holmes [15] conducted an experimental analysis of the effect of relatively small quantities of air on steam condensation on roped tubes. Bulk air concentrations of up to 4.25% by weight were used. The authors concluded

that there was a substantial improvement in heat transfer using roped tubes, even though the presence of air greatly reduces condensing performance.

Mehta and Rao [16] reported steam-side enhancements of as high as 40% in tests of 11 roped tubes under large condensate loads. All of the roped tubes exhibited some enhancement over the plain tube. The major test variables were groove pitch and depth. The researchers pointed out that their results suggested that those two parameters alone were insufficient to predict the optimum tube geometry for condensing-side enhancement.

Marto *et al.* [17] conducted tests on five single-start roped tubes and compared the results with the single-tube Nusselt prediction. The results were surprising in that the outside heat transfer coefficients for four of the five roped tubes were lower, by an average of 10%, than those predicted by the Nusselt analysis. A fifth roped tube with smaller groove pitch exhibited a 15% enhancement over the Nusselt prediction.

A 163-tube, staggered roped tube bundle was considered by Eissenberg and Bogue [18] in an investigation of inundation, vapour velocity and non-condensable gas effects. The vapour-side heat transfer coefficient was found to be 25% greater than that predicted by Nusselt's theory for inline tube bundles. It was pointed out that the comparison was not strictly valid because of the different row alignments used in the tests and in the Nusselt theory. However, steam-side enhancement was suggested by the magnitude of the improvement found.

An experimental test program carried out by Kawai and Machiyama [19] for five titanium, single-start corrugated tubes resulted in condensation enhancement averaging approximately 10% and as high as 30% over the Nusselt theory. A plain tube was not tested, and as such, no confirmation of enhancement relative to actual plain-tube experimental results was presented.

The results of the previous research appear somewhat inconsistent. However, it should be noted that the testing conditions and types of tubing used varied considerably from one investigation to the next. Viewed together, the results

suggest that vapour-side enhancements relative to plain tubes do occur with selected roped tubes. Additionally, it can be concluded that the vapour-side enhancement is in all cases less than that on the water-side at the cooling water velocities typically found in steam condensers.

1.2.2 High Concentrations of a Non-Condensing Gas.

As noted by Lee and Rose [20], when compared with studies for pure vapours, relatively few reliable collections of data have been reported for condensation from vapour–gas mixtures under well-defined conditions. Of those available, steam–air mixtures are by far the most commonly reported, undoubtedly because of the host of practical applications which make use of this combination. The most common types of heat-transfer surfaces considered are single and multiple plain tubes, and finned-tube heat exchangers. As best can be determined by the author, no results have been reported for roped tubes under these conditions. A summary of investigations conducted for plain tubes follows.

Berman's [21] examination of steam–air data reported in the Soviet Union led to the formulation of the following relation:

$$\mathrm{Sh}\,\mathrm{Re}^{-1/2} = \frac{0.455}{\left(X_{a,\mathrm{int}} - X_{a,\infty}\right)^{1/3}} \left[\frac{X_{a,\mathrm{int}}\left(1 - 0.378\,X_{a,\mathrm{int}}\right)^{1/3}}{X_{a,\infty}^{0.6}\left(1 - 0.378\,X_{a,\infty}\right)^{0.067}} \right] \tag{1.3}$$

The correlation covers a wide range of Reynolds numbers, vapour concentrations and pressures. Rose [22] notes that the value of the expression is not greatly affected by the choice of either the free-stream density or interface density, which is required in the calculation of the Sherwood number.

Rose [22] proposed approximate theoretically-based equations for vapour–gas mixtures flowing parallel to a plane horizontal condensing surface and normal to a plain horizontal tube. The horizontal tube correlation is considered here. The relation does not rely on any experimental data for its development and is designed for the limiting cases of zero and infinite condensation rate. Rose's equation was

chosen as the basis for computing the condensation rates in the present computer program, and is shown in equation (2.16) in the computer simulation chapter. A comparison with the relation of Berman in equation (1.3) showed that the two results were in good general agreement, particularly when the scatter of the data used by Berman was considered. One advantage of the Rose equation is that it stems from a uniform-density analysis and does not include the variation in density of the Berman relation. The correlation of Rose was also tested by comparing with the experimental results for steam–air condensation performed by Mills *et al.* [23], which were obtained at relatively low vapour velocities. The experimental data was analysed using a similar technique to the one employed in the present computer simulation, detailed in equations (2.15) through (2.19). The agreement between the calculated and experimental values was excellent over the whole range of data.

An extensive experimental program was carried out by Lee and Rose [20] for four vapour–gas combinations, one of which was steam–air. The vapour–gas mixtures flowed downward over a single horizontal plain tube. Vapour velocities ranged from 0.3 to 26 m/s, with gas mass fractions of up to 32%. Results for the steam–air mixtures were in good agreement with earlier data. A comparison of the experimental data with equation (2.16) confirmed the applicability of Rose's relatively simple theoretically-based correlation for all four vapour–gas combinations.

An experimental investigation of heat and mass transfer from air with high water vapour content was conducted by Taniguchi *et al.* [24]. The goal of their study was to examine condensation and convective heat transfer during latent heat recovery from boiler flue gas. The authors noted that such filmwise condensation experiments had not previously been carried out in the intermediate range of water vapour content. Three 20 mm diameter horizontally-mounted tubes were arranged in a single row with the air–steam mixture in crossflow. The humid air had a water vapour content range of 0 to 15% by weight and the Reynolds numbers ranged from 2800 to 9000. A nominal air–steam mixture temperature of 130°C was used.

Results were compared with equation (2.16) which once again confirmed the accuracy of Rose's equation. Convection heat-transfer coefficients were found to be 20 to 30% higher than suggested by the heat and mass transfer analogy. (See section 4.3 for additional discussion of the Chilton and Colburn [25] j-factor analogy). This phenomena was explained qualitatively by the fact that the ratio of Prandtl to Schmidt numbers was greater than unity.

1.3 Organisation of Thesis.

With the background information already presented, the rest of the thesis is organised as follows. Chapter 2 presents the strategies and techniques that were chosen for the plain-tube computer code. The chapter also provides the underlying theoretical basis for the algorithms used in the program, much of which also applies in the eventual analysis of the experimental results. The third chapter outlines the design and implementation of the experimental portion of the study, with an emphasis on descriptions of the experimental test facility and the procedures used to conduct the testing. The results of the experimental program follow in Chapter 4. The fully-dry-condition data is considered first, followed by the condensing results. In both cases, the plain-tube analysis precedes that of the three roped tubes. A critical discussion of the findings, which takes into account the uncertainties in the experimental data, is included along with the experimental results themselves. The condensation enhancement ratios for the three roped tubes are presented and serve as a summary of the largest part of the experimental analysis. Once the experimental input parameters and results are known, it becomes possible to evaluate the effectiveness of the computer program as a simulation. The results of this evaluation are included in the fifth chapter. A summary of the conclusions that are drawn in Chapters 4 and 5 is presented in Chapter 6, along with recommendations for further work based on issues identified in the present study.

Additional material that is less-directly relevant (but nonetheless essential) to discussions in the above-described chapters, is included in the form of appendices.

The error intervals referred to in Chapter 4 are derived from an uncertainty analysis carried out for the experimental data and presented in Appendix A. Details of the instrument calibrations described in Chapter 3 are included in Appendix B. Sample experimental and computer program results, as well as a computer program listing, make up Appendices C and D respectively.

Chapter 2

Computer Simulation.

2.1 Introduction.

There are several reasons why a numerical solution to the condensing heat-transfer process is desirable. First of all, a numerical simulation allows us to verify the underlying theoretical basis for the process as we compare it with what was observed in an experimental situation. Advantages and limitations of certain theoretical assumptions can be seen quickly as they affect the results of the computations. Secondly, and equally as important, is the ability to use the simulation to predict future results without having to run an experimental program for each combination of process parameters.

The simulation of condensation in the presence of significant quantities of non-condensables involves the simultaneous solution of many non-linear relations. Performing these calculations manually would necessarily limit the accuracy of the results or require many time-consuming iterations. Clearly this problem is well suited to a computer solution. A computer simulation allows the many iterations necessary for accuracy to be performed quickly as well as the potential to easily vary the many parameters that control the heat-transfer process.

The transfer of heat from the hot gas mixture to the cooling water within the tube is logically broken down into separate processes which can be modelled in software as separate modules or subroutines. In this way, different relations for the condensing and non-condensing gas-side heat-transfer coefficients, and the water-side heat-transfer coefficients can be evaluated without affecting other non-related parameters. The many fluid thermal and transport properties vary significantly with temperature and pressure. A computer solution provides a convenient way to include this important aspect of the process without having to manually look up the many different property values in tables. This is accomplished by using suitable correlations which are valid over the range of variables likely to be encountered.

The computer program was designed to work with plain tubes and as such does not include correlations for roped tubes. The goal of the program is to try to extend the pointwise heat exchanger principle to a system where water vapour is condensing out of a mixture that includes a non-condensable gas. In this case, the gas is air. Comparison of the results of the program with the experimental results for the plain tube will allow the computer model to be tested. If the results of the computer program are reasonable for plain tubes, correlations for roped tubes can be easily introduced once enough data is assembled on the use of roped tubes in this situation.

Existing computer programs [8,14] designed to operate under condensing conditions have been extensively used in previous research within the Department of Mechanical Engineering at the University of Glasgow. While effective for cases where condensation is not primarily limited by diffusion through non-condensables, major modification would be necessary to allow for using these programs under the condition of water vapour condensing out of air. For this reason, it was decided to write completely new code which would also have the advantage of running on the departmental UNIX system as opposed to the older University ICL mainframe. It was decided to code in standard ANSI C as this ensures a large degree of portability of the program from one set of computer hardware to the other.

2.2 Overview of Program Structure.

The basic strategy for modelling the heat and mass transfer process is to use the pointwise heat exchanger principle. This consists of dividing the tube into a number of elements and considering each element as a tube itself. The physical model of the tube is shown in Figure 2.1. Starting at the tube inlet, conditions at the exit of the first tube element are used as entry conditions for the following element and so on along the total length of the tube. Conduction along the tube length is assumed to be negligible. One advantage of breaking the tube up into smaller sections is that as the number of elements increases (with a corresponding decrease in the length of each element), the change in the various fluid properties is minimised. As this change in fluid properties becomes smaller, the overall error in calculation is reduced, all other factors being equal.

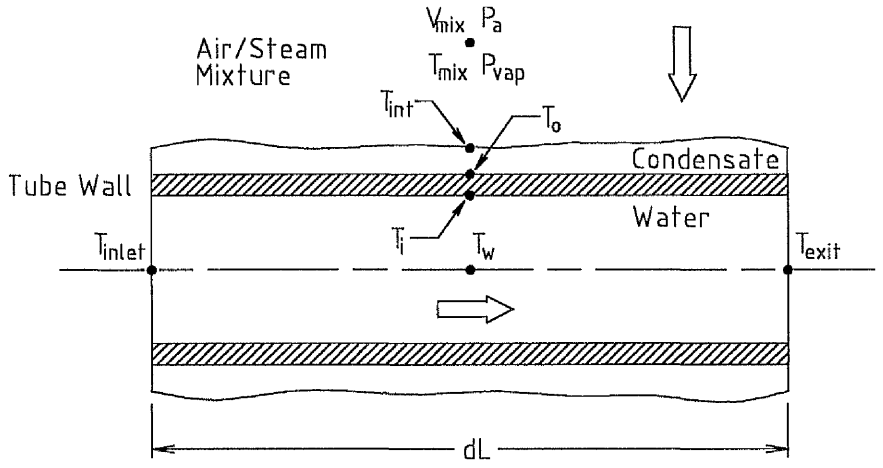

Figure 2.1 Tube Element Model.

Another important reason for employing this technique is its ability to examine situations in which parts of a tube are undergoing condensation while other areas remain dry. When the tube elements are chosen sufficiently small, it is possible to identify where along the tube length condensation will no longer occur.

The details of how the program operates are outlined in the following sections. A simplified block diagram of the program is given for reference in Figure 2.2. The computer-program listing is included in Appendix D.

2.2.1 Initialisation of Parameters.

The input parameters needed for the operation of the program are:

- The number of elements chosen for the tube, n.
- The tube length, L.
- Tube inside and outside diameters, d_i and d_o.
- The atmospheric pressure, P_{atm}.
- Mass flow of cooling water, $\dot{m}$.
- Cooling water inlet temperature, T_{inlet}.
- Gas mixture temperature, T_{mix}.
- Gas mixture velocity, V_{mix}.
- Relative humidity of gas mixture, ϕ.
- Choice of tube-side and vapour-side correlations.

Once the above information is set by the user, the program calculates some other preliminary parameters which include partial pressures of air and vapour, mole and mass fractions of the two components, and several others. Before the main program loop begins, the preliminary information is output to the screen and the initial values of the various temperatures for the first element are set equal to the inlet water temperature.

2.2.2 Dry Heat Transfer.

For each element, the dry heat-transfer rate is calculated regardless of whether condensation eventually occurs or not. This is necessary in order to determine the tube outer wall temperature. If the temperature is below the saturation temperature of the gas mixture, then condensation is possible and the analysis must be redone to include the condensate layer. This analysis is outlined in section 2.2.3. If the tube surface temperature is higher than the saturation temperature, then no condensation occurs for that element and all others that follow it. This is true because of the fact that the water bulk temperature for the next element will be

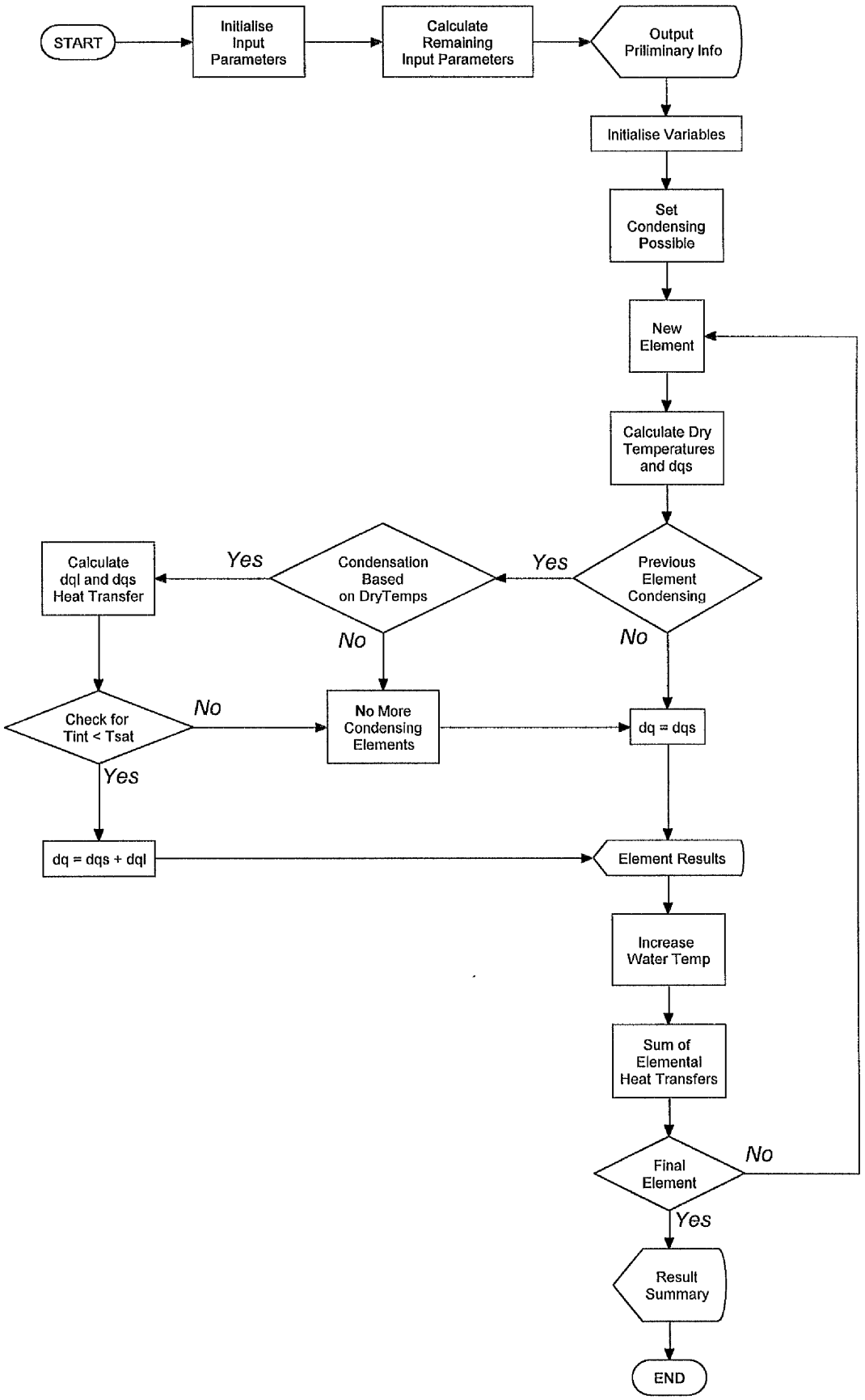

Figure 2.2 Program Flowchart.

higher than the previous one, with the same outside gas temperature. As a result, the tube outside surface temperature is necessarily higher for subsequent elements.

The approach taken to calculate the heat-transfer rate for a particular tube element is to use an energy balance of heat flowing from the hot gas mixture through the tube and into the cooling water. In the case where no condensation is taking place, the heat-transfer rate can be calculated using the electrical analogy of three resistances in series. These resistances are the external convection resistance, R_o, the tube thickness conduction resistance, R_t, and the internal convection resistance, R_i. The heat-transfer rate for a single element is found from:

$$\delta q = \frac{\Delta T_{overall}}{R_o + R_t + R_i} = \frac{T_{mix} - T_w}{R_o + R_t + R_i} \tag{2.1}$$

where the gas temperature is constant and the water bulk temperature is dependant on the heat-transfer rate itself.

The tube wall resistance is given by:

$$R_t = \frac{\ln\left(d_o/d_i\right)}{2\pi k_t \delta L} \tag{2.2}$$

where the tube thermal conductivity, k_t, is assumed to be constant over the range of temperatures used in the experiment. The length of each tube element, δL, is, of course, equal to the total length of the tube divided by the number of elements chosen.

The water-side resistance, R_i, is found from the following relation:

$$R_i \equiv \frac{\Delta T}{q} = \frac{T_i - T_w}{h_i A_i \left(T_i - T_w\right)} \tag{2.3}$$

Substituting the following two equations in equation (2.3) above:

$$A_i = \pi d_i \delta L \tag{2.4}$$

$$h_i = \frac{\mathrm{Nu}\ k_w}{d_i} \tag{2.5}$$

yields the result

$$R_i = \frac{1}{\mathrm{Nu}_i \, \pi \, k_w \, \delta L} \tag{2.6}$$

The cooling-water conductivity and the Nusselt number are dependant on the bulk water temperature. If the Seider–Tate relation is used to determine Nu, then R_i is also a function of the tube inside wall temperature. (See section 2.3.1).

The equation used to determine R_o is analogous to that for R_i in equation (2.6) i.e.,

$$R_o = \frac{1}{\mathrm{Nu}_o \, \pi \, k_{mix} \, \delta L} \tag{2.7}$$

Nu_o and hence R_o, vary with both the gas mixture temperature and the tube outside wall temperature. The temperature difference used to calculate the heat-transfer rate with the outside resistance is:

$$\Delta T = T_{mix} - T_o \tag{2.8}$$

For each element, i, of the tube the following operations are performed:

1) The bulk water temperature at the midpoint of the element is initially set to the exit temperature of the previous element. For the first element only, this takes the form of the overall water inlet temperature.

2) The inside heat-transfer resistance is calculated based on this bulk temperature and the inside wall temperature of the previous element. See section 2.3.1 for details of the correlations used in determining R_i.

3) An iterative method is used to calculate the different non-condensing parameters. The steps in this process are as follows:

   i) Calculate the external heat-transfer resistance based on T_{mix} and T_o. See section 2.3.2 for details of the correlations used in determining R_o.

   ii) Calculate the heat-transfer rate from the following relation:

$$\delta q = \frac{T_{mix} - T_{exit,\, i-1}}{R_o + R_t + R_i + \tfrac{1}{2}\left(\dot{m} C_{p,w}\right)} \tag{2.9}$$

iii) Update the bulk water temperature for element i based on the heat-transfer rate calculated in equation (2.9).

$$T_w = T_{exit,i-1} + \frac{\delta q}{2\dot{m}C_{p,w}} \tag{2.10}$$

iv) Calculate the inside heat-transfer resistance with the new value of T_w.

v) Update the inside wall temperature from:

$$T_i = T_w + \delta q R_i \tag{2.11}$$

vi) Update the outside wall temperature from:

$$T_o = T_i + \delta q R_t \tag{2.12}$$

vii) Repeat steps i) through vi) until the following condition is met:

$$\left| \frac{T_{mix} - T_o}{R_o} - \frac{T_o - T_i}{R_t} \right| < \varepsilon \tag{2.13}$$

where ε is the desired degree of accuracy for the convergence of the heat-transfer rates.

The smaller the value of ε, the greater the number of iterations required to achieve convergence. In this program, a value of $\varepsilon = 5 \times 10^{-12}$ was chosen, giving an accuracy to eleven decimal places. It is acknowledged that much fewer than eleven decimal places are really significant when the uncertainty in the input parameters is taken into account. The calculation to eleven decimal places is useful despite this, as it allows the errors due to rounding off to be minimised when performing multiple iterations.

The iterative process shown above gives, among other results, the tube outside wall temperature, necessary in determining whether condensation can take place. If the previous element was not dry, then the surface temperature is compared with the saturation temperature of the vapour corresponding to its partial pressure in the mixture. If condensation is possible, the results of the dry situation (temperatures and heat-transfer rate) are saved under new variable names before

proceeding to the next section of the program. If, on the other hand, the outside wall temperature is greater than the saturation temperature, then the analysis for this particular element is completed by initialising the inlet temperature for the following element and updating the total heat-transfer rate for the sum of elements already processed.

2.2.3 Condensing Heat Transfer.

The total amount of heat transfer from the gas mixture to the cooling water can be broken down into sensible and latent heat contributions. The formation of a condensate layer introduces another variable as compared to the dry analysis — the condensate–gas interface temperature, T_{int}. The sensible heat component is now evaluated between the gas free-stream and interface temperatures, as opposed to the free-stream and exterior tube wall temperatures in the dry situation.

The driving force for the latent heat-transfer process can be thought of in terms of vapour partial pressure differentials between the gas free-stream conditions and those at the condensate interface. The analysis based on this model does not easily lend itself to being formulated in terms of a resistance to heat transfer as used in section 2.2.2. This can be seen when looking at the relations used to calculate the latent heat-transfer rate in item iv) below. It is possible though, to use an algorithm that iterates about T_{int} and returns the value of the latent heat transfer. This is the approach used in the program. The following analysis takes place when a tube element's outside surface temperature is below the saturation temperature. Condensation is assumed throughout the length of the element and the iterative process is used to calculate the temperatures and two heat-transfer rates. The steps in the process are as follows:

i) Set a marker variable, *previous*, to the value of the condensate–gas interface temperature. In the case of the first element, this is assumed to be equal to the water inlet temperature.

ii) Calculate the external heat-transfer resistance based on T_{mix} and T_{int} used to compute the sensible heat-transfer component.

iii) Calculate the sensible heat-transfer rate from

$$\delta qs = \frac{T_{mix} - T_{\text{int}}}{R_o} \tag{2.14}$$

iv) Call a subroutine to return the value of the latent heat-transfer rate, δql, and T_{int}. The subroutine uses the method of Rose [22] for horizontal tubes undergoing condensation in the presence of non-condensing gases, the results of which are in good agreement with experimental data for steam–air mixtures. Rose's method of calculating δql requires a suitable iterative process separate from the algorithm presently being described beginning with item i). Basically, this process consists of the simultaneous solution of four non-linear equations with the following unknowns: $X_{a,int}$, the mass fraction of air at the interface; m, the net mass flux of condensate (condensation rate); Q_l, the latent heat flux; as well as T_{int}. The first equation is a consequence of the ideal-gas law and simply expresses the mass fraction of air at the interface:

$$X_{a,\text{int}} = \frac{P_{tot} - P_{sat,\text{int}}}{P_{tot} - \left[1 - \left(M_v / M_a\right)\right] P_{sat,\text{int}}} \tag{2.15}$$

The saturation pressure at the interface is not yet determined because of its dependence on the unknown interface temperature. The following approximate equation, proposed by Rose, links the condensation rate with the mass fraction of air at the interface given by equation (2.15):

$$\frac{m}{\rho_m V_\infty}\text{Re}^{1/2} = \frac{\left[1 + 2.28\ \text{Sc}^{1/3}\left(X_{a,\text{int}} / X_{a,\infty} - 1\right)\right]^{1/2} - 1}{2\,\text{Sc}} \tag{2.16}$$

where the Schmidt number is defined as:

$$\text{Sc} \equiv \frac{\mu}{\rho D} \tag{2.17}$$

with the diffusion coefficient, D, calculated from equation (2.41). The equation of Fujii *et al.* [26] for the condensate film links the heat transfer with the temperature difference ΔT for cylinders in cross flow:

$$\frac{Q_l\, d_o}{\Delta T\, k_c} = \left\{ 0.656 \left(\frac{V_\infty \rho_c\, d_o}{\mu_c} \right)^2 \left(1 + \left(\frac{\rho_{mix} \mu_{mix}}{\rho_c \mu_c} \right)^{1/2} \frac{\mu_c h_{fg}}{k_c \Delta T} \right)^{4/3} + \frac{0.276 \rho_c^2 d_o^3 h_{fg} g}{\mu_c k_c \Delta T} \right\}^{1/4} \quad (2.18)$$

where $\Delta T = T_\infty - T_{int}$. The final equation expresses the well-known relationship between the mean heat flux and the condensate mass flux, where

$$Q_l = m\, h_{fg} \quad (2.19)$$

The enthalpy change of the vapour, in cooling from the free-stream temperature to the interface temperature, is negligible compared to the enthalpy associated with the change of phase. As noted by Rose, the specific enthalpy of phase change is to be evaluated at T_{int} and the properties of the condensate layer are to be evaluated at

$$T_c = T_o + \frac{\left(T_{int} - T_o\right)}{3} \quad (2.20)$$

The iteration of equations (2.15) through (2.19) continues until the value of T_{int} differs by less than ε for two consecutive iterations. At this point δql is calculated from

$$\delta ql = Q_l \pi\, d_o \delta L \quad (2.21)$$

and the values of T_{int} and δql are returned to the main program.

v) The total heat-transfer rate is calculated from the sum of δqs and δql.

vi) The next four steps are identical to those for the non-condensing situation in section 2.2.2, items iii) through vi).

vii) Repeat steps i) through vi) until the absolute value of the difference between T_{int} and the marker *previous* is less than the accuracy chosen, ε.

It is possible (although not likely) that the increased heat-transfer rate due to the water vapour condensation will result in a calculated T_{int} that is higher than the dew point of the water vapour. The program checks for this situation and returns the dry heat-transfer results if this is the case.

2.2.4 Program Output.

In addition to displaying the user input parameters, the program outputs the following information for each element:

- Water inlet temperature, T_{inlet}.
- Tube inside and outside wall temperatures, T_i and T_o.
- Gas–condensate interface temperature, T_{int}, if condensing.
- Latent and total heat-transfer rates, δql and δq.
- Inside and outside sensible heat-transfer coefficients, h_i and h_o.

Once all of the tube elements are processed, the total latent and sensible heat-transfer rates are outputted for the complete tube length. The water exit temperature and increase over the inlet temperature are shown, as well as the overall heat-transfer coefficient.

2.3 Correlations.

Many correlations have been developed to model the flow of fluids through and across cylinders. As each correlation is based to some extent on experimental data for particular fluids at specific Reynolds numbers, it is reasonable to expect that certain correlations would be more accurate under a certain set of flow conditions. Consequently, it was decided to include three common relations for both the tube-side and vapour-side correlations to potentially allow for a wider range of flow conditions, as well as to provide a larger basis for comparison with the experimental results.

2.3.1 Water-Side Heat-Transfer Correlations.

Correlations expressing the tube-side heat-transfer coefficients for turbulent flow in tubes are usually given in terms of the Nusselt number as a function of both Reynolds number and Prandtl number. Many of the correlations widely used in engineering situations are of the following form:

$$\mathrm{Nu}_{d_i} = C\,\mathrm{Re}_{d_i}^{m}\,\mathrm{Pr}^{n} \tag{2.22}$$

where C, m, and n are constants to be determined from the experimental data. Holman [27] observes that these relations are valid for $\mathrm{Re}_{d_i} > 2300$ or more conservatively, for $\mathrm{Re}_{d_i} > 4000$ which is outside the generally accepted range for transition from laminar flow in pipes. Correlations for laminar flow were not included in the program.

The simplest of the three correlations in the program is that of Dittus and Boelter [28] for fully developed turbulent flow undergoing heating in smooth tubes:

$$\mathrm{Nu} = 0.023\,\mathrm{Re}^{0.8}\,\mathrm{Pr}^{0.4} \tag{2.23}$$

Equation (2.23) is valid for fluids with Prandtl numbers ranging from about 0.6 to 100 and all properties are evaluated at the fluid bulk temperature, T_w.

If there are substantial temperature differences present in the flow of water, there may be a significant variation in the fluid properties at the tube wall compared to the centre of the tube. For this case, Seider and Tate [29] developed the following relation which takes into account variations in viscosity with temperature:

$$\mathrm{Nu} = 0.027\,\mathrm{Re}^{0.8}\,\mathrm{Pr}^{1/3}\left(\frac{\mu}{\mu_{wall}}\right)^{0.14} \tag{2.24}$$

All of the properties in equation (2.24) are evaluated at the bulk water temperature except μ_{wall}, which is evaluated at the inside wall temperature.

In the entrance region and in short tubes, the flow is not fully developed. For these cases, Nusselt [30] recommended the following equation:

$$\mathrm{Nu} = 0.036\,\mathrm{Re}^{0.8}\,\mathrm{Pr}^{1/3}\left(\frac{d_i}{L}\right)^{0.055} \tag{2.25}$$

The fluid properties are evaluated at the bulk temperature of the water. Equation (2.25) is valid for $10 < L/d_i < 400$. The tubes used in this program fall into this category.

2.3.2 Vapour-Side Heat-Transfer Correlations.

The heat-transfer correlations for the vapour side are those that relate to the sensible heat transfer from the air–steam mixture. This takes the form of heat transfer from the mixture to the outside of the tube wall in the case of no condensation, and sensible heat transfer from the air–vapour mixture to the condensate layer in the situation where condensation takes place. Latent heat transfer, when condensation takes place, is not accounted for in these correlations. However, addition of water vapour to the hot airstream does have an effect on the convection correlations. This takes the form of altering the thermal and transport properties of the gas mixture, which necessarily affects the value of the Nusselt number and hence the outside sensible heat-transfer coefficient.

A correlation of the experimental data of Hilpert [31] for gases indicates that the average (i.e. not at a specific point around the tube circumference) heat-transfer rate is given by

$$\mathrm{Nu}_{d_o} = \frac{h\,d_o}{k_f} = C\left(\frac{\rho V_\infty d_o}{\mu_f}\right)^n \mathrm{Pr}^{1/3} \tag{2.26}$$

where the subscript f denotes the film temperature, T_f, given by

$$T_f = \frac{T_o + T_\infty}{2} \tag{2.27}$$

For the Reynolds number range of 40 to 4000, the suggested values of C and n are 0.683 and 0.466 respectively. The constants are 0.193 and 0.618 respectively for Reynolds numbers between 4000 and 40 000.

Eckert and Drake's [32] relations for gas flow across tubes can be used over a wider range of Reynolds numbers and are given below. Properties are also evaluated at the film temperature of the mixture.

$$Nu = \left(0.43 + 0.50\,Re^{0.5}\right) Pr^{0.38} \qquad \text{for } 1 < Re < 10^3 \qquad (2.28)$$

$$Nu = 0.25\,Re^{0.6}\,Pr^{0.38} \qquad \text{for } 10^3 < Re < 2 \times 10^5 \qquad (2.29)$$

The correlation of Churchill and Bernstein [33], is more complicated than equations (2.26) through (2.29), but has the advantage of being valid over the largest range of data.

$$Nu = 0.3 + \frac{0.62\,Re^{1/2}\,Pr^{1/3}}{\left[1+\left(\frac{0.4}{Pr}\right)^{2/3}\right]^{1/4}} \left[1+\left(\frac{Re}{282\,000}\right)^{5/8}\right]^{4/5} \qquad (2.30)$$

This correlation is valid over the range $10^2 < Re < 10^7$ and, like the others, properties are evaluated at the film temperature.

2.4 Fluid Properties.

An essential part of computing the heat-transfer rates is the determination of the various fluid thermal and transport properties. This applies to the water flowing within the tubes as well as to the mixture of air and water vapour outside the tubes. A convenient way of evaluating these properties over the full range of temperatures and pressures likely to be encountered was needed. Fortunately, a computer solution is available which greatly reduces the time and effort required to look up these properties in tables.

Three slightly different ways of including the fluid properties within the computer program were considered. The first method examined was the possibility of using existing correlations available in the literature. For the most part, these correlations take the form of polynomial expressions of one variable (usually temperature) in which the coefficients for the different orders of polynomials are

determined by fitting a curve to experimental data. Although they offer a solution ready-made for computer input, these correlations are often generated by compiling data over a large range of temperatures. Because they are applicable over this wide temperature range, they can either be inaccurate over any given smaller range, or require the use of many coefficients to achieve a desired level of accuracy. Partly as a result of these limitations, tables of fluid properties still continue to enjoy widespread use.

A potentially more accurate way to arrive at the fluid properties would be to find a way to incorporate these familiar tables into the computer program. In this way, only the properties within a particular temperature range would be selected. The one great disadvantage of doing this in a computer program is that it requires the construction of some form of database with all the data listed over the required range. The program would then consult this database, interpolating the data when required. Though possible to implement, this approach alone rapidly increases the complexity of the program and is somewhat of a clumsy solution.

The method chosen makes use of elements of the above two approaches. Data was collected from the various tables over ranges large enough to account for all possible experimental situations used here. The data was then correlated with a best-fit polynomial curve. The resulting curves were then plotted and checked visually to verify their fit to the data. Fifth-degree polynomials were chosen as they provided a good compromise between accuracy and ease of coding. The polynomials are listed within each property subroutine in the source code in Appendix D.

2.4.1 Water Properties.

The liquid water properties are relatively easy to calculate when compared with those of the gas mixture since they can all be evaluated at full atmospheric pressure — as opposed to the partial pressure properties used in the gas phase. The following polynomials, shown along with the source for the data, were calculated:

dynamic viscosity, μ, density, ρ, and specific heat, C_p [34] as well as thermal conductivity, k. [35]. All of the polynomials are valid within a temperature range of 0 to 100°C.

2.4.2 Air Properties.

In terms of partial pressures, dry air is by far the largest component of the mixture which flows across the tubes. For example, at an air temperature of 70°C and a relative humidity of 65%, dry air accounts for roughly 80% of the total mixture pressure. The remaining 20% is, of course, due to the water vapour. This is typical of the combinations of air temperature and relative humidity used in the experiments. Because of this, the properties of the dry air are calculated at atmospheric pressure, data for which is readily available in the literature. Data [36] was compiled over the range from 0 to 100°C and the following polynomial expressions calculated: specific heat, dynamic viscosity and thermal conductivity.

2.4.3 Vapour Properties.

Water vapour properties can be found in the literature for pure vapour at either the saturation pressure (along saturation line for gas) or at distinct pressures greater than the saturation pressure. Since any water vapour involved in latent heat transfer is necessarily at or near the saturation pressure corresponding to the temperature of the condensate layer, calculations of vapour properties are made at the saturation temperature. Data [37] was compiled for the same variables that appear in the section on air properties. Additionally, saturation pressure data [35] between 0°C and 100°C was used to create two subroutines, one giving the saturation pressure as a function of temperature, and another calculating the saturation temperature at a given vapour partial pressure.

2.4.4 Mixture Properties.

Since the gas flowing normal to the tubes is a mixture of air and water vapour, it is reasonable to expect the mixture properties to be some kind of combination of the individual properties. As it turns out, and as suggested by Reid and Sherwood [38], the methods used to combine the two properties vary depending on the property in question. Methods used to calculate each mixture property are outlined below.

Since the air–steam mixture is at atmospheric pressure, it is possible to treat the combination as an ideal gas and still have results accurate enough for engineering purposes. One consequence of the well known ideal-gas law is the calculation of the mixture density where

$$\rho_{mix} = \rho_a + \rho_v = \frac{P_a M_a}{R_u T} + \frac{P_v M_v}{R_u T} \tag{2.31}$$

and the partial pressures of the components are found from

$$P_v = \phi P_{sat} \tag{2.32}$$

$$P_a = P_{atm} - P_v \tag{2.33}$$

The specific heat (constant pressure) of the mixture, C_p, can be calculated on the basis of a mass average of the two components of the humid air, i.e.:

$$C_p = X_a C_{p,a} + X_v C_{p,v} \tag{2.34}$$

Once again, an ideal-gas model is assumed.

Reid and Sherwood [38] suggest the use of Wilke's approximation to determine the viscosity of a multicomponent mixture of gases, the general form of which is:

$$\mu = \sum_{i=1}^{n} \frac{y_i \mu_i}{\sum_{j}^{n} y_j \phi_{ij}} \tag{2.35}$$

where in a binary system, for $n = 2$, $i = a$, and $j = v$:

$$\phi_{av} = \frac{\left[1+\left(\mu_a/\mu_v\right)^{1/2}\left(M_v/M_a\right)^{1/4}\right]^2}{\left\{8\left[1+\left(M_a/M_v\right)\right]\right\}^{1/2}} \tag{2.36}$$

$$\phi_{va} = \phi_{av}\frac{\mu_v}{\mu_a}\frac{M_a}{M_v} \tag{2.37}$$

These equations are based on the kinetic theory of gases and do not assume that the mixture consists of ideal gases.

The general form of the expression used to calculate the mixture thermal conductivity is analogous to that of the viscosity, namely

$$k = \sum_{i=1}^{n} \frac{y_i k_i}{\sum_{j}^{n} y_j A_{ij}} \tag{2.38}$$

where A_{ij} is a function of the individual gas viscosities. For systems with a mixture of polar and non-polar components (water and air respectively), Reid and Sherwood suggest the Lindsay and Bromley formulation for A_{ij} :

$$A_{ij} = \frac{1}{4}\left\{1+\left[\frac{\mu_i}{\mu_j}\left(\frac{M_i}{M_j}\right)^{3/4}\frac{T+S_i}{T+S_j}\right]^{1/2}\right\}^2\frac{T+S_{ij}}{T+S_i} \tag{2.39}$$

with all the subscripts reversed for A_{ji} and where

$$S_i = 1.5\,T_{b,i} \tag{2.40}$$

$$S_{ij} = S_{ji} = \left(S_i S_j\right)^{1/2} \tag{2.41}$$

$T_{b,i}$ is the normal boiling point of component i, and S is the Sutherland constant.

2.4.5 Diffusion Coefficient.

Since condensation in the presence of non-condensing gases is controlled to a large degree by the diffusion process, the diffusion coefficient of water vapour in air is an essential parameter in the calculation of heat-transfer rates. The diffusion coefficient is necessary in order to calculate the Schmidt number used as a

parameter in most correlations that involve diffusive processes. In this program the Schmidt number is required in equation (2.16). The particular expression chosen for the diffusion coefficient is that suggested by Fujii *et al.* [39]:

$$D = 7.65 \times 10^{-5} \left(\frac{T^{11/6}}{P_{tot}} \right) \tag{2.42}$$

where D has the units of m^2/s, P_{tot} is in pascals, and T is given in kelvins. The temperature used is the arithmetic mean of the free-stream temperature and the temperature at the vapour–condensate interface.

Chapter 3

Experimental Program.

3.1 Design Considerations.

The major design criterion for the experimental rig was that it allow for heat and mass transfer from dry or humid air to the cooling water tubes. Existing rigs used within the department were designed for heat transfer testing in the presence of pure steam, or at the least, steam with relatively low fractions of incondensables. Major modifications would have been necessary to the existing rigs, particularly with respect to air injection and heating. For this reason, it was decided that a new rig would be built to carry out the experimental program.

It was clear that the major input variables controlling the heat- and mass-transfer process were the mixture temperature and velocity as well as the moisture content of the air. It was decided that these three parameters could be controlled by providing a source of relatively dry (atmospheric) air, heating it and mixing with a controlled amount of steam. The goal was to maintain these three parameters as independent of each other as possible, while still using a reasonable amount of departmental resources.

Another important requirement for the rig was related to the quality of the flow over the tube surface. The rig would have to be designed in such a way that

the air–steam mixture flow would be acceptably uniform and developed, particularly within the test section in the region closest to the tube. This requirement involved a trade-off between rig size, both in overall length and cross-section, and available space within the laboratory. In theory, a small cross-sectional area in the test section would allow for a relatively short rig while still maintaining good flow quality. However, a small test section has the potential disadvantage of accommodating tubes that may be too short to provide any appreciable water temperature rise for a given set of gas mixture properties. It soon became apparent that the rig size requirement, particularly that of the cross-sectional area, would also have a direct impact on the control of the gas mixture velocity and therefore flow rate. As a result, fan capacity, heating and steam injection quantities were affected.

The cooling water temperature rise from entry to exit of the tube is a crucial measurement in the calculation of the heat- and mass-transfer rate. When all of the experimental measurements are considered, a small water temperature rise is the limiting factor in terms of overall accuracy of the results. This is especially true in this experimental program where dry heat-transfer rates at low Reynolds numbers can be many times smaller than for condensation of pure steam. Once this potential limitation was identified, the next step was to determine how to accurately measure these small temperature differences. It was decided that the temperature measurement system should be able to reliably measure differences as low as one-tenth of a degree Celsius. This would allow for testing under conditions of low humidity ratio, mixture velocity and temperature. Achieving accurate results for this type of temperature difference required the use of a system with more stability and accuracy than standard thermocouples. For this reason, platinum resistance thermometers were chosen.

The working length of the tube was chosen as a compromise between bulk water temperature rise and test-section width. A 300 mm exposed tube length was selected since it was calculated as being just long enough to provide the necessary temperature increase with a moderate water flow rate. The water flow rate was

itself chosen as a compromise between maximum temperature rise and the need to ensure adequate mixing within the tube and measurement cell. The flow rate through the 11 mm inside diameter tubes was designed to create conditions that were beyond the transition from laminar to turbulent flow.

With the width of the test section fixed by the tube length, the height of the test section remained to be determined. The test section height should be large enough so that the upper and lower surfaces have a minimal affect on the flow along the centre of the section. A height of 150 mm was chosen, again, as a compromise between flow quality and heating and fan requirements. This height corresponds to approximately 12 tube diameters.

Once the cross-sectional area of the test section had been determined, the desired range of gas velocities past the tube could be used to calculate the volumetric flow rate of air needed. One of the objectives of the experiment was to examine the effect of different gas velocities on the roped tubes over a range that might normally be expected within a compact heat exchanger. A maximum air velocity of at least 5 m/s, corresponding to a Reynolds number of approximately 4000 (based on 12.7 mm outside diameter tubes) was used to calculate the maximum air flow rate. The flow rate quantity made it possible to select a fan size.

The temperature range of the air–steam mixture was selected so as to be high enough to allow for relatively high water vapour contents. Although not a specific objective of this particular experiment, a useful minimum design point would have been 59°C, corresponding to the dew point of the products of combustion of a stoichiometric mixture of natural gas and air. 80°C was chosen as a reasonable maximum temperature for the flow through the test section. This meant using a heater with an output sufficient to raise the maximum flow rate of air some 60°C above ambient conditions.

With the major components selected, what remained were the details of their arrangement into a functioning rig. The next sections include the specifics of the rig

components and measurement systems as well as a description of the overall construction and operation of the rig.

3.2 Rig Description.

The major components of the rig were: a fan to provide a moving airstream, a heater to raise the air temperature, a steam injection system to increase the moisture content of the air and a test section in which measurements of heat and mass transfer were made. The various components of the rig were arranged linearly, with the fan at one end and the test section at the other. The total length was approximately 4 m. This arrangement had the advantage of minimising problems with the air flow caused by bends in the sections connecting the components. An overall view of the rig is shown in Figures 3.1 and 3.2. Connecting sections made of galvanised sheet steel were used to join the major components to allow for smooth cross-section size changes. The different sections were bolted together and used a synthetic rubber seal to prevent leakage at the points of connection. Sections downstream of the heater were insulated with 50 mm thick polystyrene foam insulation. A schematic of the component location and section sizes is given in Figure 3.3. The assembled components rest on two separate steel frames fitted with wheels. This enabled the rig to be easily moved from place to place or split into two, 2 m long sections for easier handling.

A system line diagram, shown in Figure 3.4, details how the steam, water and electricity supplies and controls were attached to the rig.

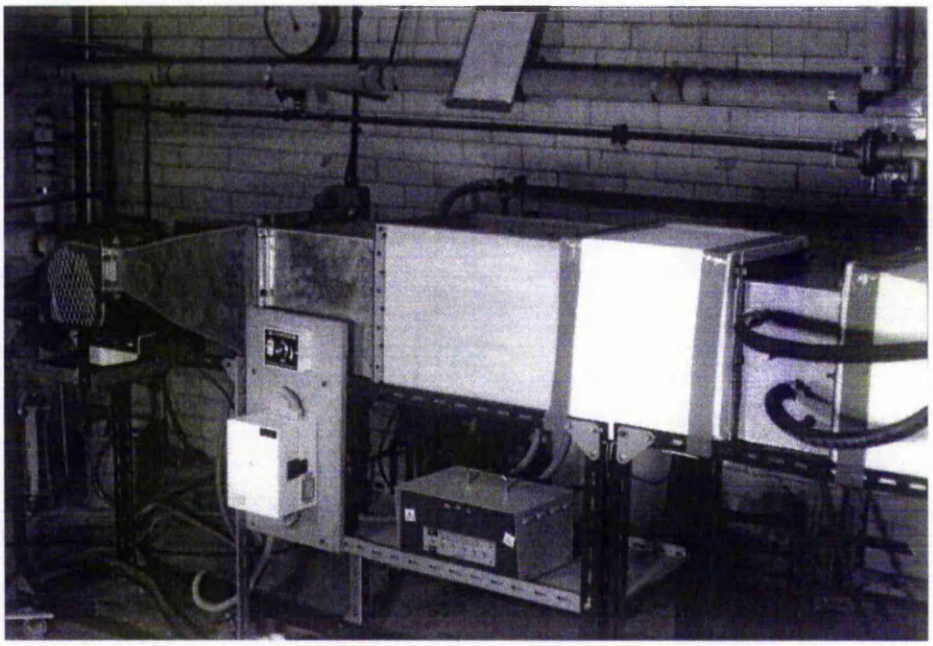

Figure 3.1 Upstream Sections of Rig. The fan is at far left. The heater circuit-selector box is visible under the heater section. The fan speed controller is located just to the left of the heater and above the white contactor box.

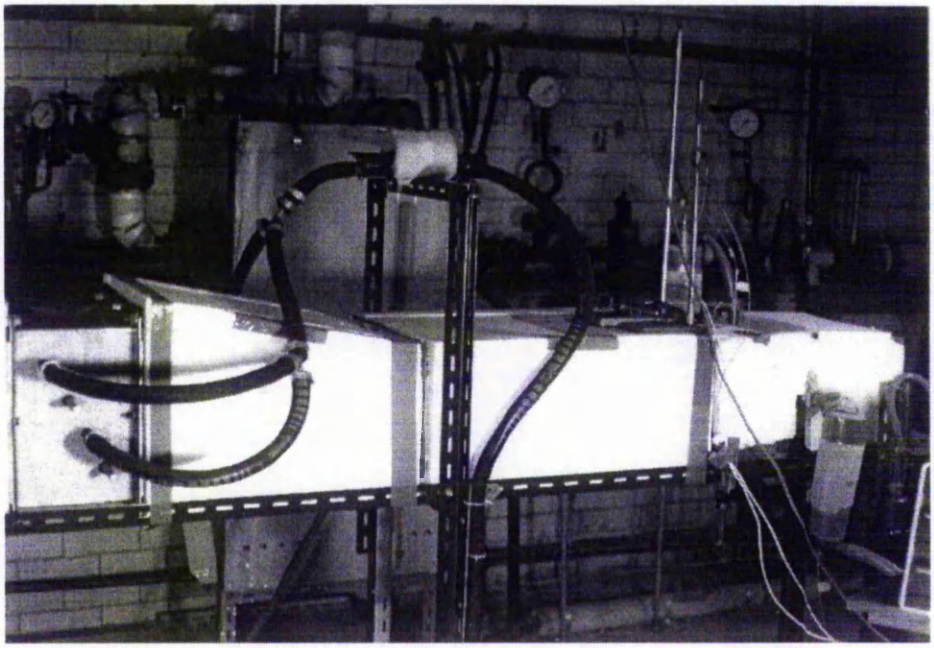

Figure 3.2 Downstream Sections of Rig. The steam injection section is at left with connecting sections leading to the test section at right.

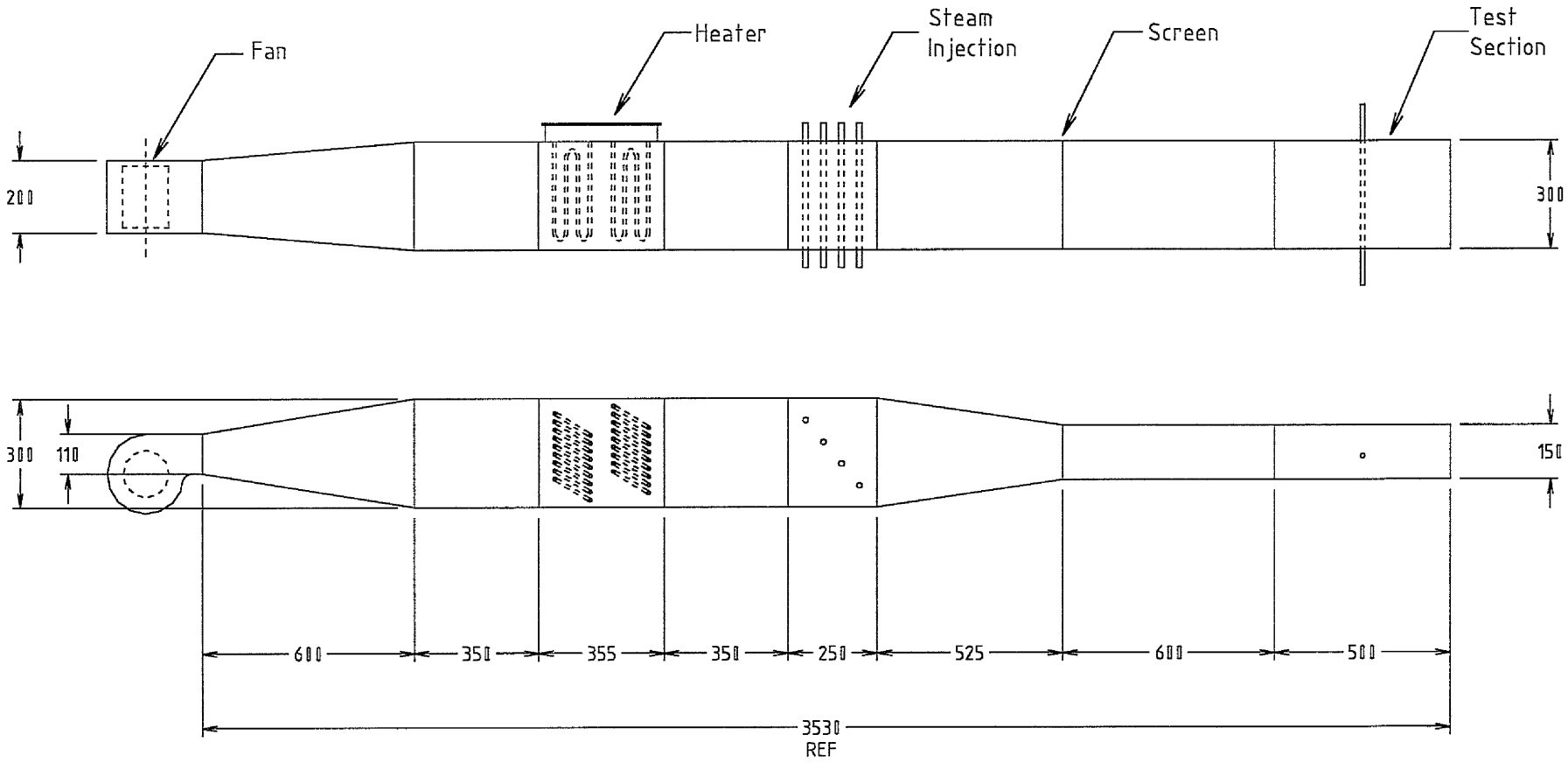

Figure 3.3 Component Location and Section Sizes. Internal dimensions given in mm.

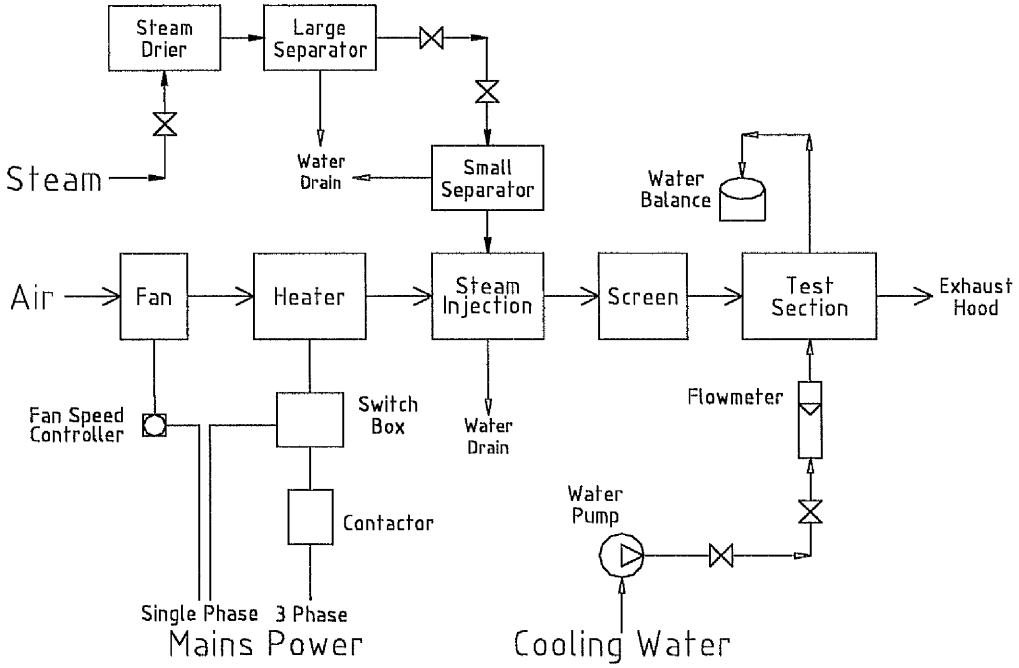

Figure 3.4 System Line Diagram.

3.2.1 Fan and Speed Controller.

A centrifugal fan was chosen over an axial fan in order to avoid swirl of the airstream flowing through the rig. The fan had a rating of 850 m^3 of air per hour at a pressure drop of 150 Pa. The air flow rate was controlled through a variable speed controller which regulated the A/C voltage to the fan. It was possible to continuously vary the velocities through the test section from a low of 1 m/s up to approximately 8 m/s.

3.2.2 Heater and Controls.

A 3-phase electric resistance heater with an output of 18 kW was located downstream of the fan. The heater's inside cross-section was 300 mm square and was fitted with eighteen 1 kW elements which were arranged in six circuits of 3 kW each. The elements were configured as two banks of nine, with the active groups of elements selected so as to give the most even heating possible. The heater system was able to provide 3, 6, 9, 12, 15 or 18 kW of heat input to the air flowing through

it. An adjustable thermostat was mounted within the heater casing and provided an automatic shut-off in the event that overheating occurred. Different minimum levels of air flow through the heater were required for each level of heat input in order to avoid the over temperature shut-off. A switch box connected the six circuits of the heater through a separate 3-phase contactor box. The contactor was in turn wired to the heater thermostat. Air exit temperatures of approximately 90°C were possible with low air flow rates.

3.2.3 Steam Injection.

Steam was supplied from the boiler house of the James Watt building. A steam line separate from the building heating system runs directly to the laboratory. Within the laboratory itself, the steam passed through a 2.3 kW electric blanket heater in order to increase its dryness. Two liquid separators were also used to increase the steam's dryness before it was injected into the air passing through the rig. Steam passed through four horizontal tubes mounted in a section located between the heater and the test section. Drilled in each tube were sixty, 0.8 mm diameter holes through which steam passed into the airstream. The 15 mm tubes were equally spaced vertically in a 300 mm square cross-section. A 1.6 mm grid stainless steel wire mesh screen was fitted downstream of the steam injection section in order to provide a more uniform velocity profile for the air–steam mixture entering the test section.

3.2.4 Water Supply.

The laboratory water supply flowed into a large storage tank from which it was pumped to the rig. The water was at room temperature, ranging from approximately 17 to 20°C. The temperature and flow rate of the water supplied to the rig were observed to be very constant over any particular test interval. Before entering the tube to be tested, the water passed through a valve which regulated the flow rate. A variable-area type flow meter was used to set the approximate flow rate, not to

measure the actual flow of water. The nominal water flow rate through the tubes was 0.04 kg/s.

3.3 Test Section.

All measurements of the experimental parameters took place within the test section which was located at the end of the rig. The test section can be seen in detail in Figure 3.5. A single tube was mounted horizontally within this section, normal to the flow of the air–steam mixture. The test section was made of mild steel and had a vapour flow cross-sectional area of 300 mm × 150 mm. A glass window was mounted in a cut-out on top which allowed for the tube to be viewed during the condensation process. The tube to be tested was secured at either end by a plate to which a threaded coupling had been welded. Two threaded brass bushings were fitted over the tube and screwed into the couplings on the plates. Four rubber o-rings were inserted into each bushing to prevent any steam–air passage and to isolate the tubes from direct conduction with the hot surfaces of the test section itself. This tube mounting arrangement allowed for quick changes of tubes with a minimum of rig dismantling between tests.

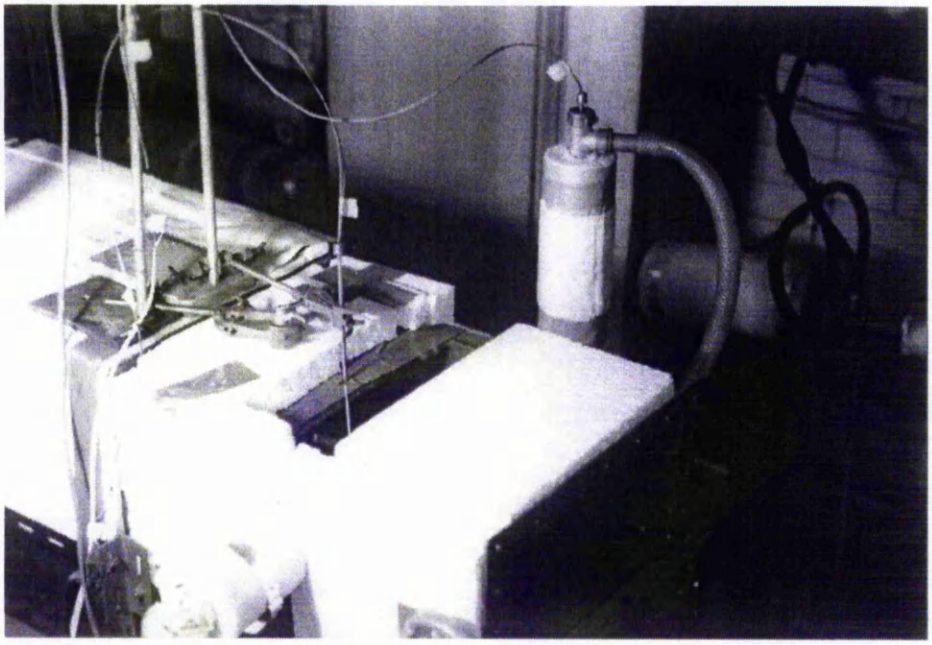

Figure 3.5 Test Section.

3.4 Tubing.

Four different tubes were tested, one plain and three roped, as shown in Figure 3.6. Each was of the same nominal outside diameter of 12.7 mm with an inside diameter of approximately 11 mm. The tubes were supplied by IMI Yorkshire Imperial Alloys and were a Cu–76%, Al–2%, Zn–remainder mixture. The tubes are manufactured by passing a plain tube through a series of dies whose number corresponds to the number of groove starts on the tube. The dies are equally spaced radially around the tube, resulting in a minimal out-of-roundness. This process results in a tube that has a series of spiral indentations winding along its length. The largest diameter of the tube remains the original plain tube diameter. For the purpose of comparison with plain tubes, it was judged reasonable to use the nominal inside and outside diameters of the roped tubes. This is especially important if roped tubes are to be considered as alternatives to plain tubes of the same outside diameter.

Two 2-start tubes were used. The first to be tested, tube **A**, had a groove depth of 0.4 mm and a pitch of 6.4 mm. The other 2-start tube, **C**, had a groove depth of 0.2 mm and a pitch of 12.8 mm. Of the three roped tubes, this one had the

least amount of spiral grooving per unit length and was the only tube tested with the shallow groove depth of 0.2 mm.

A 6-start tube, tube **B**, with a groove depth of 0.4 mm and a pitch of 6.4 mm was also tested. The combination of pitch and the high number of groove starts meant that this was the most highly indented tube in terms of grooves per unit length. A plain tube of the same nominal size was also tested.

Each tube was 600 mm long with an exposed length of 300 mm. An illustration of a typical roped tube configuration is given in Figure 3.7 and a summary of the specific tube parameters is included in Table 3.1.

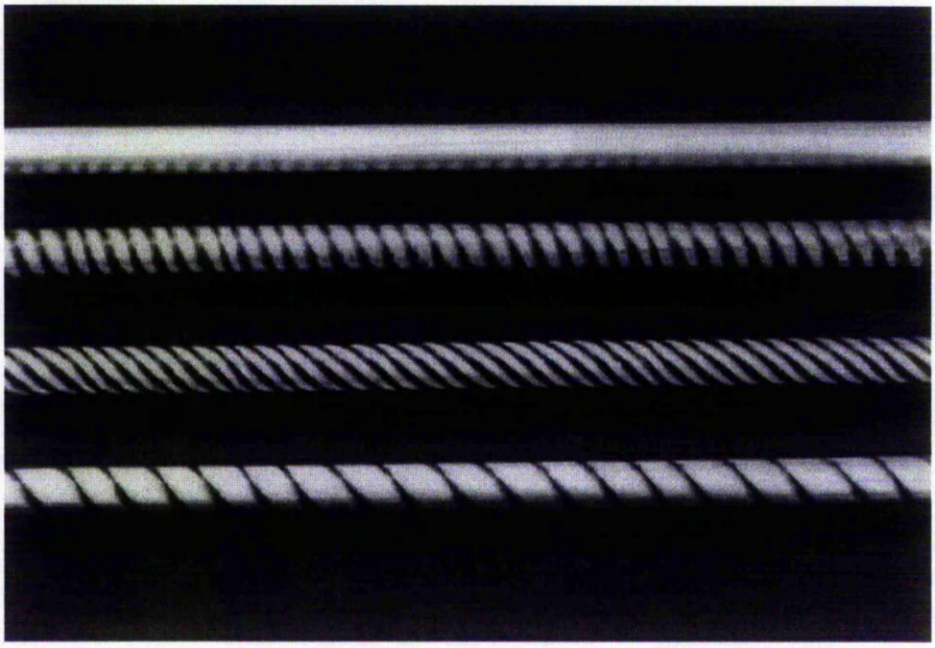

Figure 3.6 Tubes. From top to bottom, **P**, **A**, **B**, **C**.

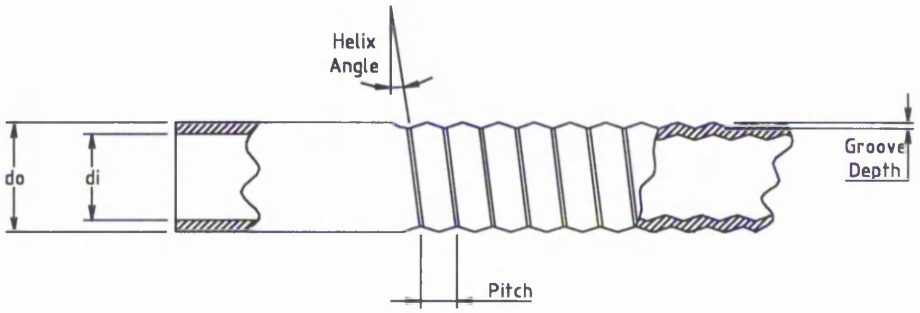

Figure 3.7 Typical Roped Tube Configuration.

Table 3.1: Tube Geometry

Tube	Number of Starts	Pitch (mm)	Helix Angle (Degrees)	Depth (mm)	d_i (mm)	d_o (mm)
A	2	6.4	17.8	0.4	11.0	12.7
B	6	6.4	43.9	0.4	11.0	12.7
C	2	12.8	32.7	0.2	11.0	12.7
P	Plain	NA	NA	NA	11.0	12.7

3.5 Instrumentation.

Instrumentation was chosen to measure and record the following experimental parameters: For the air–steam mixture, it was necessary to measure the temperature, velocity and moisture content approaching the tube in the test section. The inlet and outlet temperatures of the cooling water and the mass flow rate through the tube were also measured. Details of the instrument calibrations are included in Appendix B.

3.5.1 Water Flow Rate.

The mass flow rate of water through the tube was measured by flowing the exiting water into a 23 L container set on a balance and recording the time required to balance a 15 kg weight. The times, on the order of 380 seconds for the flow rate used in this experiment, were measured with a stopwatch. This method was judged to be more accurate than relying on a calibrated flow meter, particularly as it provided a measure of the average flow rate during a given test lasting 5 minutes.

3.5.2 Gas Mixture Velocity.

It was decided that the main stream velocity of the air–steam mixture, instead of the total flow rate through the test section, should be measured. This is because all tests were on a single tube mounted in the test section and thus required velocities only

in the plane normal to the tube. In this way, velocity variations in the vertical direction were minimised in importance.

The gas mixture velocity across the tube length was, of course, more important. A pitot-static tube was chosen as the means of measuring the horizontal velocity profile. The pitot-static tube was connected to a Furness Controls digital micromanometer with a resolution of 0.01 mm of water. The micromanometer compensated for time-varying velocity fluctuations with a built-in integration feature. Pressure difference measurements were taken at 10 mm intervals across the test section at three different nominal air velocities. The results are shown in Figure 3.8. Although there was a slight variation in velocity along the tube length, the average velocity fell near the centre of the test section in all cases. As a result, it was decided that measuring the centre-point velocity with the pitot-static tube would give a good representation of the overall mixture velocity.

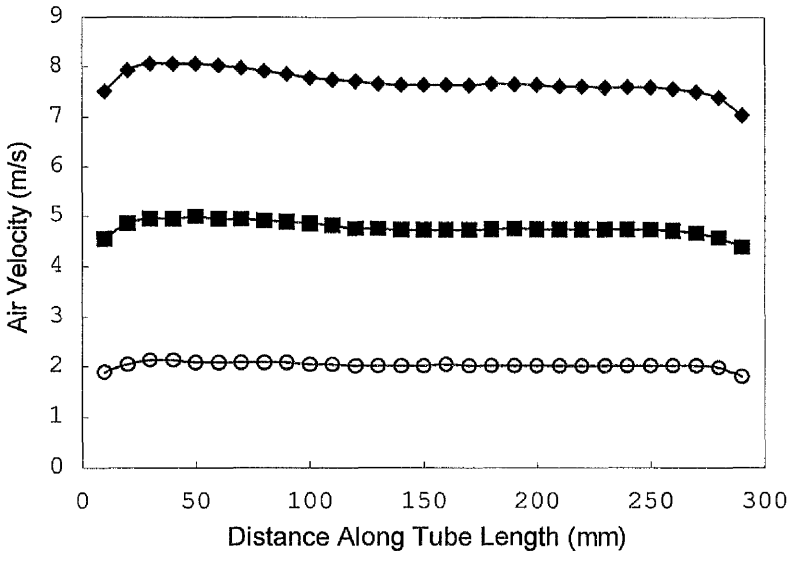

Figure 3.8 Test Section Horizontal Velocity Profiles.

The above method worked well for the case of a dry air flow around the pitot-static tube, but not as well when the airstream had a large moisture content. This may be attributed to water droplets intermittently blocking the pitot-static tube opening. For this reason, velocity measurements were made of the relatively dry

inlet air only and then corrected to take into account the addition of water vapour. Therefore, the gas mixture velocities are functions of the pitot-static pressure difference, temperature and relative humidity. It was assumed in the calculation of the velocity from the above variables that the gas mixture behaved as an ideal gas — a reasonable assumption for engineering purposes given that the mixture was at atmospheric pressure and that the maximum partial pressure of the water vapour was approximately 30 kPa.

Although the experiments described in this chapter were performed on a single tube, the test section was designed so as to be able to hold more than one row of tubes. With more than one vertical row of tubes, it is important that the vertical velocity profile be uniform. Figure 3.9, shown for reference, indicates that the vertical velocity profile should be satisfactory for more than one tube, especially in the region near the centre of the test section.

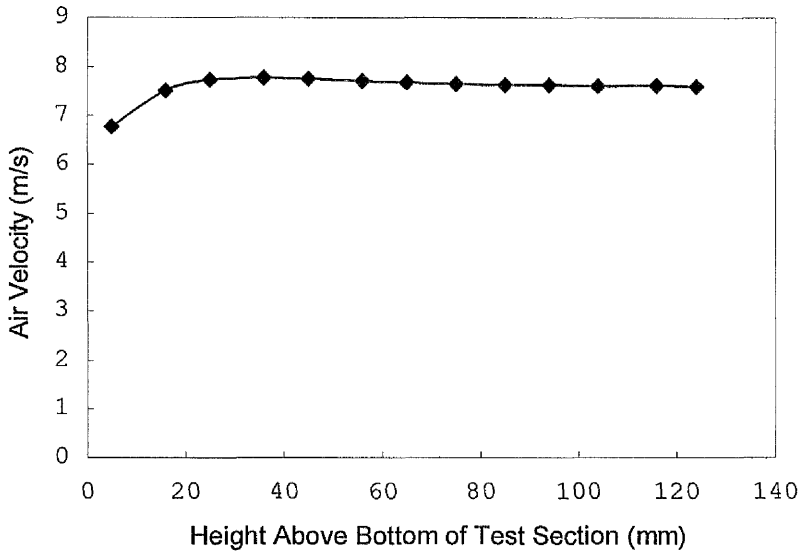

Figure 3.9 Vertical Velocity Profile.

3.5.3 Humidity Measurement.

The moisture content of the airstream was measured with a psychrometer that outputs a digital reading of both relative humidity and temperature. These combined measurements were necessary to calculate the humidity ratio or the equivalent

partial pressures of the air and water vapour. The accuracy of the relative humidity measurement is quoted as ± 1% while the temperature measurement is accurate to ± 1°C.

The psychrometer probe was large enough to significantly disturb the air flow if located upstream of the tube in the test section. To reduce the amount of turbulence, the probe was centrally located near the exit of the test section. Effectively, the psychrometer measured the humidity ratio of the air approaching the tube since the water vapour removed through condensation is a small fraction of the total water vapour present in the mixture. No noticeable variation in humidity ratio was seen across the test section.

3.5.4 Temperature Measurement.

1/10 DIN platinum resistance thermometers (PRT) were chosen as they were able to provide the desired degree of accuracy. The 4-wire, 100 Ω PRTs offer a calibrated accuracy of 0.01°C at 0°C and are very stable with time as long as they are not subjected to physical shock. Three PRTs were calibrated against a NPL-calibrated PRT over the range of 0 to 85°C using a triple-point-of-water cell and heated water bath.

One PRT was mounted in each of two specially-constructed mixing cells which were attached to the inlet and outlet ends of the tube to be tested. Because of the relatively low flow rate needed to achieve a minimum water temperature rise, it was decided that the internal flow regime should be optimised for maximum mixing of the water within the tubes and near the PRTs. The PRTs were centred within the cells, downstream of an insert which introduced turbulence in the water flow to provide a measure of the bulk or average temperature of the water. The cells themselves were insulated with 50 mm thick glass-fibre insulation and connected to the water supply via flexible plastic tubing. Once installed, the temperature measurement system was evaluated with a tube that was insulated from outside heat sources. No temperature rise, measured to an accuracy of 0.01°C, was recorded as

water flowed through the unheated tube at the flow rate used throughout this series of tests.

Temperature measurements of the incoming gas mixture were also made with a platinum resistance thermometer. A temperature profile in the horizontal direction along the tube showed a relatively smooth variation of temperature with distance. The maximum variation, shown in Figure 3.10, was less than 7% of the mean temperature found at the centre of the test section. This variation was judged to be acceptable, particularly since the mean of the temperature distribution was at the middle of the tube's length. The thermometer was located at this point, 150 mm upstream of the tube.

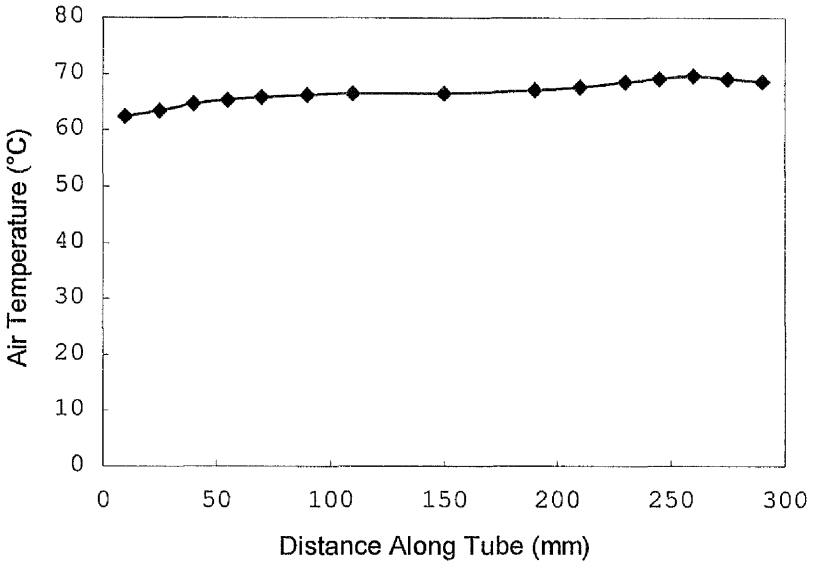

Figure 3.10 Test Section Horizontal Temperature Profile.

3.5.5 Data Recording.

A Schlumberger Orion 3530 data logger was used to record the temperature measurements. A module within the logger supplied the energising current to the PRTs while another converted the resistance measurements directly into temperatures. The logger provided temperature measurements with two-decimal-place precision when sampling at 10 measurements per second.

3.6 Experimental Procedures.

3.6.1 Tube Preparation.

It is well known that dropwise condensation is sometimes difficult to avoid in filmwise condensation experiments, especially with a tube that is new or hasn't had any special surface treatment. Nevertheless, it is extremely important that dropwise condensation be prevented, or at the very least, be kept to an absolute minimum. This is the case because dropwise condensation heat-transfer rates can be many times higher than filmwise condensation rates, where the condensate layer presents an additional resistance to heat and mass transfer. The need to ensure filmwise condensation in this experimental situation is in contrast to what sometimes occurs in practical applications where dropwise condensation can be used to increase heat transfer within an exchanger.

Various methods have been proposed for the preparation of tubes used in filmwise condensation experiments. The efforts of Ben Boudinar [8] in the preparation of roped tubes used in filmwise condensation experiments show that any one procedure won't necessarily be successful in every instance. In this experiment, it was found that using tubes that had been used extensively in previous experiments and that had sufficiently uniform surface oxidation, gave good results. It was observed that dropwise condensation would sometimes occur immediately when restarting a series of tests on a particular tube after the tube had been exposed to steam condensation the previous day. This may be explained by the build-up of contaminant particles present in the steam supply. For this reason, the tubes were routinely cleaned first with ethyl alcohol and then rinsed with distilled water between tests. In this way, dropwise condensation was able to be avoided almost exclusively.

3.6.2 Rig Start-Up.

The following procedure was used to begin a series of tests on a particular tube:

(a) The external surface of the tube was cleaned as described above.

(b) The cooling water pump was turned on and the supply to the rig was adjusted to the appropriate value by checking with the float meter located on the rig.

(c) The logger was turned on and the temperatures displayed.

(d) The fan speed was adjusted to one of three approximate settings.

(e) Heater contactor and control box were plugged in and turned on.

(f) The heater elements were selected on the heater control box.

(g) Heater power was turned on.

(h) The air temperature was monitored on the logger for approximately 20 minutes until it reached a stable temperature.

(i) The air velocity was measured with the pitot-static meter and the velocity was adjusted to one of the three predetermined values.

3.6.3 Individual Tube Testing.

For each tube, the first test involved no injection of steam. The procedure for the dry tests was as follows:

(j) Logging of the temperatures was started. Values were recorded at 15 second intervals over 5 minutes for a total of 20 measurements per test. The results for the three temperatures recorded were averaged by the logger and summarised on the logger printout.

(k) As the logger was recording temperatures, the flow rate of water was measured using the 15 kg weight and balance.

Once the dry test was completed it was possible to start the steam injection system for the condensing tests. The series of operations is described below.

(l) The steam system, including the two separators, was drained of accumulated water.

(m) All steam valves were opened allowing steam to flow into the rig. The amount of steam injection was adjusted while monitoring the relative humidity reported by the psychrometer. The relative humidity was seen to fluctuate within

approximately ± 1 percentage point of an average value as reported by the psychrometer. For this reason, the psychrometer readings recorded were the average of the values seen over the 5 minute test periods.

(n) Once the mixture temperature had stabilised sufficiently, measurements were taken for a particular relative humidity value while following steps (j) and (k) above.

(o) Step (n) was repeated for six other steam injection rates, performed in order of increasing water vapour content.

(p) The steam and heater were shut off, the rig allowed to cool and then the process was repeated starting at step (d) for the other two gas mixture velocities.

Chapter 4

Experimental Results and Discussion.

4.1 Introduction.

The first section of this chapter offers a critical evaluation of how well, in practice, the experimental program design met the goals described in the previous chapter. The sections that follow these general observations include the specific experimental results and a discussion of their significance. Since the dry tests are a helpful way of examining the subsequent condensing tests, the dry cases are presented first. Further, the plain-tube tests provide a logical baseline for evaluating the roped tubes, and as such the roped tube results follow those for the plain tube. A discussion of the computer-program output and its comparison with the experimental results is included in Chapter 5.

4.1.1 General Remarks.

Initial tests with the plain tubes in a non-condensing environment yielded overall water temperature rises that were much higher than expected from predictions based on published correlations of convection coefficients. A pattern emerged which showed an additional water temperature rise of between approximately 0.05 and 0.1°C, regardless of the air velocity. This effect was very significant, especially at

the lowest air velocity where it amounted to approximately 50 to 100% of the projected convection heat transfer. The source of the problem was found to be a poor o-ring installation which allowed for conduction into the tube itself through the hot fittings and test section walls. The problem was corrected when additional o-rings were used within the tube fittings.

Condensing tests using steam injection from the building steam supply had to be timed with the building heating cycle so that the steam pressure would not fluctuate excessively during the course of a test. This didn't pose a major problem because there was sufficient time between cycles to perform a single complete test at a specific air humidity content. Subsequent tests were performed after the building steam pressure had stabilised.

Another limitation of the experimental program was the inability to verify the total heat-transfer rate calculated from the water temperature rise with an energy balance on the air–vapour side. In fact, an accurate measurement of the decrease in gas-side temperature would have been very difficult, particularly at non-condensing conditions. The convection heat-transfer rate for the plain tube was on the order of only 50 Watts at the highest air velocity. This translates into an air temperature decrease (averaged over the volume through the test section) of approximately 0.15°C. This kind of decrease in air temperature is difficult to measure under bulk conditions due to uneven mixing of the air both upstream and downstream of the tube. Fortunately, the measurement of the bulk water temperature increase is much more straightforward, even with similar temperature differences.

A similar situation existed with respect to verifying the latent heat transfer by collecting the condensate falling from the tube. A conventional receiver-type conduit was unsuitable because a certain amount of the condensate would be subject to re-evaporation in the hot airstream. This same situation was identified by Taniguchi *et al.* [24], for which a new device was used to draw in both the condensate and surrounding gas via a vacuum pump. The collected fluids were then passed through a condenser and corrected by an amount proportional to the quantity

of drawn gas. The solution used in that study proved successful in collecting the condensate, but its complexity precluded its use in the present experimental apparatus.

Measuring the temperature of the outside tube wall would also have led to another indirect method for calculating the condensing heat transfer. This method simplifies the calculation of the condensing heat-transfer coefficient considerably if it assumed that the temperature difference across the condensate layer is zero. In practice, with the condensate interface temperature only slightly higher than the outside tube wall temperature, the approximation would be a good one. The drawback to directly measuring the tube wall temperature is that thermocouples would need to be mounted in the tube wall — an operation that requires a great deal of care to ensure accurate measurements. Even if such a set-up were practical within the scope of these experiments, several wall temperatures would need to be measured and their results averaged.

For the reasons outlined above, special attention was paid to ensuring an accurate measurement of the water temperature rise, both in terms of adequate mixing at both ends of the tube, and in all areas related to the actual temperature measurement apparatus.

4.2 Dry Heat Transfer Results.

An assessment of the convection heat transfer performance of plain and roped tubes was not one of the explicit goals of this particular experiment. It is, however, necessary in order to determine the condensing performance. Since the total heat transferred from the hot, humid airstream was made up of sensible and latent contributions, it was necessary to devise a method to separate these two components in the experimental results. Measuring the total heat transferred to the cooling water is a relatively straightforward process, easily calculated through the knowledge of the water flow rate and temperature rise. The difficulties involved in a experimental measurement of the latent heat-transfer rate alone have been discussed in the

previous section. This leads to a situation where the latent heat-transfer rate must be calculated from the difference between the total and sensible heat-transfer rates. Fortunately, there is a connection between the sensible heat-transfer coefficients during the condensing process and the convection coefficients under dry conditions. This relationship is discussed in section 4.3.

4.2.1 Plain Tube.

The convection gas-side heat-transfer coefficient is needed for later calculations involving the latent heat-transfer rates. The first task when analysing the dry tube data is to attempt to separate the outside heat-transfer resistance, R_o, from the water side and tube wall conduction resistance. If a fouling resistance is not considered as a factor, the electrical resistance analogy given in equation (2.1) is, i.e.,

$$Q_{tot} = \frac{T_\infty - T_w}{R_o + R_t + R_i}$$

The total heat-transfer rate, Q_{tot}, is known from the product of the water mass flow rate, heat capacity and temperature rise. The bulk temperatures of the air and cooling water are also known experimentally. The tube wall resistance to conduction, R_t, is calculated (as outlined in Chapter 2) using a value of 104 W/m°C for the thermal conductivity of the tube material.

The remaining variable, the tube-side resistance, R_i, could have been determined experimentally by measuring the tube inside wall temperature and comparing it with the bulk cooling water temperature. This measurement is difficult to obtain accurately and would only provide local values of the tube wall temperature — an average reading over the tube length being preferable. The inside heat-transfer coefficient was not a specific object of study in this experiment, but rather its determination provided a means for calculating the condensing performance of the tubes. Also, correlations for the tube-side heat-transfer coefficients have been widely developed and accepted, especially for the turbulent

flow of water in plain tubes. For these reasons, the value of the water- side heat-transfer resistance was calculated using the relation of Dittus and Boelter given in equation (2.23). The nominal water flow rate of 0.04 kg/s corresponded to a Reynolds number of approximately 4400, with a Prandtl number of approximately 7.4. Both values were within the range recommended for use with the Dittus–Boelter relation for fully developed turbulent flow of a liquid undergoing heating. There are several other correlations of Nusselt number expressed as a function of Reynolds and Prandtl number, most notably the correlation of Seider and Tate shown in equation (2.24). For the purposes of calculating the experimental results, this correlation is less convenient because it includes a term that relies on water properties calculated at the inside tube wall temperature — a parameter that was not directly measured in the experiment. In any case, the estimated convection coefficient as calculated by Seider–Tate is less than 3% greater than that actually calculated using the Dittus–Boelter correlation. The influence of the choice of correlation on total heat-transfer rates is discussed further in the chapter dealing with the computer-program results.

When evaluating the accuracy of the calculation of the water-side heat-transfer coefficient, it is useful to examine the relative sizes of the three heat-transfer resistances. As shown in Table 4.1 below, in the worst-case scenario of the highest gas velocity, the gas-side resistance is over 25 times higher than the water-side resistance. This ratio is more than 50 at the lowest gas velocity. When the goal is to calculate the tube outside temperature (and hence the heat-transfer coefficient), inaccuracies in the inside heat-transfer coefficient calculation, while still present, diminish in importance. The same principle applies to the determination of the tube wall resistance to conduction, R_t, — only to a greater extent. Depending on gas velocity, the tube wall conduction resistance is approximately 1400 to 3000 times smaller than the gas-side convection resistance. The corresponding temperature difference across the tube wall is, of course, very small. In this experiment it ranged from approximately 0.02 to 0.04°C. These results are not surprising and they serve

as a reminder of why much of the attention is directed towards gas-side enhancement of convection heat transfer over tubes. (Note that this is not at all the case in situations where pure or near-pure water vapour is condensing on similar tubes. As discussed in the introduction, in steam condensation on similar plain and roped tubes, other investigators have determined that the greatest resistance to heat transfer was to be found on the water side.)

Table 4.1: Temperatures and H.T. Resistances for Plain Tube

V_∞ (m/s)	T_w (°C)	T_i (°C)	T_o (°C)	T_∞ (°C)	R_i (°C/W)	R_t (°C/W)	R_o (°C/W)
1.5	17.84	18.58	18.59	56.67	0.042	7.3×10^{-4}	2.18
2.8	18.52	19.65	19.67	62.26	0.042	7.3×10^{-4}	1.57
6.4	18.64	20.87	20.91	75.62	0.043	7.3×10^{-4}	1.05

The dry, experimental external convection heat-transfer coefficient was calculated from

$$h_o = \frac{1}{\pi\, d_o R_o} \tag{4.1}$$

with the air velocity past the tube calculated as recommended by Zukauskas [40]:

$$V_{mix} = V_\infty \left[1 \Big/ \left(1 - \frac{\pi}{4} \frac{d_o}{H} \right) \right] \tag{4.2}$$

where the d_o/H term is the blocking ratio for the test section of height H. In this case, the free-stream velocity was multiplied by a factor of 1.07. The overall heat-transfer coefficient, $U_{overall}$, is calculated from:

$$U_{overall} = \frac{Q_{tot}}{A_o\, \Delta T_{LM}} \tag{4.3}$$

where ΔT_{LM} is the log mean temperature difference (LMTD) given by:

$$\Delta T_{LM} = \frac{T_{w,2} - T_{w,1}}{\ln\left(\frac{T_\infty - T_{w,1}}{T_\infty - T_{w,2}}\right)} \tag{4.4}$$

The subscripts *1* and *2* represent the inlet and outlet conditions respectively and $U_{overall}$ is based on the tube outside surface area, A_o. Not surprisingly, given the dominance of R_o, the overall heat-transfer coefficient is only marginally lower than h_o. Table 4.2 summarises the results for the experimental heat-transfer coefficients of the three velocities considered.

Table 4.2: Dry Heat-Transfer Coefficients for Plain Tube

V_∞ (m/s)	Re_d	h_o (W/m^2°C)	$U_{overall}$ (W/m^2°C)
1.5	1131	38	38
2.8	2074	53	52
6.4	4627	79	76

The Reynolds numbers were evaluated at the film temperature properties,

$$T_f = \frac{(T_{o,1} + T_{o,2})/2 + T_\infty}{2} \tag{4.5}$$

i.e., at the average of the inlet and outlet external wall temperatures and the free-stream gas temperature.

The flow regime for the gas side was within the range of Reynolds numbers of approximately 1000 to 2×10^5, in which the flow is turbulent in the separated region downstream of the tube. The experimental gas-side coefficients are 3 to 7% greater than those predicted by the Churchill–Bernstein correlation, equation (2.30). If the relations of Eckert–Drake and Hilpert are considered, the experimental heat-transfer coefficients are also greater than the theoretical coefficients. (A detailed discussion of the choice of gas-side correlation is given in Chapter 5). One possible reason for an increased gas-side convection coefficient is the presence of free-stream turbulence inside the rig. Quantifying the amount of undesirable non-

uniform flow is difficult. Measures have, however, been taken in the design of the rig to minimise it. Non-condensing experimental results are included in Table C1.

4.2.2 Roped Tubes.

The spirally wound indentations, or roping, were expected to enhance the overall heat-transfer rate, even in non-condensing environments. Since the effective surface area of the roped tubes was approximately equal to that of plain tubes of equivalent diameter, it was assumed that there were no effects that could have been attributed to extended surfaces. Enhancement of both the air and water-side convection coefficients was expected with the roped tubes.

Of the two potential enhancements, the water-side heat-transfer enhancement (along with a corresponding increase in friction factor) is the more widely examined in the literature. This was discussed in greater detail in Chapter 1. Further, the inside heat-transfer coefficients for the roped tubes, like the plain tube, were not specifically compared for reasons outlined in section 4.2.1. It is clear, however, that the inside heat-transfer coefficients for the roped tubes should be greater than that of the plain tube at equivalent flow conditions. The effect of this enhancement is to lower the inside heat-transfer resistance, R_i. If the plain-tube water-side correlation is used with the roped tubes, it follows that the air-side resistance, R_o, will be under-predicted. This results in the calculation of an external convection coefficient which is slightly higher than in actual fact. Fortunately, this degree of over-prediction is very small since the internal resistance is only a small fraction of the total resistance. For example, if an enhancement in the internal heat-transfer coefficient of 100% is assumed for a particular roped tube, then R_i shown in Table 4.1 falls to only 0.9% and 1.9% of the total resistance for the lowest and highest air velocities respectively. This would correspond to an error in calculating h_o in the range of 1 to 2%. Since the degree of internal enhancement was not explicitly quantified as part of this experimental program, the plain-tube internal correlations were used. Note

that specific expressions for internal enhancement due to roping can easily be added to the computer program if desired. (See discussion in Chapter 5).

Enhancement of the external convection heat-transfer coefficient was found to occur with the roped tubes as compared to the plain tube. A summary of the results is given in Table 4.3 below. However, the magnitude of the calculated increase was small, with little or no enhancement observed at the lowest air velocity of 1.5 m/s. At 2.8 m/s, a modest enhancement averaging approximately 6% for the three roped tubes was found. At the highest air velocity of 6.4 m/s the average enhancement was slightly less than 10%. It is difficult to draw any conclusions about the relative convection performance of the three roped tubes because of the error inherent in the calculation of the convection coefficient. With all enhancements within 4% of the average for all tubes, the results suggest that there is little difference between the three tubes. The error interval for this quantity was calculated at 14%, 10% and 5% for the slowest to fastest air velocity respectively. (See Appendix A for details of the calculation of the error intervals). Much of the uncertainty at the slowest air velocity, and hence lowest heat-transfer rate, was due to the small water temperature rise of approximately 0.11°C. At the fastest air velocity, the uncertainty in the measurement of the external tube diameter was the dominant factor in the overall uncertainty in h_o.

Table 4.3: Comparison of Air-Side Coefficients for All Tubes

	Tube						
	Plain	**A**		**B**		**C**	
V_∞ (m/s)	h_o (W/m^2°C)	h_o (W/m^2°C)	% Diff.	h_o (W/m^2°C)	% Diff.	h_o (W/m^2°C)	% Diff.
1.5	38	38	−1	38	0	39	3
2.8	53	55	3	56	5	58	9
6.4	79	88	10	85	8	88	11

The slight convection enhancement over the plain tube outlined above is almost certainly due to an increase in turbulence close to or within the boundary layer. Since the roped tubes present roughly the same frontal profile as the plain tube, the grooves and ridges of the roped tubes likely increase the friction-induced turbulence, with a minimal effect on the form drag past the tube. Within the range of Reynolds numbers used in this experiment, the frictional contribution to drag and turbulence is much lower than the pressure effects. This means that when it comes to the outside convection coefficient, the limited influence of the roping is relatively well-predicted. The overwhelming number of roped tube applications have been under conditions of condensation of pure steam. As a result, it is difficult to compare the present experimental convection results for cross-flow with other studies. However, the convection results generally confirm the anticipated small enhancement over an equivalent plain tube.

4.3 Condensing Heat Transfer Results.

This section presents the condensing calculations and results that are common to both the plain and roped tubes. Results that are specific to either the plain or roped tubes are presented in sections 4.3.1 and 4.3.2 respectively.

With the total heat transfer treated as a sum of the latent and sensible contributions, the assumption was made that the external convection coefficients during condensation are equal to the dry-case coefficients for h_o. This assumption formed part of an investigation by Idem *et al.* [41]. Their review of the literature indicated that the wet-case sensible heat transfer could either be augmented or reduced as compared to the dry situation. Results depended on the quantity of condensation, flow regime, as well as the type of surface used. Although no results were presented specifically for roped tubes, it is assumed that some small increase in the wet-surface sensible transfer rate can be expected. The mechanism by which this happens is presumably due to waves on the condensate film which induce additional turbulence and thus mixing in the boundary layer. It is also possible,

though not quantified here, that because to the natural surface irregularity of the roped tubes, the condensate retained in the concave sections of the tube acts to offset some of the sensible enhancement. Notwithstanding these possibilities, the overall effect is assumed to have a negligible bearing on the calculation of the latent heat transfer, particularly when the ratio of latent to sensible contributions is high.

Figures 4.1 through 4.3 show the breakdown of the total heat-transfer rate into the sensible and latent components for each of the three velocities. The plain-tube data presented in these plots gives an idea of the relative importance of each component at the seven distinct vapour concentrations tested. The variable chosen for the x-axis is a measure of the available vapour above saturation conditions at the interface, and as such, required the calculation of the interface temperature. The ratios are also typical of those calculated for the three roped tubes. At the lowest mixture velocity tested, the latent heat-transfer rate varies from 36% of the total heat-transfer rate, to 91% at the greatest vapour content. At the highest velocity these latent fractions become 10% and 70% respectively. Also, the limiting case of zero water-vapour pressure above saturation conditions (i.e., dry conditions) can be extrapolated from the total heat-transfer rate curve on the same plots. The total heat-transfer curve obviously does not depend on any assumptions for the sensible portion. Therefore, the point where this curve crosses the y-axis can be a useful, albeit rough, check of the calculation of the wet, sensible heat-transfer calculation. Judging by the graphs, the calculations of the sensible contributions appear reasonable at all three velocities.

The analogy between temperature-driven heat transfer and diffusion-driven mass transfer is a useful way of quantifying the performance of condensing heat exchangers. The j-factor analogy of Chilton and Colburn [25],

$$j = \left(\frac{h_o}{m c_p}\right) \mathrm{Pr}^{2/3} \quad \approx \quad j_h = \left(\frac{h_D}{m}\right) \mathrm{Sc}^{2/3} \tag{4.6}$$

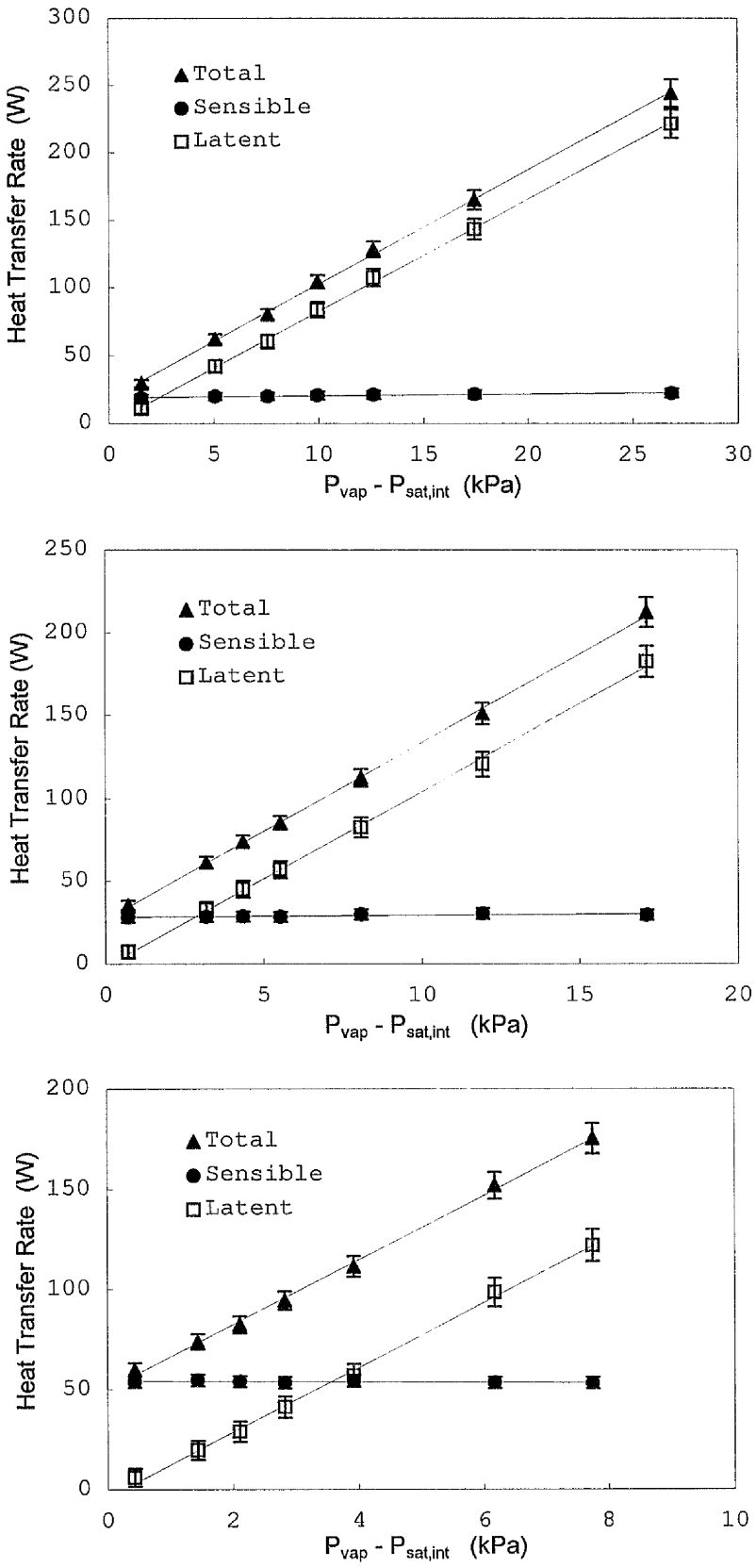

Figures 4.1 through 4.3 Heat Transfer Breakdown for Plain Tube.
(Top) V_{mix} = 1.5 m/s. (Middle) V_{mix} = 2.8 m/s. (Bottom) V_{mix} = 6.4 m/s.

links the two processes and suggests that they are approximately equal as long as the rate of mass transfer is low. It follows that the rate of mass transfer can be expressed in a form similar to the heat-transfer rate due to convection, i.e.,

$$\dot{m} = h_D A(\rho_{vap} - \rho_{\text{int}}) = h_D A \frac{M_w}{R_u}\left(\frac{P_{vap}}{T_\infty} - \frac{P_{\text{int}}}{T_{\text{int}}}\right) = \frac{q_l}{h_{fg}} \tag{4.7}$$

where the condensation coefficient, h_D, replaces the convection coefficient, h_o, and the driving force in the process is the concentration difference rather than a temperature potential. The substitution of the partial pressure terms is a result of the assumption that the mixture behaves as an ideal gas.

The similarity between the two processes suggests a functional relationship for the Sherwood number similar to expressions for the Nusselt number in convection situations. Following from equation (4.6), the Sherwood number can be expressed in a way similar to equation (2.26), with the Schmidt number taking the place of the Prandtl number, i.e.,

$$\text{Sh} = C\,\text{Re}^m\,\text{Sc}^{1/3} = \frac{h_D\, d_o}{D} \tag{4.8}$$

The constants C and m can be determined experimentally for each tube and the condensing performance can then be plotted as a function of Reynolds number. This is accomplished by combining equations (4.7) and (4.8) to obtain the following relation:

$$C\,\text{Re}^m = \frac{h_D\, d_o}{D\text{Sc}^{1/3}} = \frac{q_l\, R_u d_o}{h_{fg} M_w A_o\, D\, \text{Sc}^{1/3}\left(\frac{P_{vap}}{T_\infty} - \frac{P_{\text{int}}}{T_{\text{int}}}\right)} \tag{4.9}$$

The terms on the far right side of the above equation are, like the Reynolds number, all known experimentally. If a log-log plot is made, the resultant slope and y-intercept correspond to the constants m and $\log(C)$ respectively. The plots used to calculate these constants are presented in the sections that follow.

As discussed in section 3.5.2, the dry gas velocity measurement required a correction in order to account for the addition of water vapour. The assumption was

made that the total momentum through the test section was approximately constant both with and without the steam introduction. This approximation was considered valid due to the relatively small initial velocity of the injected steam and the absence of any change in the fan setting. With momentum conserved:

$$\rho_a V_a = \rho_{mix} V_{mix} \tag{4.10}$$

and with the mixture density calculated using the ideal-gas law, the following equation is used to calculate the average mixture velocity through the test section:

$$V_{mix} = V_a \rho_a \left(\frac{R_u T_{mix}}{P_a M_a + P_v M_v} \right) \tag{4.11}$$

The subscript a denotes the conditions of dry air before the addition of water vapour. The addition of steam to the air flow naturally resulted in an increase in the air–vapour mixture temperature over that of the dry air leaving the heater section of the rig. The amount of this temperature rise was clearly related to the amount of steam added. The effect was greatest at the slowest air velocity; with a maximum temperature rise of approximately 14°C when the steam injection was sufficient to raise the relative humidity of the mixture to a value greater than 90%. The maximum air–vapour mixture temperature rise was on the order of 9°C for the intermediate mixture velocity and 4°C for the fastest velocity. The combined effects of mixture density change and temperature increase resulted in the following corrections to V_a: At the highest air velocity, V_{mix} was approximately 4% higher than V_a when using the largest steam injection rate. At the intermediate and slowest velocities, the maximum corrections to V_a were 10% and 16% respectively. Sample condensing results are included in Appendix C.

4.3.1 Plain Tube.

The log-log plot in Figure 4.4 indicates a good correlation between the latent heat-transfer rate for the plain tube and the sensible heat transfer predicted empirically for tubes in crossflow. The best-fit line for the latent heat transfer,

$$Sh = 0.645\,Re^{0.511}\,Sc^{1/3} \tag{4.12}$$

compares favourably with the correlation of Hilpert for forced convection only (see section 2.3.2):

$$Nu = 0.683\,Re^{0.466}\,Pr^{1/3} \tag{4.13}$$

When the present experimental results for the mass transfer j-factor, j_h, are compared with the dry, sensible Colburn j-factor, j, the former is found to be approximately 11% greater than the latter across the range of velocities tested. This suggests that the wet-surface sensible heat transfer is greater than the fully-dry heat transfer, as discussed in section 4.3.

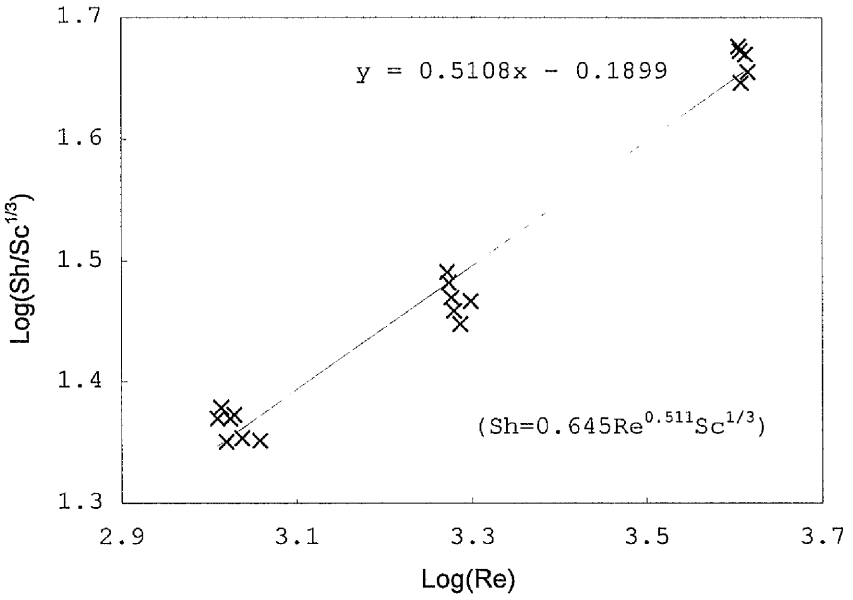

Figure 4.4 Determination of Coefficients in Colburn Analogy: Plain Tube.

When the experimentally-determined latent heat fluxes are plotted against the corresponding theoretically-calculated ones, a measure of the average performance over the range of humidity values can be calculated from the slope of the best-fit line through the data. The results calculated using this method are shown in Figures 4.9 through 4.11 for all tubes. The abscissa in these plots is a function of the product of the vapour concentration difference between the free stream and interface, and the latent heat of vaporisation. The quantity calculated above is multiplied by the condensation coefficient as calculated by the computer program in

order to normalise the units with those of the experimentally-determined latent heat flux. This allows for the direct comparison of results between tubes since it accounts for the small, but significant, variation of test conditions (most notably free-stream temperature and vapour content), during runs with the different tubes. This method of comparing results is only practical if a computer program is available to calculate the condensation coefficient from the experimental input parameters, as is the case here. It also assumes that the method used to calculate the condensation coefficient is a reasonable one. The small scatter about the linear best-fit line for the plain tube at the three different velocities suggests that this is in fact the case.

If the slopes of the graphs for only the plain tubes are examined, they yield information as to the overall degree of approximation of the computer-program results with the experimental results. In general, the computer program slightly over-predicts the amount of latent heat transfer, as compared with the present experimental results. Most of the predicted results do, however, fall within the limits of the uncertainty in the experimental results. This is discussed in greater detail in Chapter 5. It is important to note that for the purposes of comparing the performances of the roped tubes and the plain tubes, the computer-program results serve only as a common point of reference in the previous analysis.

The influence of changes in the free-stream velocity at equivalent vapour partial pressure differences can be seen in Figure 4.5. For example, the effect of changing the velocity from 1.5 to 6.4 m/s is to increase it by approximately 4.3 times. The unit experimental latent heat flux, per kPa of partial pressure difference, increases by a factor of 1.35/0.69, or roughly 2.0 times. Assuming similar fluid transport properties at equivalent vapour contents, the velocity ratio also applies to the ratio of Reynolds numbers. Using Hilpert's exponent of 0.466 (see equation (4.13)) for the ratio of Reynolds numbers, a latent heat transfer increase of 2.0 times can in fact be expected for the above change in velocity. This assumes, of course, that the Colburn analogy applies. Similar comparisons can be made between the

other velocities tested. As demonstrated in equation (2.16), the condensation rate depends on several unrelated experimental variables. With velocity held constant, the major influences on the condensation rate are terms which are in some way related to the concentration of air and, by extension, water vapour. This includes the Schmidt number, mixture density, and air mass fraction terms. If an adequate estimate of the interface temperature is made, the "available" vapour fraction can be expected to yield acceptable results. The available fraction is most conveniently expressed as the difference between the vapour partial pressure at free-stream conditions and that at the saturation temperature. The error associated with the estimation of the interface temperature is reduced as the difference between the gas free-stream temperature and tube surface temperatures increases. The temperature estimate is also made easier at lower condensation rates and therefore smaller condensate thicknesses. In these situations, the interface temperature approaches that of the tube outer wall.

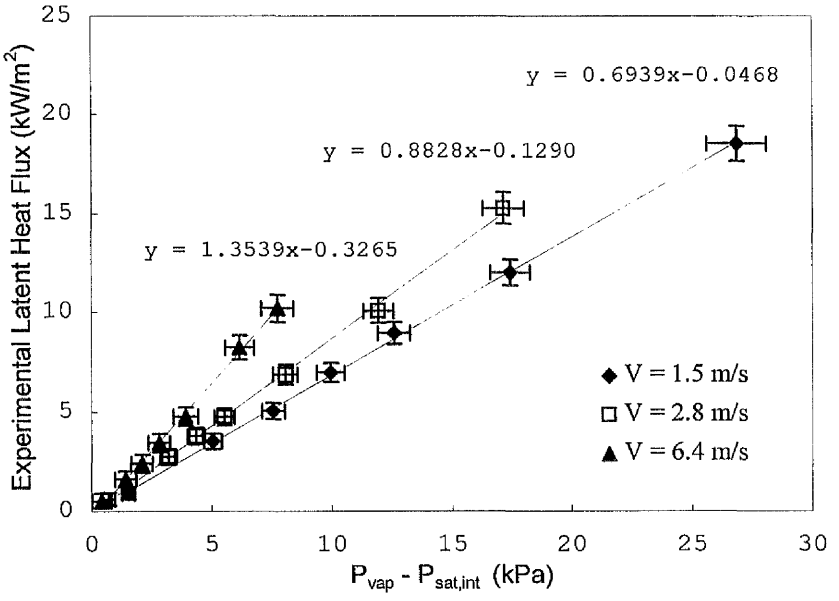

Figure 4.5 Latent Heat Transfer Performance with Velocity: Plain Tube.

The above analysis is by no means exhaustive. However, it tends to validate the potential application of the partial pressure difference as a substitute for the more complicated term involving the computer-calculated condensation coefficient

outlined in the previous paragraphs. In this way, engineering estimates of condensing performance under different vapour concentration conditions can be easily extrapolated from existing condensing results. The interface temperature in the present experimental program may be estimated with a fair degree of accuracy by approximating with the tube outer wall temperature. (See computer-program results for details).

4.3.2 Roped Tubes.

The mass transfer analysis for the three roped tubes is similar to that for the plain tube. Figures 4.6 through 4.8 were used to determine the coefficients to test in equation (4.8). Even with only three sets of velocity points plotted, it can be seen qualitatively that the data does not fit well with the form of the equation assumed in the convection-versus-mass-transfer analogy. This is particularly true of tubes **A** and **C** where the middle velocity group lies substantially off of the best-fit line. Two possible reasons for this can be put forward. First, it is conceivable that the functional analogy between convective heat transfer and condensing mass transfer is less than perfect in the case of the roped tubes. Second, (and indirectly related to the first possibility) it may be that the representation of the data over this range of Reynolds numbers and humidity content requires the use of separate correlations (or a single more sophisticated expression) for sub-intervals of the data — this in order to better represent the full range. This seems plausible, especially considering the proximity of the lowest velocity ($Re \approx 1130$) to the transition point for fully-turbulent flow. Although it is difficult to draw additional conclusions from these three plots, it is observed that the slope of the best-fit line is substantially higher for both tubes **A** and **B** than for the plain tube and tube **C**. This suggests greater condensing performance with increasing velocity for the first two tubes over the plain tube and tube **C**. Both of the latter two tubes performed similarly with respect to the coefficients determined for equation (4.12).

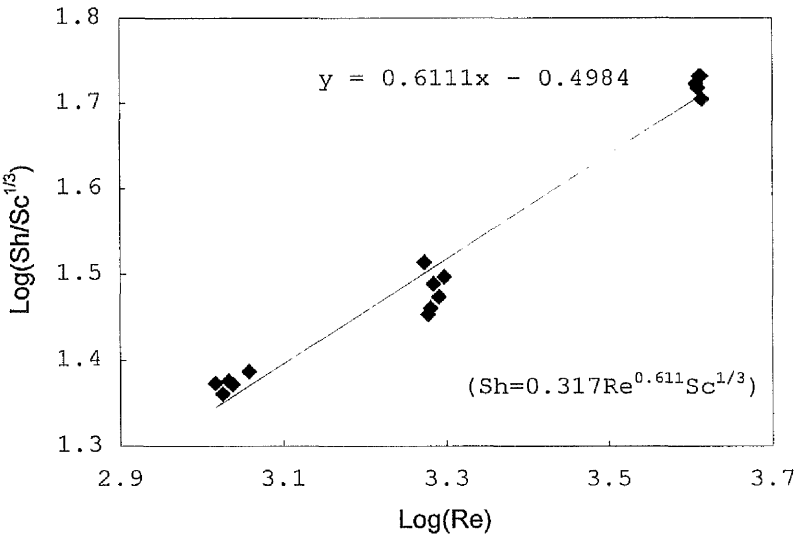

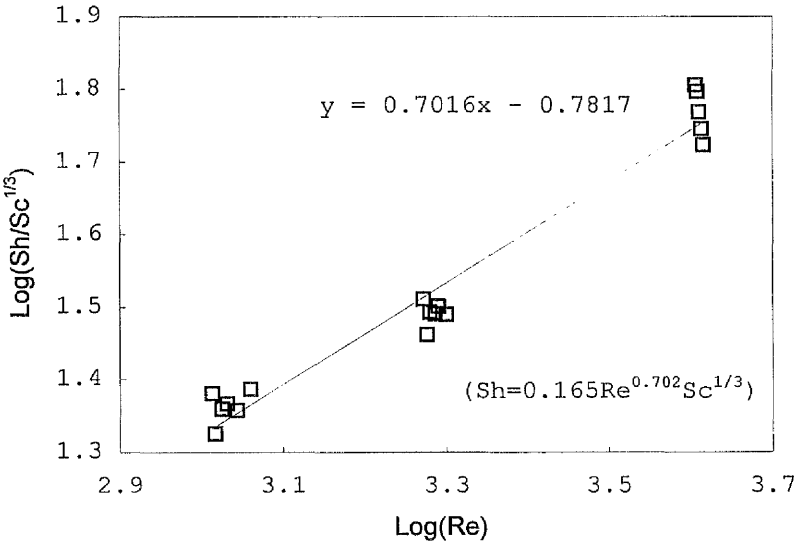

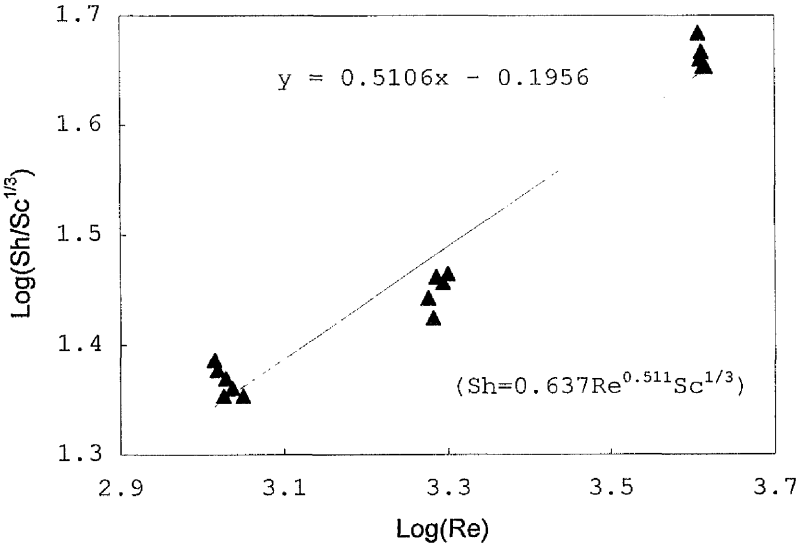

Figures 4.6 through 4.8 Determination of Coefficients in Colburn Analogy: (Top) Tube **A**. (Middle) Tube **B**. (Bottom) Tube **C**.

An effective way of comparing the condensing performance of the three roped tubes is to apply the experimental-versus-theoretical analysis used for the plain tube. By plotting all four tube results on the same graph, it is possible to perform a quantitative comparison of the average performance of all tubes against the baseline performance of the plain-tube computer model. The advantages and limitations of this method are the same as those for the plain-tube-only analysis. The plots for the experimental latent heat flux in Figures 4.9 through 4.11 appear to be good linear fits with the expected theoretical heat flux as calculated by the computer program. Further, the best-fit curves generally tend to converge towards the limiting case of no latent heat transfer at the origin of the graphs.

At the lowest velocity of approximately 1.5 m/s, limited enhancement of latent heat transfer is observed for the roped tubes. As seen in Figure 4.9, no appreciable enhancement is evident at the lower levels of air humidity — up to approximately 10 kW/m^2 of heat flux. This point corresponds to a mass-transfer rate of approximately 4 kg per second per square meter of tube surface. Even at higher water vapour concentrations (upwards of 90% relative humidity), there is only a relatively small increase in latent heat-transfer rates. The average enhancements over the full vapour concentration range, based on the slopes of the best-fit lines, are summarised in Table 4.4. Overall, tubes **A** and **B** perform almost equally, with an average enhancement of 7% over the equivalent plain-tube experimental results. Tube **B** shows a very slight advantage over **A**, most notably at the lower condensation rates. The enhancement for tube **C** is even lower, averaging 5% over the full range. It is evident from the combined plots that the performance range of the four tubes is small. Combining this with the fact that the possible error in the plotted values is not insubstantial, it was not possible to rank the roped tubes in order of increasing enhancement. The error intervals are best seen in Figure 4.5. The minimum uncertainty for the latent heat flux is approximately 5% at the highest condensation rates. The corresponding uncertainty in the theoretical values depends primarily on the water vapour concentration, with a minimum of 5% for the highest

vapour contents. However, it may be said with a moderate degree of confidence that tube **C** offers the least degree of enhancement of the three roped tubes. The fact that all four best-fit curves cross the x-axis slightly to the left of the graph origin, suggests the possibility that the sensible heat transfer quantity was marginally under-estimated in the calculations at this particular velocity. This would have no effect on the comparative aspect of the tube performance analysis because the same vertical offset would apply to all tubes equally. It should be noted that the offset in the curves falls within the limits of the experimental uncertainty and may not necessarily be related to the sensible heat calculation.

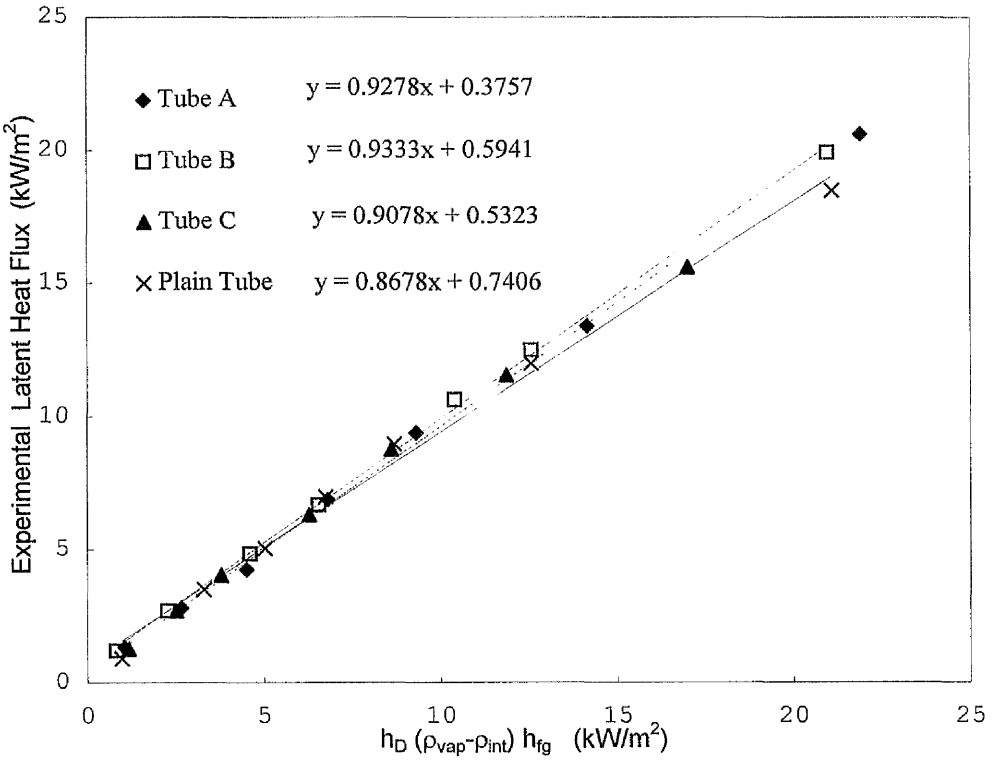

Figure 4.9 Comparison of Condensing Performance. V_{mix} = 1.5 m/s.

At the nominal air–steam mixture velocity of 2.8 m/s, Figure 4.10 indicates that the condensing heat-transfer enhancements for tubes **A** and **B** are roughly equal. An improvement of 9% in the latent heat transfer relative to the plain tube is observed in both cases. As was the case for the lowest velocity tested, the degree of enhancement is most apparent when the condensate loading is greatest. There is no

significant improvement in heat flux until the condensation rate is greater than approximately 3 kg/s·m^2. The average condensing performance of tube **C** was almost exactly the same as that of the plain tube, the enhancement for the former being less than 1%. The minimum uncertainties for both plotted quantities are approximately 5%. At the lowest water vapour content, the possible error is much larger — on the order of 40% for the theoretically-calculated latent transfer. The maximum uncertainty in the experimental latent heat flux is roughly the same at the lowest of the seven condensation rates. This is a consequence of the relatively small latent fraction of the total heat transferred, and applies generally to the results at all three velocities. The convergence of the four best-fit curves near the graph origin indicates a potentially better calculation of the sensible heat transfer contribution than at the lowest air–vapour velocity.

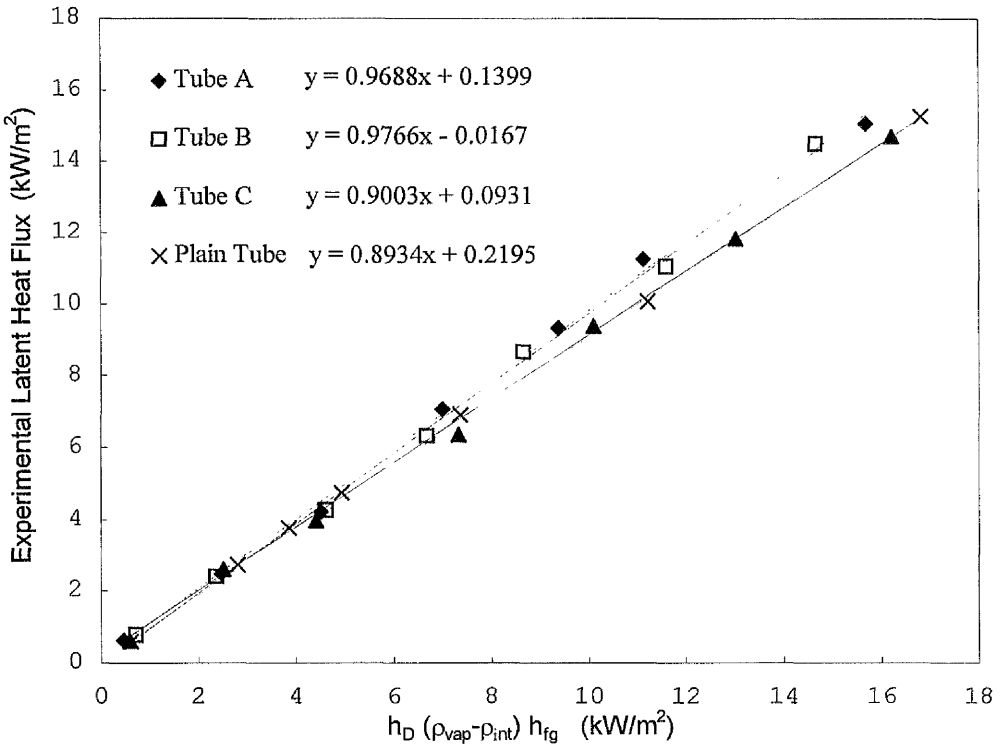

Figure 4.10 Comparison of Condensing Performance. V_{mix} = 2.8 m/s.

The enhancements calculated for tubes **A** and **B** at a nominal gas velocity of 6.4 m/s, and making use of Figure 4.11, are substantially greater than those observed at the two lowest velocities. Once again, these two particular tubes show similar

condensing performances, with an increase in latent heat-transfer rates of 15 and 14%, respectively. It is notable that the points at which the best-fit curves cross the x-axis are slightly offset from the origin for the plain tube and tubes **B** and **C**. At this particular velocity, and unlike the results for the lowest velocity, it is possible that this was the result of an over-estimation of the sensible heat-transfer flux. Tube **A** does not fit this pattern since its best-fit curve exhibits virtually no offset. Tube **C** does not demonstrate any appreciable latent heat-transfer enhancement over the plain tube, even at the greatest condensation rate tested. It should be noted that the maximum condensation rates achieved at this greatest free-stream velocity were necessarily smaller than those possible at the lower velocities. This was due to limitations in the maximum amount of steam available for injection into the much greater air flow through the test section. As a result, the highest condensation rate was roughly 4 kg/s·m^2. However, the point where tubes **A** and **B** show improvement relative to the plain tube is considerably less than at the two lowest velocities, with a condensate flux of 1.5 kg/s·m^2 corresponding to 4 kW/m^2 of heat flux.

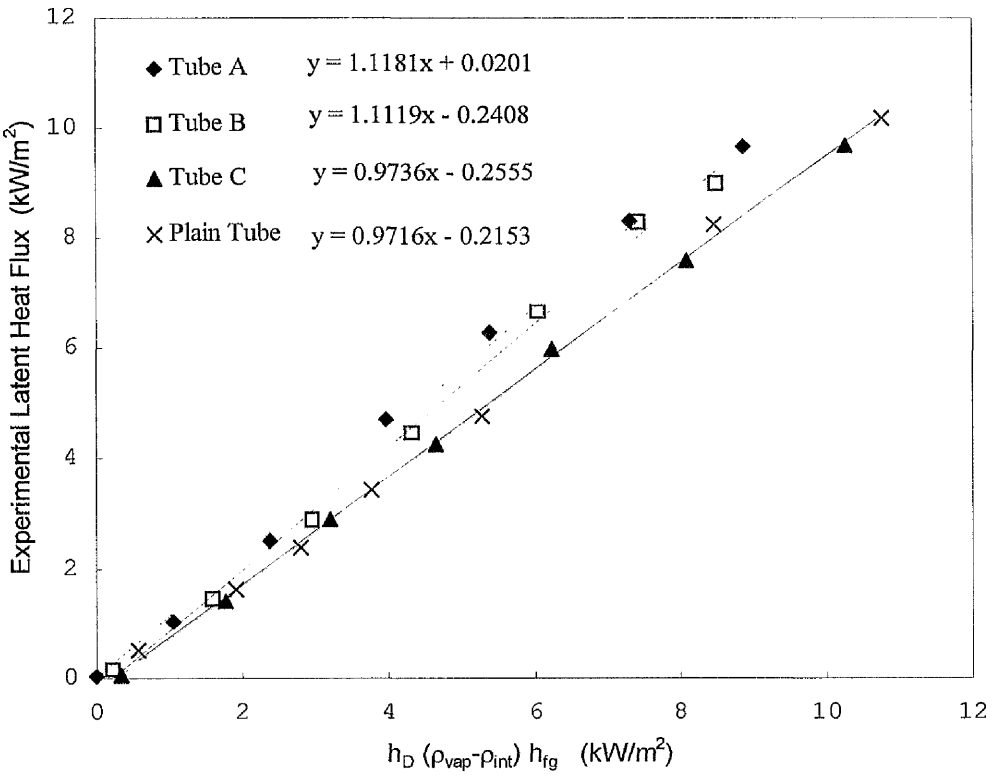

Figure 4.11 Comparison of Condensing Performance. V_{mix} = 6.4 m/s.

Table 4.4: Latent Heat Transfer Enhancement Based on $h_D \Delta P h_{fg}$

	Tube						
	Plain	**A**		**B**		**C**	
V_∞ (m/s)	% Theory	% Theory	% Diff.	% Theory	% Diff.	% Theory	% Diff.
1.5	86.8	92.8	7	93.3	7	90.8	5
2.8	89.3	96.9	9	97.7	9	90.0	1
6.4	97.2	112	15	111	14	97.4	0

As discussed previously for the plain tube, and as shown in Figure 4.5, there are definite advantages in being able to quantify the latent heat transfer performance in terms of quantities which are directly measurable experimentally. This particular method may be extended to the roped tubes also, with the condensing performance based solely on the partial pressure difference criterion. The graphs used to establish the average latent heat transfer are shown in Figures 4.12 through 4.14. The results are summarised in Table 4.5. The results calculated using the strict theoretical method described by equations (2.15) through (2.19) (see Table 4.4 above), may be compared directly with the results in Table 4.5. Upon comparison it is clear that the latter method provides a very good estimate of the latent heat transfer performance of the roped tubes. The difference between the two sets of results is, in all cases, less than or equal to 4 percentage points. The second set of results indicates average condensing heat transfer enhancements which are either equal to, or slightly less than the computer-predicted values. The good correlation between the two sets of results is admittedly partially due to the accurate choice of T_{int} as calculated by the computer program. However, at the conditions selected for this experimental program, the accuracy of the results should be relatively insensitive to errors in the choice of the interface temperature.

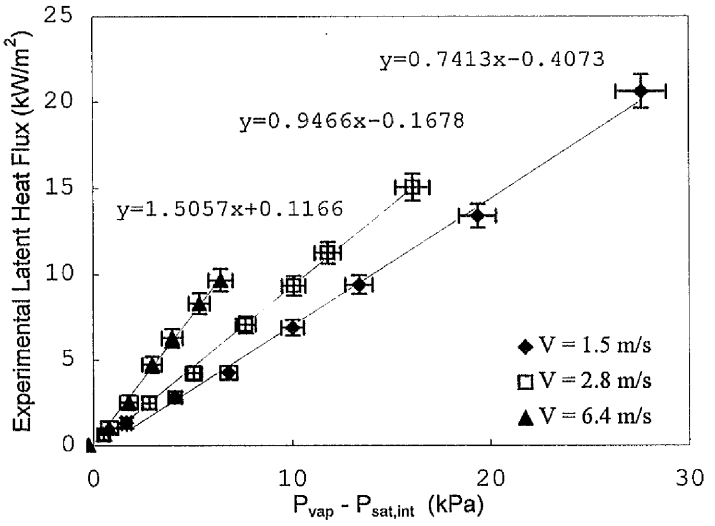

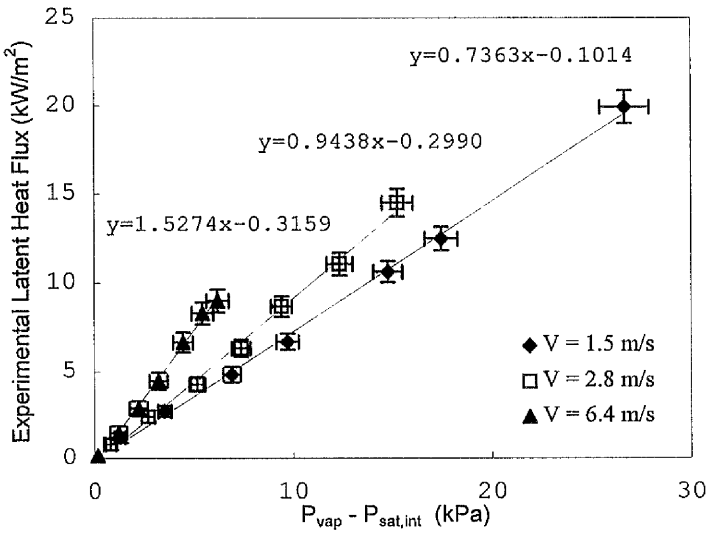

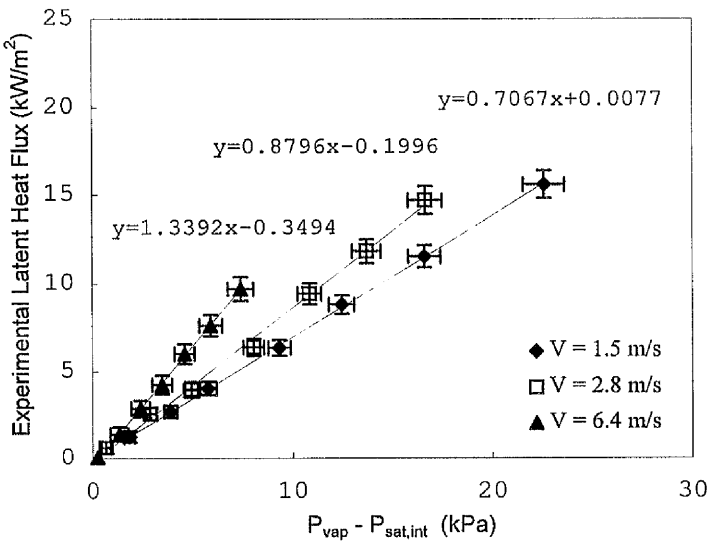

Figures 4.12 through 4.14 Latent Heat Transfer Performance with Velocity: (Top) Tube **A**. (Middle) Tube **B**. (Bottom) Tube **C**.

Table 4.5: Latent Heat Transfer Enhancement Based on $\Delta P = P_{vap} - P_{sat,int}$

	Tube						
	Plain	**A**		**B**		**C**	
V_∞ (m/s)	$Q_l/\Delta P$ ($W/m^2 \cdot Pa$)	$Q_l/\Delta P$ ($W/m^2 \cdot Pa$)	% Diff.	$Q_l/\Delta P$ ($W/m^2 \cdot Pa$)	% Diff.	$Q_l/\Delta P$ ($W/m^2 \cdot Pa$)	% Diff.
1.5	0.694	0.741	7	0.736	6	0.707	2
2.8	0.883	0.946	7	0.944	7	0.880	0
6.4	1.354	1.506	11	1.527	13	1.339	–1

The analysis of the condensing performance of the roped tubes is simplified if the many factors which influence condensation rates are combined into two general groups. Although these two groups are not necessarily completely independent of each other, for the purposes of this investigation they are considered separately.

Firstly, there are those factors which affect the localised mixing of the air–vapour stream in the vicinity of the tube surface. The most obvious of these factors is the free-stream velocity, the variation of which is easily seen in Figures 4.12 through 4.14. Much more important though, for the purposes of comparing the performance of different roped tubes, is the influence of the exterior roping on additional turbulent mixing beyond what might be expected for a plain tube of equivalent diameter. Quantifying the exact way in which each of the tube geometry characteristics affects the flow past the tube is clearly not possible using the combination of three roped tubes in the present experimental program, nor was it the intention of this investigation to do so. Nevertheless, the dry, sensible heat transfer performance may be considered as a somewhat reliable, although imperfect, indication of global surface "irregularity" effects under condensing conditions. Under this assumption, the results summarised in Table 4.3 suggest little or no significant improvement in condensation due to increased mixing at the lowest velocity of 1.5 m/s. Measurable, though modest, condensing enhancements can be postulated at the two higher velocities, the degree of enhancement increasing with

velocity. It should be pointed out once again that the error intervals for the dry-sensible results on which these assumptions were made, were significant compared to the small enhancements calculated. The fact that tube **C**, (with the least amount of grooving in terms of all roping parameters), showed both the greatest degree of dry-sensible enhancement *and* the least amount of latent enhancement, suggests at the very least, that the mechanism of additional turbulent mixing does not fully account for the observed increase in condensing performance of the roped tubes.

The second group of factors which influence the condensate rate are those related generally to the thinning of the condensate layer. As stated earlier, the present investigation deals with situations in which the condensation rates are relatively small. The small condensate loading may explain the similarity in the performance of the 2-start tube, **A**, relative to the 6-start tube, **B**. This would be true if the degree of condensate loading was insufficient to take advantage of a greater ability of one tube over the other to drain condensate. Since the condensing results for tubes **A** and **B** indicate an enhancement over that suggested purely by the dry convection results, it is assumed that the total latent heat-transfer enhancement is a result of the combination of the two major factors presented here. At much higher condensation rates, condensate thinning through enhanced drainage would be expected to account for the great majority of the overall improvement in latent heat-transfer rates. This conclusion cannot be drawn in the present experimental investigation. For the three roped tubes, the amount of enhancement *beyond* that predicted by the surface irregularity of the tubes is greatest at the lowest velocity, this also being the set of conditions under which condensation rates were highest. This is consistent with the increased relative importance of drainage effects at higher condensate loadings. As the velocity increased to 2.5 and 6.4 m/s (with an associated reduction in condensate loading), the general trend for tubes A and B was to smaller improvements potentially attributable to condensate thinning.

One way that tube **C** differed from the other roped tubes was that its groove depth was only half that of the others, 0.2 mm as compared to 0.4 mm for tubes **A**

and **B**. This detail may have accounted for the fact that little or no enhancement over the plain tube was observed under condensing conditions. It is possible (though highly speculative without additional confirmation), that the smaller roping depth resulted in a reduction in the amount of exposed groove due to wetting with condensate. This would presumably reduce any surface roughness contribution discussed earlier. This particular analysis is complicated further by the fact that tube **C** also had the least degree of roping of all the roped tubes, its groove pitch being twice that of the other 2-start tube, tube **A**. What can be said conclusively, however, is that tube **C** offers no significant enhancement over the equivalent plain tube at the condensing conditions examined in this experimental program.

The free-stream air–vapour velocity acting on the condensate layer can cause significant effects related to decreased condensate retention and waviness of the condensate film. While the oncoming air–vapour flow direction is perpendicular to the gravitational flow of the condensate, the effect is similar to that described in investigations [14,42] of vapour shear in the gravitational direction. Small droplets were observed being blown off of the lower regions of the tubes, particularly when the free-stream velocity of 6.4 m/s was tested. It was impossible to determine quantitatively which tube benefited the most from this phenomenon. It did appear, very roughly, that the effect applied equally to all tubes.

In summary, the results of the condensing tests indicated little or no gas-side condensing enhancement for the least-grooved, 2-start tube, **C**. The other 2-start tube, **A**, and the 6-start tube, **B**, displayed similar modest enhancements at all gas velocities and condensation rates tested. Their enhancement ratios ranged from approximately 1.07 at the lowest air–vapour velocity to 1.15 at the highest velocity.

Chapter 5

Computer Program Evaluation.

5.1 Introduction.

This chapter consists primarily of an evaluation of the computer program's ability to model and predict the experimental results presented in the previous chapter. Sample program output is presented first. The influence of the choice of the various input parameters on the computer-program output is also examined; the focus of that section being the correlations and number of tube elements chosen. A direct comparison of the computer results with the plain-tube experimental results follows. As previously mentioned, the computer program includes correlations to predict results for plain tubes in crossflow under conditions where water vapour condenses out of a humid airstream. A discussion of the possibility of extending the computer program to include roped tubes is also included, with the relative experimental performance of the plain and roped tubes providing the basis for this analysis.

5.1.1 Program Sample Output.

Two examples of the computer-program output are included in Appendix C. The first example, shown in Figure C1, illustrates results typical of situations where the entire length of the tube is subject to condensation. The input parameters were

chosen to reflect those used in one of the experimental tests so that the computer results in this example would be representative of the experimental results. In addition to the total heat-transfer rate given in the summary of the output, it is worth noting the percentages of the total rate attributable to each of the sensible and latent heat transfers. The relatively small difference between the tube outer wall temperature and the gas–condensate interface temperature is also noteworthy. Both of these observations relate to issues discussed in the chapter examining the experimental results.

Figure C2 demonstrates a case in which only a portion of the tube is wet, with the downstream end fully-dry. This situation was not duplicated in the experimental program, but rather serves as a demonstration of the capabilities of the computer program under different classes of input parameters. In order to simulate the partially-wet conditions, a sufficiently high water temperature rise along the tube (relative to the amount of available water vapour) was required. This allows the tube surface temperature at some particular location to exceed the saturation point of the water vapour. For this particular example, this was most easily accomplished by using a longer tube length of 5 m. The computer program identifies the 10^{th} element as being the last fully-wet one, implying that the 11^{th} element is at least only partially wet.

5.2 Influence of the Choice of Input Variables.

As outlined in Chapter 2, the choice of the gas-side convection correlation had implications for the computation of both the dry and wet-sensible heat-transfer rates. The computer-program convection predictions are shown in Figure 5.1 along with the experimental results for the fully-dry plain tube. The three correlations included in the program yielded results, for all velocities, which were within 6% of the average for all correlations. The correlation of Churchill and Bernstein was chosen as the basis for the computation of the latent heat transfer (from the difference between total and sensible heat-transfer rates) because it yielded results

that were closest to the experimental convection results. Less importantly, the correlations of Eckert–Drake and Hilpert were not ideal for a comparison with the present collection of experimental data because these sets of equations are discontinuous at Reynolds numbers of 1000 and 4000 respectively (i.e., somewhat close to the lowest and highest nominal free-stream velocities at Reynolds numbers of approximately 1100 and 4600).

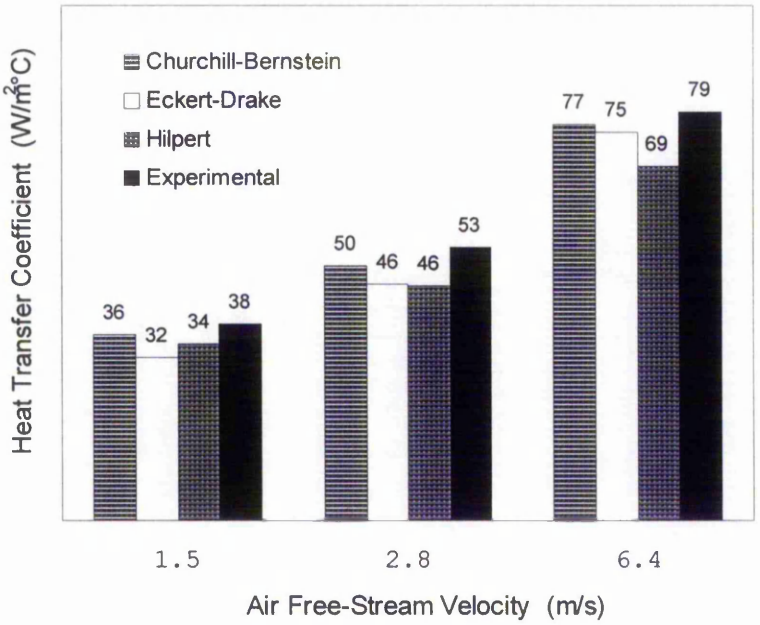

Figure 5.1 Effect of Choice of Correlation on Air-Side Convection Coefficient.

The influence of the water-side heat-transfer correlation as it applies to the computation of the latent heat-transfer quantities is shown in Table 5.1. Input parameters recorded in the plain-tube experimental program were used in the computation of the three internal convection coefficients and associated latent heat-transfer rates. Sample results are presented for the full range of latent heat-transfer rates at a nominal gas velocity of 6.4 m/s. Table 5.1 indicates that the relations of Dittus–Boelter and Seider–Tate produce very similar water-side heat-transfer coefficients, with those for the latter being approximately 3% higher than the former. In the worse-case scenario of the highest latent heat-transfer rate, favouring one of these two relations over the other results in a difference of only one-tenth of 1% in the latent heat-transfer computation. At lower latent heat-transfer rates, the

difference is even smaller because of the lesser relative importance of the water-side heat-transfer resistance. The same reasoning applies to the results at the two lower velocities with their higher associated gas-side resistances. The Nusselt correlation yields convection coefficients roughly 14% higher than those calculated using the Dittus–Boelter relation. Nusselt's correlation was not used in the examination of the present experimental data since its intended use is for very short tubes and for the entrance region of longer tubes. However, had it been used, the computed latent heat-transfer rates would have been less than one-half of 1% smaller than those actually computed using the Dittus–Boelter correlation.

Table 5.1: Effect of Water-Side Correlation on Latent Heat-Transfer Calculation

	Correlation					
	Dittus–Boelter		Seider–Tate		Nusselt	
q_{tot} (W)	h_i (W/m^2°C)	q_l (W)	h_i (W/m^2°C)	q_l (W)	h_i (W/m^2°C)	q_l (W)
60	2319	5.93	2387	5.93	2653	5.91
74	2277	19.42	2342	19.40	2604	19.32
82	2324	28.60	2393	28.57	2661	28.46
94	2323	40.97	2393	40.92	2660	40.77
111	2268	56.93	2331	56.87	2592	56.63
152	2275	98.46	2345	98.33	2607	97.93
175	2279	121.86	2350	121.71	2612	121.21

Theoretically, increasing the number of tube elements used in the pointwise heat exchanger model should increase the accuracy of the computer prediction. This was observed in practice, with each ten-fold increase in the number of tube elements resulting in roughly a two-decimal-place increase in the convergence of the value of the OHTC. Using the input variables of Figure C2 as an example and with a single tube element chosen, the result was an OHTC calculation of 37.2666 W/m^2°C. With 10 tube elements, the computed value of the OHTC was

marginally higher at 37.4266 W/m^2°C. The OHTC always follows this pattern of slight increase with number of elements considered, converging to a value of 37.4289 W/m^2°C at 100 elements. With small changes in the fluid properties along the tube length, the increased accuracy due to a greater number of elements can quickly be overshadowed by the uncertainty in the input parameters. In these instances, the greatest benefit of using additional elements is the program's ability to identify more precisely the location on the tube at which condensation is no longer possible. Quite obviously, the degree of precision of this result varies directly with the number of tube elements chosen.

5.3 Condensing Results.

The overall effectiveness of the computer program can be judged by comparing the latent heat-transfer predictions with the plain-tube experimental results. Since the gas velocity and humidity ratio are the two major variables affecting the condensation process, the computer results should be reasonably accurate over both ranges in order to provide an acceptable simulation. Both conditions are most-easily tested by examining the three graphs in Figures 5.2 through 5.4, data for which is included in Appendix C, Table C5. These graphs plot the computer-predicted latent heat fluxes based on input parameters identical to those found in the experimental tests. Points plotted above the dashed, diagonal line indicate an over-prediction by the computer program — points below this line indicate the opposite. Taken as a whole, the three plots demonstrate qualitatively that the general methodology of the computer program is sound. This is suggested by the generally linear distribution of the computer-predicted fluxes as well as their overall degree of approximation of the experimental results. There are individual intervals of the data which are less well-predicted than others, however, and this deviation is discussed in the paragraphs which follow.

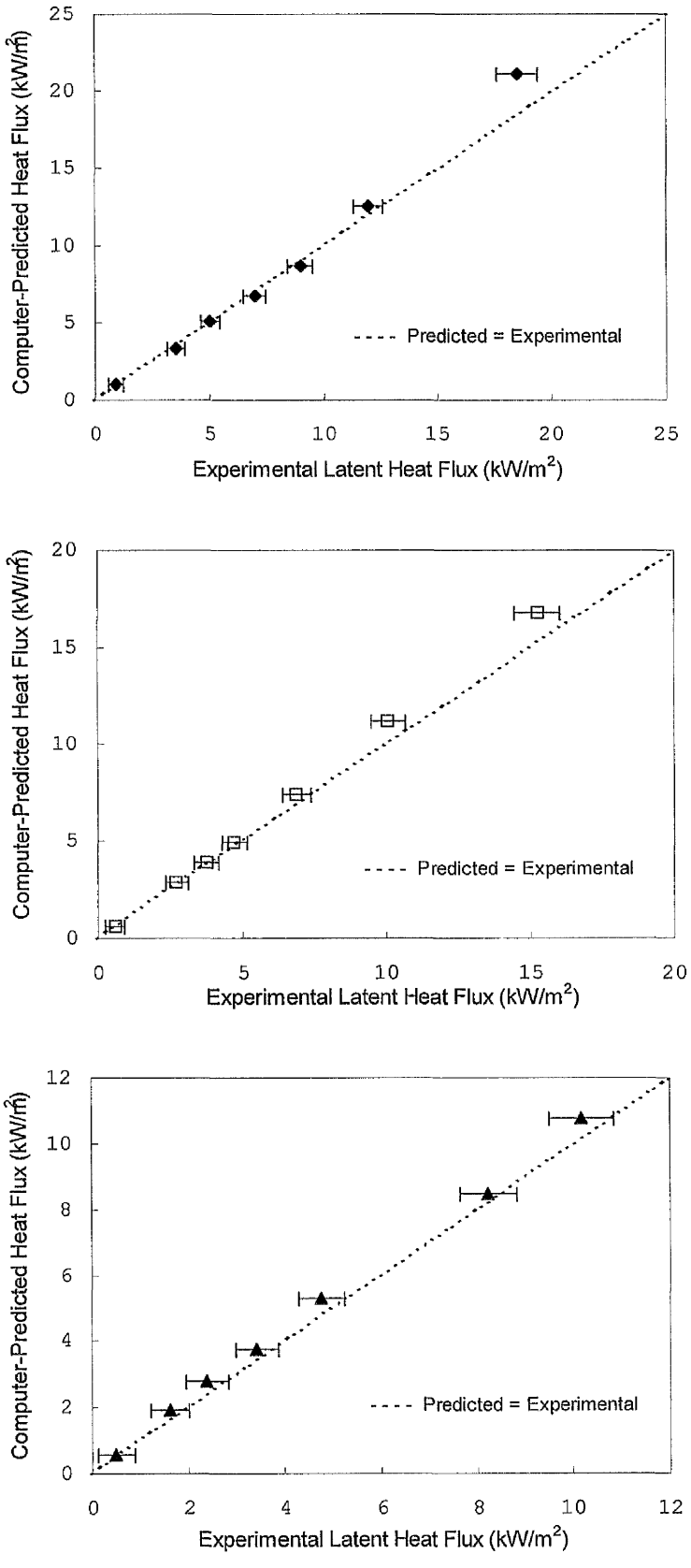

Figures 5.2 through 5.4 Comparison of Computer Prediction and Experimental Results: (Top) V_{mix} = 1.5 m/s. (Middle) V_{mix} = 2.8 m/s. (Bottom) V_{mix} = 6.4 m/s.

Figure 5.2 indicates that the computer program predicts the experimental results, within the limits of the experimental uncertainty, for most of the vapour-content range. At the lowest nominal gas velocity, the predictions at the six lowest water-vapour concentrations deviate from the experimental results by an average of 4%. Three of these computed values are marginally lower than the experimental results, two are higher, and one is equal. The only data point which is significantly different from the experimental result is the one associated with the highest condensation rate at 92% relative humidity. In this case, the latent heat flux is over-predicted by 14%.

At the intermediate gas-mixture velocity, Figure 5.3 reveals a situation similar to that at the lowest gas-mixture velocity, with the difference being that all of the computed values are slightly higher than their corresponding experimental values. Results associated with the five lowest vapour concentrations are an average of 4% higher than their experimental equivalents and within the limits of the experimental uncertainty. The tests at the two highest humidity levels do not fall within these limits, however, with both computations over-predicting the experimental results by approximately 11%.

Figure 5.4 demonstrates that the computer program also over-predicts all latent heat fluxes at the highest nominal gas velocity. The overall pattern at this velocity is for decreasing predicted/experimental ratios with increasing vapour content. This ratio averages 1.14 for the five lowest vapour concentrations, and 1.04 for the two highest concentrations. However, in absolute terms, the differences between the computed and experimental values are small. If all of the computer-predicted values were lowered by a constant 0.4 kW/m^2, the resulting ratios of predicted/experimental results would vary from 0.98 to 1.02 for the five largest heat fluxes.

The over-prediction associated with the offset seen at the highest nominal velocity can be explained by a possible overestimation of the experimental convection coefficient. If the estimate for h_o was lower by roughly 9%, this would

have accounted for the difference of 400 W/m^2 between the experimental and computer-predicted latent heat fluxes mentioned above. This example illustrates a potential shortcoming of the analysis of the computer-program results since they are based on a necessarily limited group of experimental measurements. For single predictions, it is difficult to determine conclusively that differences in the results are due to the computer program and not to uncertainties in the experimental data. Taken together, the data for all velocities and condensation rates suggests that it is the computer simulation that generally over-predicts the actual results. Figure 5.5 summarises the ratios of predicted to experimental latent heat transfer for all tests. The average ratio for the full set of data is 1.06, with a standard deviation of 0.07. The somewhat random distribution of the plotted points with vapour content suggests that the uncertainty in the experimental results has at least some small effect on the computer predictions. In general, the computer results are very satisfactory and verify the application of the equations suggested by Rose [22] over the range of input parameters tested.

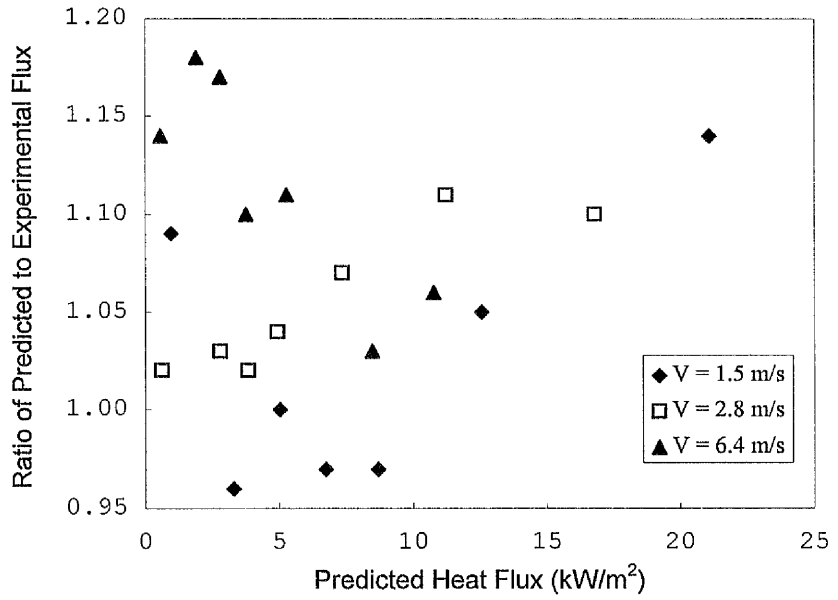

Figure 5.5 Predicted vs. Experimental Latent Heat Fluxes for All Velocities.

5.3.1 Extension of the Program to Roped Tubes.

With the applicability of the computer solution verified for the plain tubes, the next logical step is to consider the extension of the simulation to the roped tubes. The number of data sets considered in the experimental program were sufficient to draw conclusions as to the relative condensing efficiency of the three roped tubes. However, as discussed in Chapter 4, the large number of tube geometry variables, combined with the combination of only three roped tubes tested, makes generalisations based on groove geometry difficult. For this reason, enhancement correlations as functions of tube geometry would strictly require additional experimental data for humid air mixtures. Alternatively, more widely available shell-side enhancement equations for the condensation of pure steam on roped tubes might be tested to see if they may be adapted to the conditions considered in the present program. Whatever method is chosen for the gas side, the computer program would benefit, to some degree, from the application of a correlation which takes into account the influence of roping on the water-side heat-transfer coefficient.

With a slightly more restricted application of the computer program, it is possible to easily modify the code to yield satisfactory predictions for the three specific roped tubes tested. Used over the same range of input variables, the program would benefit from the addition of a multiplier of 0.94 to account for the average degree of over-prediction discussed previously. The roped-tube results would be further improved by introducing enhancement factors based on the experimental results presented in Table 4.4. If the following single line of code from the *Getdql* routine (See Appendix D for the program listing):

```
Qlat = m * hfg(Tint);                    (5.1)
```

is changed to

```
Qlat = m * hfg(Tint) * 0.94 * E[i];      (5.2)
```

(where `E[i]` is the experimentally-observed enhancement-ratio matrix for the three different nominal velocities), then the overall agreement between the predicted and

experimental results is very satisfactory for each of the roped tubes tested. A sample group of modified computer-program results for tube **A** are included in Appendix C, Table C6. This example indicates that the above simple modification to the plain-tube computer program results in predictions which are within 10% of the experimentally-determined values for all velocities. (Excluding the very lowest vapour concentrations with the highest associated experimental uncertainties). Of course, the success of this modification to the plain-tube code hinges on the fact that the `E[i]` coefficients were previously determined experimentally. However, in the more usual case where no experimental results are available, the above example illustrates the effectiveness of creating a subroutine whose output parameters function identically to `E[i]`. The same simple modification to the main program code described by equations (5.1) and (5.2) can then be made, with a single call to the new routine substituted for `E[i]`.

Chapter 6

Conclusions.

6.1 Summary.

In situations where a lean mixture of water vapour condenses out of a hot airstream, the experimental results indicate that some types of roped tubes can benefit from a modest condensation enhancement over the equivalent plain tube. In keeping with the much lower condensation rates encountered in the present study, the degree of enhancement was found to be less than that reported in most studies of pure steam condensation on roped tubes. The maximum enhancement observed in the present investigation was 15%.

Two of the three tubes showed noticeable enhancement at all velocities. With the condensing performance roughly equal for the two, it was not possible to establish a general rule for the influence of the number of starts and helix angle on condensing performance under these conditions. It was postulated, but not confirmed, that performance differences due to tube geometry become more apparent at higher condensation rates. The third, least-grooved tube in terms of the total amount of roping per unit length and groove depth, showed little or no significant condensing enhancement.

The degree of condensation enhancement was shown to increase with increasing free-stream air–vapour velocity. The effect was seen throughout the range of vapour concentrations. Reasons to explain this were examined, focusing on the two mechanisms of improved condensate drainage and increased boundary-layer mixing. The results tend to suggest that the latter effect dominates at the condensation rates tested here.

As a more minor point, it was shown that the latent heat-transfer rates could be adequately represented as a linear function of the vapour content expressed in terms of partial-pressure differences. This results in a simplified method of predicting condensing performance which doesn't rely on the calculation of a condensation coefficient. Condensing performance projected using this method tended to be slightly conservative.

Regarding the computer-program predictions for the plain tube performance, the results were found to be in good agreement with the experimental results. The influence of the choice of the water-side convection correlation was examined and found to be very small — this being the result of the high ratio of external to internal heat-transfer resistances. A similar analysis of the three gas-side correlations that were considered revealed a slightly greater, yet still very limited variation in the computed heat transfers. Overall, the computer model over-predicted the experimental condensation rates by an average of 6% and in all cases by no more than 18%.

The extension of the plain-tube computer code to include roped tubes was also discussed. A suggested method of accomplishing this goal was successfully demonstrated for the specific case of one of the roped tubes examined in this study.

6.2 Recommendations for Further Work.

With the experimental results showing relatively small enhancements at low free-stream velocities, it is felt that additional study should primarily focus on situations where the air–vapour mixture velocity is maximised. A practical example which

meets this criterion is the examination of the condensing performance in roped tube bundles, where localised inter-tube velocities can be significantly greater than the free-stream velocity. Of additional interest would be a comparison of the scaleability of the humid-air performance, from single tube to tube bundle, with the same scaling for condensation of pure steam. In this way, the more extensive collection of roped-tube data for steam might possibly be used in the prediction of humid-air condensation on roped tube bundles.

While the overall degree of condensation enhancement has been described in the present study, the relative size of the contributions due to individual enhancement mechanisms has not been definitively analysed. A useful starting point in this direction would be a breakdown of the whole into the two effects broadly categorised as improved condensate drainage and increased boundary-layer mixing. Conducting tests for humid air with no appreciable velocity would help minimise the latter effect and thus facilitate isolation of the former.

With regard to possible improvements to the existing experimental rig, efforts should centre on the addition of a facility to measure energy and/or mass balances on the air–vapour stream. With a large number of tubes installed, it may be possible to accurately measure bulk changes in humidity content and temperature upstream and downstream of the tube bundle. Alternatively, the addition of a device similar to that used by Taniguchi *et al.* (described in Chapter 4), would allow for a direct measurement of the condensation rate.

The core of the computer program can be extended to roped tubes as discussed previously, with the starting point being the addition of correlations for the water-side convection coefficient. It should also prove useful as the basis for computing condensation rates from humid air for other types of heat exchanger tubes such as finned tubes.

In summary, the author considers the present study as an overview of what can be expected from roped tubes undergoing condensation from humid air, and this over a relatively large range of velocities and condensation rates. It is hoped that

this investigation can provide at least some of the framework for the analysis of the substantial gaps in knowledge which invariably remain to be filled in.

References

[1] A. E. Bergles, "Survey of augmentation of two phase heat transfer." Paper presented at semi-annual meeting of ASHRAE, Dallas, Texas, February 1976.

[2] I. H. Newson, "Enhanced heat transfer condenser tubing for advanced multistage flash distillation plants." *Proc. 5th Int. Symposium on Fresh Water from the Sea*. vol. 2, pp. 107-115, 1974.

[3] R. Gregorig, "Zeitschrift fur angewandte." *Mathmatikund Physik*, vol. 5, pp. 36-49, 1954.

[4] W. Nusselt, "Die oberflachenkondensation des wasserdampfes." *Zeitschrift Ver. Dt. Ing.*, vol. 60, pp. 541-546, 1916.

[5] W. M. Rohsenow, "Heat transfer and temperature distribution in laminar film condensation." *Trans. ASME*, vol. 78, pp. 1645-1648, 1956.

[6] W. H. Adams, *Heat Transmission*. McGraw-Hill, 1954.

[7] M. Baghernejad, *Condensate Inundation in Horizontal Roped Tube Bundles*. Ph.D. Dissertation, Univ. of Glasgow, 1987.

[8] M. Ben-Boudinar, *Effect of Condensate Inundation on Roped Tubes*. M.Sc. Dissertation, Univ. of Glasgow, 1988.

[9] T. J. Rabas, "Data and correlation review of the enhancement for steam condensation on spirally indented tubes." *Boiling and Condensing Heat Transfer*, HTD of ASME, vol. 85, pp. 99-106, 1987.

[10] J. G. Withers and E. H. Young, "Steam condensing on vertical rows of horizontal corrugated and plain tubes." *Ind. and Eng. Chem. Process Design and Dev.*, vol. 10, pp. 19-30, 1971.

[11] J. P. Catchpole and B. C. H. Drew, "Evaluations of some shaped tubes for steam condensation." Steam Turbine Condensers, NEL Glasgow Report No. 619, pp. 66-82, 1976.

[12] J. Cunningham and H. K. Milne, "The effect of helix angle on the performance of roped tubes." *Proc. 6th International H. T. Conference*, vol. 2, Toronto, pp. 601-605, 1978.

[13] J. Cunningham and M. Baghernejad, "The effect of vapour shear and condensate drainage in condensers using roped tubes." *Desalination*, vol. 45, pp. 135-142, 1983.

[14] W. J. Fidler, *The Effects Of Vapour Shear and Inundation on Roped Tubes.* M.Sc. Dissertation, Univ. of Glasgow, 1991.

[15] J. Cunningham and A. Holmes, "The effect of air on condensation on a roped tube." *Desalination*, vol. 38, pp. 65-74, 1981.

[16] M. H. Mehta and M. R. Rao, "Heat transfer and frictional characteristics of spirally enhanced tubes for horizontal condensers." Advances in Enhanced Heat Transfer, ASME, pp. 11-22, 1979.

[17] P. J. Marto, D. J. Reilly and J. H. Fenner, "An experimental comparison of enhanced heat transfer condensing tubing." Advances in Enhanced Heat Transfer, ASME, pp. 1-10, 1979.

[18] D. M. Eissenberg and D. Bogue, "Tests of an enhanced horizontal tube condenser under conditions of horizontal steam cross flow." *Proc. 4th Int. H. T. Conference*, Paris, vol. 1, paper HE 2.1, 1970.

[19] S. Kawai and T. Machiyama, "Some notes on the experimental evaluations of condensing heat transfer characteristics on titanium corrugated tubes." Waseda University Science and Engineering Research Laboratory Report, pp. 40-43, 1972.

[20] W. C. Lee and J. W. Rose, "Forced convection film condensation on a horizontal tube with and without non-condensing gases." *Int. J. Heat Mass Transfer*, vol. 27, pp. 519-528, 1984.

[21] L. D. Berman, "Determining the mass transfer coefficient in calculations on condensation of steam containing air." *Thermal Engineering*, vol. 16, pp. 85-99, 1969.

[22] J. W. Rose, "Approximate equations for forced-convection condensation in the presence of a non-condensing gas on a flat plate and horizontal tube." *Int. J. Heat Mass Transfer*, vol. 23, pp. 539-546, 1980.

[23] A. F. Mills, C. Tan and D. K. Chung, "Experimental study of condensation from steam–air mixtures flowing over a horizontal tube: overall condensation rates." *Proc. 5th Int. H. T. Conference.*, Tokyo, vol. 5, Paper CT 1.5, pp. 20-23, 1974.

[24] H. Taniguchi, K. Kudo, Q. Hwang and A. Fujii, "Heat and mass transfer from air with high water vapour content." *Japanese Soc. of Mech. Eng. Int. J.*, series 2, vol. 31, pp. 299-305, 1988.

[25] T. H. Chilton and A. P. Colburn, "Mass transfer (absorption) coefficients." *Industrial Engineering Chemistry*, vol. 26, pp. 1183-1187, 1934.

[26] T. Fujii, H. Uehara and C. Kurato, "Laminar filmwise condensation of a flowing vapour on a horizontal cylinder." *Int. J. Heat Mass Transfer*, vol. 15, pp. 235-246, 1972.

[27] J. P. Holman, *Heat Transfer*. McGraw-Hill, 1986.

[28] F. W. Dittus and L. M. K. Boelter, *Univ. Calif. (Berkeley) Pub. Eng.*, vol. 2, p. 443, 1930.

[29] E. N. Sieder and C. E. Tate, "Heat transfer and pressure drop of liquids in tubes." *Ind. Eng. Chem.*, vol. 28, p. 1429, 1936.

[30] W. Nusselt, "Der wärmeaustausch zwischen wand und wasser im rohr." *Forsch. Geb. Ingenieurwes.*, vol. 2, p. 309, 1931.

[31] R. Hilpert, "Wärmeabgabe von geheizen drahten und rohren." *Forsch. Geb. Ingenieurwes.*, vol. 4, p.220, 1933.

[32] E. R. G. Eckert and R. M. Drake, *Analysis of Heat and Mass Transfer,* McGraw-Hill, 1972.

[33] S. W. Churchill and M. Bernstein, "A correlating equation for forced convection from gases and liquids to a circular cylinder in crossflow." *J. Heat Transfer*, vol. 99, pp. 300-306, 1977.

[34] G. W. C. Kaye and T. H. Laby, *Tables of Physical and Chemical Constants.* Longman, 1986.

[35] UK Committee on the Properties of Steam, *UK Steam Tables in SI Units 1970.* Edward Arnold, 1970.

[36] A. J. Chapman, *Fundamentals of Heat Transfer*. MacMillan, 1987.

[37] E. A. Schmidt, *Properties of Water and Steam in SI Units*. Springer, 1969.

[38] R. C. Reid and T. K. Sherwood, *The Properties of Gases and Liquids, Their Estimation and Correlation.* McGraw-Hill, 1966.

[39] T. Fujii, Y. Kato and K. Mihara, "Expressions of transport and thermodynamic properties of air, steam and water." Univ. Kyushu Research Institute of Industrial Science Report. No. 66, pp. 81-95, 1977.

[40] A. Zukauskas, "Heat transfer from tubes in crossflow." *Advances in Heat Transfer*, vol. 8, pp. 93-160, 1972.

[41] S. A. Idem, A. M. Jacobi and V. W. Goldschmidt, "Heat transfer characterization of a finned-tube heat exchanger (with and without condensation)." *J. Heat Transfer*, vol. 112, pp. 64-70, 1990.

[42] L. D. Berman, "Influence of vapour velocity on heat transfer with filmwise condensation on a horizontal tube." *Teploenergetika*, vol. 26, pp. 16-20, 1979.

[43] S. J. Kline and F. A. McClintock, "Describing uncertainties in single-sample experiments." *Mechanical Engineering*, vol. 75, pp. 3-8, 1953.

Appendix A

Uncertainty Analysis.

The uncertainty in the results is calculated using the second-power equation of Kline and McClintock [43] given below. This method describes the error interval for a function, R, of n independent variables, v_1, v_2, ..., v_n. δR is the resultant uncertainty of the combination of each of the constituent uncertainties, δv_1, δv_2, ..., δv_n.

$$\delta R = \left[\left(\frac{\partial R}{\partial v_1}\delta v_1\right) + \left(\frac{\partial R}{\partial v_2}\delta v_2\right) + \ldots + \left(\frac{\partial R}{\partial v_n}\delta v_n\right)\right]^{1/2} \tag{A.1}$$

Non-Condensing Results

The uncertainty in the non-condensing, gas-side heat-transfer coefficient, h_o, is calculated beginning from the sum of the individual heat-transfer resistances:

$$R_o = R_{overall} - R_t - R_i \tag{A.2}$$

$$\frac{1}{h_o A_o} = \frac{1}{U_{overall} A_o} - \frac{\ln(d_o/d_i)}{2\pi k_t L} - \frac{1}{h_i A_i} \tag{A.3}$$

The expression for h_o is simplified by the substitution of a, b and c for the terms in the denominator,

$$h_o = \frac{1}{\left(\frac{1}{U_{overall}}\right) - \left(\frac{\ln\left(d_o/d_i\right)d_o}{2\,k_t}\right) - \left(\frac{\left(d_o/d_i\right)}{h_i}\right)} = \frac{1}{Z} = \frac{1}{a-b-c} \qquad \text{(A.4)}$$

so that the dimensionless uncertainty in the heat-transfer coefficient becomes:

$$\frac{\delta h_o}{h_o} = \frac{\delta Z}{Z} = \frac{1}{Z}\left[\delta a^2 + \delta b^2 + \delta c^2\right]^{1/2} \qquad \text{(A.5)}$$

with:

$$\delta a^2 = \left(\frac{\delta U_{overall}}{U^2_{overall}}\right)^2$$

$$\delta b^2 = b^2\left\{\left[\left(\frac{\delta d_o}{d_o}\right) - \left(\frac{\delta d_i}{d_i}\right)\right]^2\left(\frac{1}{\ln\left(d_o/d_i\right)}\right)^2 + \left(\frac{\delta d_o}{d_o}\right)^2 + \left(\frac{\delta k_t}{k_t}\right)^2\right\}$$

$$\delta c^2 = \left(\frac{\delta d_o}{d_i h_i}\right)^2 + \left(\frac{d_o \delta d_i}{d_i^2 h_i}\right)^2 + \left(\frac{d_o \delta h_i}{d_i h_i^2}\right)^2$$

The uncertainty in the overall heat-transfer coefficient is calculated from:

$$U_{overall} = \frac{Q_{tot}}{A_o \Delta T_{LM}} = \frac{\dot{m}_w C_p\left(T_{w,2} - T_{w,1}\right)}{A_o\,\Delta T_{LM}} = \frac{m_w C_p \Delta T_w}{t\,\pi d_o L\,\Delta T_{LM}} \qquad \text{(A.6)}$$

so that:

$$\frac{\delta U_{overall}}{U_{overall}} = \left[\left(\frac{\delta m}{m}\right)^2 + \left(\frac{\delta C_p}{C_p}\right)^2 + \left(\frac{\delta \Delta T_w}{\Delta T_w}\right)^2 + \left(\frac{\delta t}{t}\right)^2 + \left(\frac{\delta d_o}{d_o}\right)^2 + \left(\frac{\delta L}{L}\right)^2 + \left(\frac{\delta \Delta T_{LM}}{\Delta T_{LM}}\right)^2\right]^{1/2} \qquad \text{(A.7)}$$

where:

$$\left(\frac{\delta \Delta T_w}{\Delta T_w}\right)^2 = \frac{\delta T^2_{w,2} + \delta T^2_{w,1}}{\left(T_{w,2} - T_{w,1}\right)^2}$$

and

$$\left(\frac{\delta\Delta T_{LM}}{\Delta T_{LM}}\right)^2 = \left(\frac{\delta T_{w,2} - \delta T_{w,1}}{T_{w,2} - T_{w,1}}\right)^2 + \left[\frac{1}{\ln\left(\left(T_\infty - T_{w,1}\right)/\left(T_\infty - T_{w,2}\right)\right)}\right]^2 \left[\left(\frac{\delta T_\infty - \delta T_{w,2}}{T_\infty - T_{w,2}}\right) - \left(\frac{\delta T_\infty - \delta T_{w,1}}{T_\infty - T_{w,1}}\right)\right]^2$$

The uncertainty in the water-side heat-transfer coefficient is calculated by applying equation (A.1) to the Dittus–Boelter correlation, equation (2.23), so that:

$$\frac{\delta h_i}{h_i} = \left[\left(\frac{\delta k_w}{k_w}\right)^2 + \left(\frac{\delta d_i}{d_i}\right)^2 + \left(\frac{0.8\,\delta \mathrm{Re}}{\mathrm{Re}}\right)^2 + \left(\frac{0.4\,\delta \mathrm{Pr}}{\mathrm{Pr}}\right)^2\right]^{1/2} \tag{A.8}$$

where the potential errors in the Reynolds and Prandtl numbers on the water side are given by:

$$\frac{\delta \mathrm{Re}}{\mathrm{Re}} = \left[\left(\frac{\delta m}{m}\right)^2 + \left(\frac{\delta t}{t}\right)^2 + \left(\frac{\delta \mu_w}{\mu_w}\right)^2 + \left(\frac{\delta d_i}{d_i}\right)^2\right]^{1/2}$$

$$\frac{\delta \mathrm{Pr}}{\mathrm{Pr}} = \left[\left(\frac{\delta C_p}{C_p}\right)^2 + \left(\frac{\delta \mu_w}{\mu_w}\right)^2 + \left(\frac{\delta k_w}{k_w}\right)^2\right]^{1/2}$$

The uncertainty in the velocity of the airstream is derived from:

$$\tfrac{1}{2}\rho_a V^2 = \Delta P = \rho_w H_w g \tag{A.9}$$

so that

$$V = \sqrt{\frac{2\rho_w g H_w R T_\infty}{P_a}} \tag{A.10}$$

and

$$\frac{\delta V}{V} = \frac{1}{2}\left[\left(\frac{\delta \rho_w}{\rho_w}\right)^2 + \left(\frac{\delta H_w}{H_w}\right)^2 + \left(\frac{\delta T_\infty}{T_\infty}\right)^2 + \left(\frac{\delta P_a}{P_a}\right)^2\right]^{1/2} \tag{A.11}$$

Condensing Results

The uncertainty in the sensible contribution to the heat-transfer flux is:

$$\frac{\delta Q_s}{Q_s} = \left[\left(\frac{\delta T_\infty^2 + \delta T_{\text{int}}^2}{\left(T_\infty - T_{\text{int}}\right)^2} \right) + \left(\frac{\delta h_o}{h_o} \right)^2 \right]^{1/2} \tag{A.12}$$

T_{int} is calculated by iteration from equations (2.15) through (2.19) and as such the estimation of the uncertainty depends upon the choice of a convergence interval, ε. Irrespective of the choice of ε, it is recognised that T_{int} is a maximum of approximately one half of one degree Celsius higher than the outside wall temperature. Taking 100% of this temperature difference results in a very conservative estimate of 0.5°C for the error in the interface temperature. The uncertainty in the convection coefficient is as in the non-condensing case.

The uncertainty in the latent heat transfer per unit area of tube, Q_l, is calculated by subtracting the sensible heat flux from the total heat flux so that:

$$\frac{\delta Q_l}{Q_l} = \left[\frac{\delta Q_{tot}^2 + \delta Q_s^2}{\left(Q_{tot} - Q_s\right)^2} \right]^{1/2} \tag{A.13}$$

where the uncertainty in the total experimental heat-transfer flux, Q_{tot}, follows from equation (A.6):

$$\frac{\delta Q_{tot}}{Q_{tot}} = \left[\left(\frac{\delta m_w}{m_w} \right)^2 + \left(\frac{\delta C_p}{C_p} \right)^2 + \left(\frac{\delta t}{t} \right)^2 + \left(\frac{\delta d_o}{d_o} \right)^2 + \left(\frac{\delta L}{L} \right)^2 + \left(\frac{\delta \Delta T_w}{\Delta T_w} \right)^2 \right]^{1/2} \tag{A.14}$$

The uncertainty in the calculation of the vapour pressure , P_{vap}, is:

$$\frac{\delta P_{vap}}{P_{vap}} = \left[\left(\frac{\delta \phi}{\phi} \right)^2 + \left(\frac{\delta P_{sat,T_\infty}}{P_{sat,T_\infty}} \right)^2 \right]^{1/2} \tag{A.15}$$

with the error in the saturation pressure of the vapour calculated at the free-stream temperature. The error in the saturation pressure at the interface is taken at the interface temperature.

Uncertainties in Experimental Measurements

Tube Wall Properties

$\delta L = 0.002$ m

$\delta d_i = \delta d_o = 0.0005$ m

$\delta k_t = 1$ W/m°C

Water Flow Rate

$\delta t = 1$ s

$\delta m_w = 0.1$ kg

Temperatures

$\delta T_\infty = 1$°C

$\delta T_{w,1} = \delta T_{w,2} = 0.01$°C

Relative Humidity

$\delta \phi = 1\%$

Velocity Calculation

$\delta H_w = 0.01$ mmH_2O

$\delta P_a = 1$ kPa

Fluid Properties

(Water)

$\delta C_p = 0.1$ J/kg°C

$\delta \rho = 0.02$ kg/m^3

$\delta k = 2 \times 10^{-5}$ W/m°C

$\delta \mu = 3 \times 10^{-7}$ kg/m·s

Appendix B

Instrument Calibrations.

Platinum Resistance Thermometer Calibrations.

The three platinum resistance thermometers used were calibrated with an NPL-calibrated, glass-bulb type PRT that was connected to an A/C bridge with an accuracy of ± 0.0002 Ω. The same data logger and current module used in the calibrations were also used for all tests. The calibration curves are shown in the figure below. (PRT1 and PRT5 were used to measure the water inlet and outlet temperatures respectively, while PRT19 measured the free-stream gas temperature).

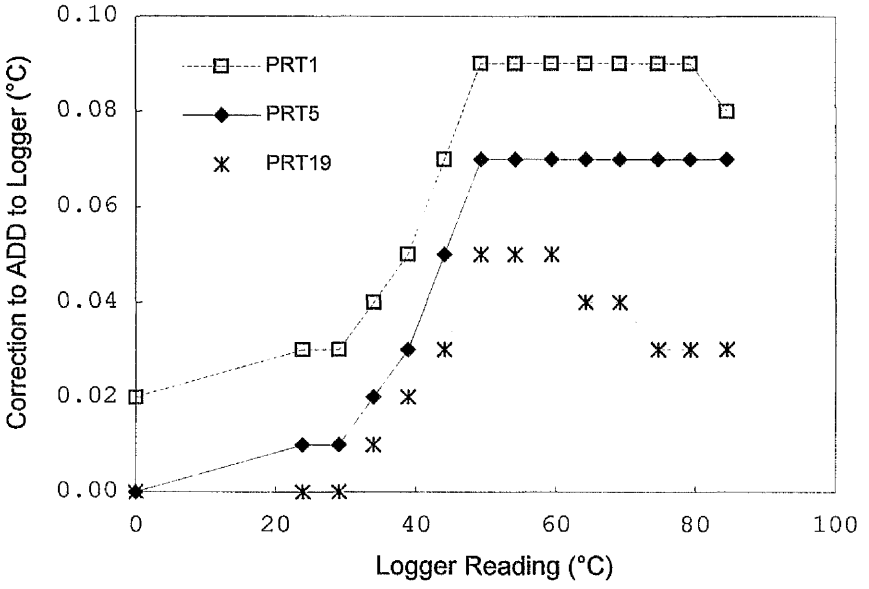

Air Humidity Measurement.

The digital psychrometer used in the tests was compared with another psychrometer over the range of humidity levels encountered in the experimental program. Both psychrometer readings fluctuated slightly due to the small inconsistency in the steam pressure levels in the laboratory. However, when time-varying fluctuations were accounted for, the results were within the ± 1% relative-humidity accuracy claimed by the manufacturer.

Air Velocity Measurement.

The combination of pitot-static tube and Furness Controls digital micromanometer was calibrated to output time-averaged pressure difference readings with a stated accuracy of 0.01 mm of water at 20°C. The conversion from mmH_2O output to velocity in meters per second was calculated from the following:

$$V_a = \sqrt{\frac{2\Delta p}{\rho_a}} = \sqrt{\frac{2\rho_w g H_w}{\rho_a}}$$

With the air treated as an ideal gas,

$$V_a = \sqrt{\frac{2\rho_w g H_w R_u T_K}{P_{atm} M_a}} = \sqrt{\frac{2(997.6)(9.81)mmH_2O(8314.4)T_K}{1000 P_{atm}(28.97)}}$$

$$V_a = 74.95\sqrt{\frac{mmH_2O\ T_k}{P_{atm}}}$$

where the temperature is given in Kelvins and the atmospheric pressure in Pascals.

Appendix C

Sample Experimental and Computer Results.

Table C.1: Non-Condensing Experimental Results

Tube	V_∞ (m/s)	T_∞ (°C)	$T_{w,in}$ (°C)	$T_{w,out}$ (°C)	ΔT_w (°C)	$T_{w,ave}$ (°C)	t (s)	Q_{tot} (W)	h_i (kW/m^2°C)	h_o (W/m^2°C)	$U_{overall}$ (W/m^2°C)
Plain	1.5	56.57	17.79	17.90	0.11	17.84	376.9	17	1.97	38	38
	2.8	62.26	18.44	18.60	0.16	18.52	373.7	27	2.00	53	52
	6.4	75.62	18.48	18.80	0.32	18.64	387.0	52	1.95	79	76
A	1.5	56.42	17.49	17.60	0.11	17.55	380.2	17	1.95	38	37
	2.8	61.53	19.03	19.19	0.16	19.11	382.5	27	1.98	55	53
	6.4	75.12	21.28	21.60	0.32	21.44	382.3	54	2.03	88	84
B	1.5	55.42	17.98	18.09	0.11	18.03	380.1	16	1.96	38	38
	2.8	59.83	18.40	18.57	0.17	18.49	379.6	27	1.98	56	54
	6.4	74.93	18.60	18.93	0.33	18.77	380.8	55	1.98	85	82
C	1.5	54.27	17.27	17.37	0.10	17.32	368.6	17	2.00	39	39
	2.7	59.39	18.39	18.56	0.17	18.48	380.4	28	1.97	58	56
	6.4	74.91	18.64	18.98	0.34	18.81	380.6	57	1.98	88	85

Table C.2: Condensing Experimental Results at Lowest Velocity

Tube	ϕ (%)	V_∞ (m/s)	T_ϕ (°C)	T_∞ (°C)	$T_{w,in}$ (°C)	$T_{w,out}$ (°C)	ΔT_w (°C)	$T_{w,ave}$ (°C)	t (s)	Q_{tot} (W)	Q_s (W)	Q_l (W)
Plain	20	1.51	59	59.84	18.08	18.25	0.18	18.17	373.8	30	19	11
	38	1.55	60	63.40	18.26	18.63	0.37	18.44	373.7	62	20	42
	49	1.57	61	63.84	18.28	18.76	0.48	18.52	376.7	80	20	60
	56	1.59	63	66.06	18.30	18.92	0.62	18.61	373.7	104	21	84
	65	1.62	64	67.11	17.63	18.39	0.77	18.01	375.8	128	21	107
	80	1.67	66	70.34	18.52	19.54	1.02	19.03	386.2	165	22	143
	92	1.76	72	74.72	18.39	19.89	1.50	19.14	385.8	244	23	221
A	22	1.52	58	60.42	18.35	18.56	0.21	18.46	379.5	35	19	16
	33	1.54	60	62.25	18.34	18.66	0.32	18.50	379.5	53	19	34
	45	1.57	61	64.43	18.17	18.60	0.43	18.39	380.7	71	20	51
	59	1.59	62	65.34	18.27	18.89	0.62	18.58	380.4	102	20	82
	69	1.62	64	67.47	18.32	19.13	0.81	18.72	380.4	133	21	112
	84	1.68	67	70.36	18.33	19.43	1.10	18.88	379.5	182	21	161
	95	1.77	72	74.76	18.36	19.99	1.62	19.17	379.5	268	22	246

Table C2: (Continued)

Tube	ϕ (%)	V_∞ (m/s)	T_ϕ (°C)	T_∞ (°C)	$T_{w,in}$ (°C)	$T_{w,out}$ (°C)	ΔT_w (°C)	$T_{w,ave}$ (°C)	t (s)	Q_{tot} (W)	Q_s (W)	Q_l (W)
B	21	1.51	57	59.18	18.44	18.64	0.20	18.54	378.0	33	18	14
	33	1.52	58	59.31	18.44	18.75	0.30	18.60	378.0	51	18	33
	46	1.57	61	65.00	18.45	18.92	0.47	18.68	378.0	78	20	58
	60	1.58	61	63.34	18.15	18.76	0.61	18.45	386.4	99	19	80
	72	1.64	65	69.04	18.35	19.24	0.89	18.79	377.3	149	21	127
	80	1.67	66	70.35	18.39	19.42	1.03	18.91	377.5	171	22	150
	96	1.76	71	74.30	18.46	20.03	1.57	19.24	377.5	261	22	238
C	24	1.51	57	58.90	18.24	18.44	0.21	18.34	380.2	34	19	15
	35	1.53	58	60.49	18.32	18.63	0.31	18.47	380.2	52	19	33
	44	1.54	59	61.12	18.36	18.77	0.41	18.56	380.2	68	19	48
	61	1.57	60	61.88	18.39	18.96	0.57	18.67	380.6	95	19	76
	68	1.62	63	67.00	18.45	19.22	0.77	18.83	380.6	127	21	105
	80	1.66	65	69.17	18.49	19.46	0.97	18.97	380.6	160	22	138
	93	1.71	68	71.41	18.52	19.78	1.27	19.15	380.6	209	22	187

Table C.3: Condensing Experimental Results at Intermediate Velocity

Tube	ϕ (%)	V_∞ (m/s)	T_ϕ (°C)	T_∞ (°C)	$T_{w,in}$ (°C)	$T_{w,out}$ (°C)	ΔT_w (°C)	$T_{w,ave}$ (°C)	t (s)	Q_{tot} (W)	Q_s (W)	Q_l (W)
	14	2.80	62	63.87	18.41	18.62	0.21	18.51	373.7	35	28	7
	25	2.84	63	65.12	18.38	18.74	0.36	18.56	373.2	61	28	33
	30	2.85	63	65.19	17.63	18.08	0.44	17.85	376.3	74	29	45
Plain	36	2.87	63	65.89	18.36	18.86	0.51	18.61	373.2	85	29	57
	42	2.92	66	68.78	18.25	18.92	0.67	18.59	376.3	112	30	82
	56	3.00	67	71.27	18.77	19.70	0.93	19.23	386.9	151	30	121
	71	3.08	69	72.48	18.89	20.20	1.31	19.54	386.2	212	30	183
	15	2.78	60	62.42	19.21	19.42	0.21	19.32	382.5	35	27	8
	25	2.82	62	63.92	19.33	19.68	0.35	19.51	382.5	58	28	30
	35	2.86	63	65.56	20.08	20.56	0.48	20.32	383.6	79	28	50
A	46	2.92	64	68.27	20.49	21.18	0.69	20.84	383.6	113	29	84
	55	2.96	65	68.82	20.92	21.78	0.86	21.35	382.9	140	28	112
	63	2.98	65	69.14	21.15	22.14	0.99	21.64	382.9	163	28	135
	72	3.06	68	70.85	21.22	22.49	1.27	21.86	382.4	208	28	180

Table C.3: (Continued)

Tube	ϕ (%)	V_∞ (m/s)	T_ϕ (°C)	T_∞ (°C)	$T_{w,in}$ (°C)	$T_{w,out}$ (°C)	ΔT_w (°C)	$T_{w,ave}$ (°C)	t (s)	Q_{tot} (W)	Q_s (W)	Q_l (W)
B	16	2.78	60	61.73	18.46	18.69	0.23	18.57	380.7	38	28	10
	25	2.81	61	62.93	18.48	18.83	0.35	18.65	380.3	57	29	29
	36	2.85	62	63.83	18.49	18.97	0.48	18.73	380.3	80	29	51
	45	2.90	63	66.44	18.53	19.17	0.64	18.85	380.1	105	30	75
	55	2.94	63	68.02	18.56	19.37	0.81	18.96	380.1	134	30	104
	63	2.98	65	69.02	18.58	19.57	0.99	19.08	380.6	163	30	132
	73	3.03	66	69.83	18.64	19.87	1.23	19.25	380.6	203	30	174
C	16	2.78	59	61.47	18.49	18.71	0.22	18.60	380.4	36	29	7
	26	2.81	61	61.94	18.54	18.91	0.36	18.73	380.6	60	29	31
	35	2.85	62	64.82	18.58	19.05	0.47	18.82	380.6	78	31	47
	46	2.91	64	66.61	18.61	19.26	0.65	18.93	380.8	107	31	76
	54	2.97	66	69.93	18.63	19.51	0.88	19.07	380.7	145	33	112
	66	3.00	66	69.39	18.65	19.70	1.05	19.17	380.7	173	31	142
	72	3.06	68	70.99	18.69	19.95	1.26	19.32	380.7	208	32	176

Table C4: Condensing Experimental Results at Highest Velocity

Tube	ϕ (%)	V_∞ (m/s)	T_ϕ (°C)	T_∞ (°C)	$T_{w,in}$ (°C)	$T_{w,out}$ (°C)	ΔT_w (°C)	$T_{w,ave}$ (°C)	t (s)	Q_{tot} (W)	Q_s (W)	Q_l (W)
Plain	8	6.48	74	77.44	18.54	18.89	0.36	18.71	373.4	60	54	6
	10	6.52	76	78.22	18.18	18.63	0.45	18.40	380.3	74	55	19
	12	6.54	76	78.25	18.69	19.18	0.49	18.93	373.5	82	54	29
	14	6.56	76	78.11	18.65	19.21	0.56	18.93	373.6	94	53	41
	16	6.60	77	78.78	17.60	18.28	0.67	17.94	379.6	111	54	57
	21	6.70	79	80.36	18.93	19.87	0.93	19.40	386.1	152	53	98
	24	6.76	80	80.97	19.00	20.08	1.08	19.54	386.1	175	53	122
A	7	6.45	75	76.06	21.35	21.69	0.34	21.52	382.3	56	55	1
	10	6.47	75	75.86	21.41	21.81	0.41	21.61	382.3	67	54	12
	13	6.51	75	76.47	21.48	21.99	0.52	21.74	382.8	84	54	30
	16	6.56	76	77.36	21.54	22.21	0.68	21.87	382.8	111	54	56
	19	6.61	76	78.08	21.58	22.37	0.79	21.97	383.7	129	54	75
	22	6.66	77	79.02	21.60	22.51	0.91	22.06	371.1	154	55	99
	24	6.71	78	79.73	21.64	22.65	1.01	22.15	371.0	171	55	116

Table C4: (Continued)

Tube	ϕ (%)	V_∞ (m/s)	T_ϕ (°C)	T_∞ (°C)	$T_{w,in}$ (°C)	$T_{w,out}$ (°C)	ΔT_w (°C)	$T_{w,ave}$ (°C)	t (s)	Q_{tot} (W)	Q_s (W)	Q_l (W)
B	7	6.44	75	75.97	18.62	18.97	0.35	18.80	381.0	58	56	2
	10	6.47	75	75.85	18.65	19.10	0.44	18.88	380.8	73	56	17
	13	6.51	75	76.43	18.69	19.23	0.55	18.96	380.3	90	56	34
	16	6.55	75	77.04	18.71	19.37	0.66	19.04	380.3	109	56	53
	19	6.61	76	78.53	18.74	19.57	0.82	19.16	380.2	136	56	80
	21	6.65	77	79.08	18.79	19.73	0.94	19.26	380.2	155	56	99
	23	6.68	77	79.10	18.78	19.77	0.99	19.27	380.2	163	56	108
C	7	6.46	76	76.77	18.71	19.08	0.36	18.90	380.6	60	59	1
	10	6.49	76	76.88	18.75	19.20	0.46	18.98	380.8	75	59	17
	13	6.53	76	77.09	18.78	19.35	0.56	19.06	380.8	93	58	35
	16	6.56	76	77.33	18.82	19.48	0.66	19.15	380.9	109	58	51
	19	6.61	76	78.40	18.07	18.88	0.80	18.48	387.4	130	59	71
	21	6.68	78	80.00	18.57	19.45	0.89	19.01	370.3	150	60	91
	24	6.74	79	80.56	18.67	19.70	1.03	19.18	370.3	175	59	116

Table C5: Comparison of Computer-Predicted and Experimental Latent Heat Flux for Plain Tube

Nominal V_∞ (m/s)	ϕ (%)	Experimental Q_l (kW/m^2)	Predicted Q_l (kW/m^2)	Predicted / Experimental
1.5	20	0.90	0.98	1.09
	38	3.51	3.31	0.94
	49	5.03	5.03	1.00
	56	6.99	6.75	0.97
	65	8.97	8.70	0.97
	80	11.98	12.56	1.05
	92	18.50	21.09	1.14
2.8	14	0.61	0.62	1.02
	25	2.73	2.81	1.03
	30	3.77	3.85	1.02
	36	4.74	4.94	1.04
	42	6.89	7.36	1.07
	56	10.07	11.22	1.11
	71	15.26	16.81	1.10
6.4	8	0.50	0.57	1.14
	10	1.62	1.91	1.18
	12	2.39	2.80	1.17
	14	3.42	3.77	1.10
	16	4.76	5.28	1.11
	21	8.23	8.47	1.03
	24	10.18	10.76	1.06

Table C6: Results of Modified Plain-Tube Program as Applied to Tube A

Nominal V_∞ (m/s)	ϕ (%)	Experimental q_l (W)	Predicted q_l (W)	Predicted / Experimental
	22	16	13	0.81
	33	34	32	0.94
	45	51	54	1.06
1.5	59	82	81	0.99
	69	112	111	0.99
	84	161	169	1.05
	95	247	260	1.06
	15	8	6	0.75
	25	30	30	1.00
	35	50	51	1.02
2.8	46	84	85	1.01
	55	112	114	1.02
	63	135	135	1.00
	72	180	190	1.06
	7	1	0	0.00
	10	12	13	1.10
	13	30	30	1.00
6.4	16	56	51	0.91
	19	75	69	0.92
	22	99	94	0.95
	24	116	113	0.97

HEAT TRANSFER PREDICTIONS

Length of Tube, l :	300 mm	
Tube Outside Diameter, od :	12.7 mm	
Outside Surface Area :	0.0119695 m2	
Tube Inside Diameter, id :	11.0 mm	
Inside Surface Area :	0.0103673 m2	
Conductivity of Tube, Kt :	104.00 W/mDegC	
Number of Elements, N :	15	
Water-Side Correlation Used :	Dittus-Boelter	
Gas-Side Correlation Used :	Churchill-Bernstein	
Atmospheric Pressure, Ptot :	101325 Pa	
Relative Humidity, phi :	65.00 %	
Air Partial Pressure, Pair :	83558 Pa	
Water Vapour Pressure, Pvap :	17767 Pa	
Saturation Temperature, Tsat :	57.55 DegC	
Inlet Temperature,Tin (DegC):	18.00	67.00
Mass Flow Rate (kg/s):	0.04000	----
Re at inlet :	4408	1319
Pr at inlet :	7.311	0.701
Velocity, V (m/s):	0.421	1.732
Specific Heat, Cp (J/kgDegC):	4182.79	1109.93
Conductivity, k (W/mDegC):	0.6009	0.0276
Viscosity, mu (x 10E-5 kg/ms):	105.024	1.742
Density, rho (kg/m3):	998.596	1.0444

Element	Tw_in	Tinside	Toutside	Tintfc	dqLatnt	dqTot	hinside	houtside
1	18.0000	24.1669	24.2590	24.6369	8.3794	9.7244	2292.323	39.786
2	18.0581	24.2166	24.3087	24.6860	8.3743	9.7177	2293.876	39.786
3	18.1162	24.2663	24.3583	24.7351	8.3691	9.7109	2295.427	39.785
4	18.1742	24.3159	24.4079	24.7842	8.3640	9.7042	2296.977	39.785
5	18.2322	24.3655	24.4574	24.8332	8.3588	9.6975	2298.526	39.785
6	18.2902	24.4151	24.5070	24.8822	8.3536	9.6907	2300.073	39.785
7	18.3481	24.4647	24.5565	24.9312	8.3484	9.6840	2301.618	39.784
8	18.4060	24.5142	24.6060	24.9801	8.3432	9.6772	2303.162	39.784
9	18.4639	24.5637	24.6554	25.0291	8.3380	9.6704	2304.705	39.784
10	18.5217	24.6132	24.7048	25.0779	8.3328	9.6636	2306.246	39.784
11	18.5794	24.6626	24.7542	25.1268	8.3276	9.6569	2307.785	39.783
12	18.6372	24.7121	24.8036	25.1756	8.3223	9.6501	2309.324	39.783
13	18.6948	24.7614	24.8529	25.2244	8.3171	9.6433	2310.860	39.783
14	18.7525	24.8108	24.9022	25.2732	8.3118	9.6364	2312.395	39.783
15	18.8101	24.8601	24.9515	25.3219	8.3066	9.6296	2313.929	39.782

Total Latent HT Rate:	125.1470 W	86.22 %	
Total Sensible HT Rate:	20.0098 W	13.78 %	
Total Heat Transfer Rate	145.1567 W		
Water Exit Temperature:	18.8677 DegC		
Water Temperature Rise:	0.8677 DegC		
Overall HT Coefficient:	247.4949 W/m2DegC		

Figure C.1 Sample Computer Program Output for Fully-Wet Plain Tube.

HEAT TRANSFER PREDICTIONS

Length of Tube, l :	5000 mm	
Tube Outside Diameter, od :	12.7 mm	
Outside Surface Area :	0.1994911 m2	
Tube Inside Diameter, id :	11.0 mm	
Inside Surface Area :	0.1727876 m2	
Conductivity of Tube, Kt :	104.00 W/mDegC	
Number of Elements, N :	15	
Water-Side Correlation Used :	Dittus-Boelter	
Gas-Side Correlation Used :	Churchill-Bernstein	
Atmospheric Pressure, Ptot :	101325 Pa	
Relative Humidity, phi :	12.00 %	
Air Partial Pressure, Pair :	98045 Pa	
Water Vapour Pressure, Pvap :	3280 Pa	
Saturation Temperature, Tsat :	25.59 DegC	
Inlet Temperature,Tin (DegC):	22.50	67.00
Mass Flow Rate (kg/s):	0.02661	----
Re at inlet :	3273	1201
Pr at inlet :	6.471	0.706
Velocity, V (m/s):	0.281	1.637
Specific Heat, Cp (J/kgDegC):	4180.03	1025.11
Conductivity, k (W/mDegC):	0.6078	0.0276
Viscosity, mu (x 10E-5 kg/ms):	94.097	1.899
Density, rho (kg/m3):	997.659	1.0970

Element	Tw_in	Tinside	Toutside	Tintfc	dqLatnt	dqTot	hinside	houtside
1	22.5000	23.8392	23.8411	23.8568	2.8157	24.6483	1741.894	38.050
2	22.7216	24.0359	24.0376	24.0530	2.5099	24.2425	1746.035	38.049
3	22.9396	24.2293	24.2308	24.2460	2.2060	23.8404	1750.104	38.048
4	23.1539	24.4195	24.4207	24.4357	1.9042	23.4421	1754.100	38.047
5	23.3647	24.6064	24.6074	24.6222	1.6046	23.0476	1758.025	38.046
6	23.5719	24.7901	24.7910	24.8055	1.3072	22.6569	1761.880	38.046
7	23.7756	24.9707	24.9714	24.9857	1.0122	22.2702	1765.665	38.045
8	23.9759	25.1481	25.1486	25.1627	0.7195	21.8874	1769.381	38.044
9	24.1727	25.3225	25.3228	25.3367	0.4292	21.5085	1773.030	38.043
10	24.3661	25.4938	25.4939	25.5077	0.1414	21.1338	1776.612	38.042
11	24.5561	25.6695	25.6833	-------	-------	20.9031	1780.139	38.041
12	24.7441	25.8505	25.8643	-------	-------	20.8110	1783.635	38.040
13	24.9312	26.0308	26.0445	-------	-------	20.7193	1787.113	38.039
14	25.1175	26.2104	26.2240	-------	-------	20.6280	1790.573	38.038
15	25.3030	26.3892	26.4027	-------	-------	20.5371	1794.013	38.037

Total Latent HT Rate:	14.6498 W	4.41 %
Total Sensible HT Rate:	317.6263 W	95.59 %
Total Heat Transfer Rate	332.2761 W	
Water Exit Temperature:	25.4877 DegC	
Water Temperature Rise:	2.9877 DegC	
Overall HT Coefficient:	37.4276 W/m2DegC	

Figure C.2 Sample Computer Program Output for Partially-Wet Plain Tube.

Appendix D

Computer Program Listing.

```
/*                  ****************************************
                    *                                      *
                    *            Robert Prosperi           *
                    *                                      *
                    *           Glasgow University         *
                    *  Department of Mechanical Engineering *
                    *                                      *
                    *                (ANSI C)              *
                    *                                      *
                    *             April 12, 1997           *
                    *                                      *
                    ****************************************          */

#include <stdio.h>
#include <float.h>
#include <math.h>
#ifdef __MSDOS__
#include <conio.h>
#endif

typedef enum  {dittus,seider,nusselt}      inside_corr_type;
typedef enum  {hilpert,eckert,churchill}   outside_corr_type;
typedef enum  {no,maybe,yes}               condense_type;
typedef enum  {false,true}                 boolean;

#define inches     0.0254        /* Convert Inches to Meters */
#define Kt         104.0         /* Thermal Conductivity of Tube (W/m.K) */
#define Ru         8314.4        /* Universal Gas Constant (J/kgmole.K) */
#define g          9.80665       /* Gravitational Constant (N/kg) */
#define mma        28.97         /* Molar Mass of Air (kg/kgmole) */
#define mmw        18.02         /* Molar Mass of Water (kg/kgmole) */
#define accuracy   5E-12         /* Convergance Accuracy Required */
#define Pi         3.141592654   /* Constant Pi */

long               n;           /* Number of Tube Elements */
double             l;           /* Length of Tube (m) */
double             H;           /* Height of Test Section (m) */
double             dl;          /* Length of Tube Element (m) */
double             mfw;         /* Mass Flow Rate of Water (kg/s) */
double             id;          /* Tube Inside Diameter (m) */
double             od;          /* Tube Outside Diameter (m) */
double             TG1;         /* Gas Inlet Temperature (DegC) */
double             Vgas;        /* Gas Velocity (m/s) */
double             phi;         /* Relative Humidity (fraction) */
double             Tinlet;      /* Initial Water Inlet Temperature (DegC) */
double             Tex;         /* Element Exit Water Temperature (DegC) */
double             Ptot;        /* Atmospheric Pressure (Pa) */
double             Pvap;        /* Partial Pressure of Water Vapour (Pa) */
double             Pair;        /* Partial Pressure of Air (Pa) */
double             mofra;       /* Mole Fraction of Air (fraction) */
double             mofrv;       /* Mole Fraction of Water Vapour (fraction) */
double             mafra;       /* Mass Fraction of Air (fraction) */
double             mafrv;       /* Mass Fraction of Water Vapour (fraction) */
double             qlat;        /* Sum of Elemental Latent HT Rates (W) */
double             qtot;        /* Sum of Elemental Total HT Rates (W) */
double             sattemp;     /* Saturation Temperature of Vapour (DegC) */
inside_corr_type   inside_corr;     /* Water-Side HT Correlation to use */
outside_corr_type  outside_corr;    /* Vapour-Side HT Correlation to use */
boolean            file_output;     /* True for File Output, False for CRT */
```

```
double      sqr(double  x);

double      pwr(double  base,
                double  exponent);

double      Psat(double  t);

double      Tsat(double  pressure);

double      hfg(double  t);

double      Cpw(double  t);

void        Water_Prop(double  t,
                       double  *reyn,
                       double  *pran,
                       double  *k,
                       double  *vel);

void        Gas_Prop(double  t,
                     double  *reyn,
                     double  *pran,
                     double  *k,
                     double  *Cp);

void        GetRi(double  Twater,
                  double  Twall,
                  double  *r);

void        GetRo(double  T,
                  double  Tgas,
                  double  *r);

void        Getdql(double  *Tintface,
                   double  Tout,
                   double  *dql);

void        Show_Prelim_Info(void);

void        Show_End_Summary(void);


/*############################################################################*/
int     main(void)

{
   long             element;     /* Tube Element Number */
   double           dq_dry;      /* Heat Transfer Rate for Dry Element (W) */
   double           Tout_dry;    /* Outside Wall Temp for Dry Element (DegC) */
   double           Tin_dry;     /* Inside Wall Temp for Dry Element (DegC) */
   double           dq;          /* Total Heat Transfer Rate for Element (W) */
   double           dqs;         /* Sensible HT Rate for an Element (W) */
   double           dql;         /* Latent HT Rate for an Element (W) */
   double           Tw;          /* Element Bulk Water Temperature (DegC) */
   double           Tin;         /* Inside Wall Temperature (DegC) */
   double           Tout;        /* Outside Wall Temperature (DegC) */
   double           Ti;          /* Gas/Condensate Interface Temp (DegC) */
   double           Ri;          /* Inside HT Resistance (DegC/W) */
   double           Rt;          /* Tube Wall HT Resistance (DegC/W) */
   double           Ro;          /* Outside HT Resistance (DegC/W) */
   double           previous;    /* Previous Element Interface Temp (DegC) */
   double           Vair;        /* Velocity of Inlet Air Alone (m/s) */
   condense_type    condensing;  /* Element Condensing Flag (No/Maybe/Yes) */
```

```
    file_output = false;

          /*   freopen("results.dat","w",stdout);
               file_output = true;                    */

    n = 15;
    l = 0.300;
    H = 0.150;
    Ptot = 101325.0;
    mfw = 15 / 375.8;
    id = 0.011;
    od = 0.5 * inches;
    TG1 = 67.1084;
    Vair = 1.3;
    phi = 0.65;
    Tinlet = 17.6253;
    inside_corr = dittus;
    outside_corr = churchill;

    Pvap = phi * Psat(TG1);
    Pair = Ptot - Pvap;
    Vgas = Vair *  1.205 * Ru * (TG1 + 273.15) / (Pair*mma + Pvap*mmw);
    Vgas = Vgas / (1 - (Pi*od)/ (4*H));
    if (phi > 0.0) sattemp = Tsat(Pvap);
    mofra = Pair / Ptot;
    mofrv = 1 - mofra;
    mafra = mofra * mma / (mofra * mma + mofrv * mmw);
    mafrv = 1 - mafra;
    dl = l / n;
    Rt = log(od / id) / (2 * Pi * Kt * dl);

#ifdef __MSDOS__
      clrscr();
#endif

    Show_Prelim_Info();

    Tex = Tinlet;
    Tin = Tex;
    Tout = Tex;
    Ti = Tex;
    qtot = 0.0;
    qlat = 0.0;
    condensing = maybe;



    for (element = 1; element <= n; element++) {
        Tw = Tex;
        GetRi(Tw,Tin,&Ri);

        do {
            GetRo(Tout,TG1,&Ro);
            dq = (TG1 - Tex) / (Ro + Rt + Ri + 1 / (2 * mfw * Cpw(Tw)));
            Tw = Tex + dq / (2 * mfw * Cpw(Tw));
            GetRi(Tw,Tin,&Ri);
            Tin = Tw + dq*Ri;
            Tout = Tin + dq*Rt;
        }  while (!(fabs((TG1-Tout)/Ro - (Tout-Tin)/Rt) < accuracy));
```

```
        if (condensing != no)
           if (phi > 0.0) {
              if (Tout >= sattemp)
                 condensing = no;
              else {
                 condensing = maybe;
                 Tin_dry = Tin;
                 Tout_dry = Tout;
                 dq_dry = dq;
              }
           }
           else
              condensing = no;

        if (condensing == maybe) {
           do {
               previous = Ti;
               GetRo(Ti,TG1,&Ro);
               dqs = (TG1 - Ti) / Ro;
               Getdql(&Ti,Tout,&dql);
               Ti = (Ti + previous) / 2;
               dq = dqs + dql;
               Tw = Tex + dq/(2 * mfw * Cpw(Tw));
               GetRi(Tw,Tin,&Ri);
               Tin = Tw + dq*Ri;
               Tout = Tin + dq*Rt;
           }  while (!(fabs(Ti-previous) < accuracy));

           if (Ti < sattemp) {
              condensing = yes;
              Tout = Tin + dql*Rt;
              qlat = qlat + dql;
              }
           else {
              dql = 0.0;
              dq = dq_dry;
              Tin = Tin_dry;
              Tout = Tout_dry;
           }
        }

        printf("%4ld  %9.4f%9.4f%9.4f",element,Tex,Tin,Tout);
        if (condensing == yes)
           printf("%9.4f%9.4f",Ti,dql);
        else if (condensing == no)
           printf("  -------  -------");
        else
           printf("  ? ? ? ?  ? ? ? ?");
        printf("%9.4f%10.3f%8.3f\n",dq,1/(Ri*Pi*id*dl),1/(Ro*Pi*od*dl));

        Tex = Tex + dq / (Cpw(Tw) * mfw);
        qtot = qtot + dq;
     }

     Show_End_Summary();

     fclose(stdout);
     return 0;
  }
  /*##############################################################################*/
```

```
/*****************************************************************************/
double     sqr(double  x)

/*======
          Square a Given Number, x.
                                        =====*/
{
   return x*x;
}
/*****************************************************************************/
double     pwr(double  base,
               double  exponent)

/*=====
          Raises a Number (base) to a Given Power (exponent).
                                                              =====*/

{
   if (base > 0.0)
      return exp(exponent * log(base));
   else if (base == 0.0)
      return 0.0;
   else {
      printf("Warning - Negative Base in pwr Function\n");
      return 0.0;
   }
}
/*****************************************************************************/
double     Psat(double  t)

/*=====
             Calculate Saturation Pressure for a Given Temperature.
             VALID for 0 < t < 100 DegC.
             UNITS: Saturation Pressure in Pa, Temp in DegC.
             DATA from "UK Steam Tables in SI Units 1970".
                                                          =====*/

{
   double     a0, a1, a2, a3, a4, a5;    /* Coeffs of Degree Zero to Five */

   a0 = 6.12516098949974E+02;    a1 = 4.36933838983877E+01;
   a2 = 1.48002634331512E+00;    a3 = 2.54204108505460E-02;
   a4 = 2.89795112322884E-04;    a5 = 2.71462032626696E-06;
   return t * (t * (t * (t * (t * a5 + a4) + a3) + a2) + a1) + a0;
}
/*****************************************************************************/
double     Tsat(double  pressure)

/*=====
         Calculate Saturation Temperature for a Given Pressure.
         VALID for 613 < Pressure < 101325 Pa.
         UNITS: Saturation Pressure in Pa, Temp in DegC.

    Representation of Tsat as a Polynomial Function of P is NOT Effective.
    A Simple Bracketting Method Using Psat Function Works Well Since
    the First Derivative of Psat(Temp) is Positive Over the Interval.
                                                          =====*/

{
   double     ptrial;          /* Current Trial Value of Pressure (Pa) */
   double     left;            /* Left Bracket (Pa) */
   double     right;           /* Right Bracket (Pa) */
   boolean    finished;        /* Used When Tsat is Close to Zero */
```

```
   left = 0.0;
   right = 100.0;
   finished = false;
   do {
       ptrial = Psat((left + right) / 2);
       if (ptrial < pressure)
          left = (left + right) / 2;
       else
          right = (left + right) / 2;
       if (ptrial < 613)
          finished = true;
   }  while (!(fabs(ptrial - pressure) < accuracy*10) && (finished == false));
   return (left + right) / 2;
}
/*****************************************************************************/
double     hfg(double  t)

/*=====
        Calculate Specific Heat of Condensation for a Given Temperature.
        VALID for 0 < t < 100 DegC.
        UNITS: hfg in J/kg, Temperature in DegC.
        DATA from "UK Steam Tables in SI Units 1970".
                                                                      =====*/

{
   double     a0, a1, a2, a3, a4, a5;    /* Coeffs of Degree Zero to Five */

   a0 = 2.50158037044541E+06;    a1 = -2.37393254258484E+03;
   a2 = 9.76941187918792E-01;    a3 = -2.37212933881319E-02;
   a4 = 1.07589400096309E-04;    a5 = -4.07226801172310E-07;
   return t * (t * (t * (t * (t * a5 + a4) + a3) + a2) + a1) + a0;
}
/*****************************************************************************/
double     Cpw(double  t)

/*=====
       Calculate Specific Heat at Constant Pressure of Water.
       VALID for 0 < t < 100 DegC, Atmospheric Pressure.
       UNITS: J/kg.DegC.
       DATA from Kaye & Laby, "Tables of Physical and Chemical Constants".
                                                                      =====*/

{
   double     a0, a1, a2, a3, a4, a5;   /* Coeffs of Degree Zero to Five */

   a0 = 4.21670185239030E+03;    a1 = -3.41645030246307E+00;
   a2 = 1.13267367406859E-01;    a3 = -1.81766661368302E-03;
   a4 = 1.49585991952496E-05;    a5 = -4.70815238214041E-08;
   return t * (t * (t * (t * (t * a5 + a4) + a3) + a2) + a1) + a0;
}
/*****************************************************************************/
void       Water_Prop(double  t,              /* Bulk Temperature (DegC) */
                      double  *reyn,          /* Reynolds Number */
                      double  *pran,          /* Prandtl Number */
                      double  *k,             /* Conductivity (W/m.DegC) */
                      double  *vel)           /* Water Mean Velocity (m/s) */

/*=====
     Calculate Water Properties as a Function of Temperature.
     VALID for 0 < t < 100 DegC, Atmospheric Pressure.
     DATA for rho,mu: Kaye & Laby,"Tables of Physical and Chemical Constants".
     DATA for k: "UK Steam Tables in SI Units 1970".
                                                                      =====*/
```

```
{
   double     a0, a1, a2, a3, a4, a5;    /* Coeffs of Degree Zero to Five */
   double     mu;                        /* Dynamic Viscosity (kg/m.s) */
   double     rho;                       /* Density of Water (kg/m3) */

   a0 =  9.99851787420866E+02;     a1 = 6.10494033492148E-02;
   a2 = -8.29800148570132E-03;     a3 = 6.41040886833811E-05;
   a4 = -3.96647525721798E-07;     a5 = 1.09538595867921E-09;
   rho = t * (t * (t * (t * (t * a5 + a4) + a3) + a2) + a1) + a0;

   a0 =  5.69000000000000E-01;     a1 = 1.97416666666652E-03;
   a2 = -1.32291666666542E-05;     a3 = 1.24999999999653E-07;
   a4 = -1.30208333332941E-09;     a5 = 5.20833333331781E-12;
   *k = t * (t * (t * (t * (t * a5 + a4) + a3) + a2) + a1) + a0;

   a0 = 1.78381212659454E-03;     a1 = -5.93979363702911E-05;
   a2 = 1.32933140514451E-06;     a3 = -1.87379091332240E-08;
   a4 = 1.42835335689436E-10;     a5 = -4.40101961964643E-13;
   mu = t * (t * (t * (t * (t * a5 + a4) + a3) + a2) + a1) + a0;

   *vel = 4 * mfw / (rho * Pi * id * id);
   *reyn = rho * *vel * id / mu;
   *pran = Cpw(t) * mu / *k;
}
/*****************************************************************************/
void       Gas_Prop(double  t,          /* Gas Mixture Temperature (DegC) */
                    double  *reyn,      /* Reynolds Number */
                    double  *pran,      /* Prandtl Number */
                    double  *k,         /* Conductivity of Mix (W/m.DegC) */
                    double  *Cp)        /* Spec Heat of Mixture (J/kg.DegC) */

/*=====
      Calculate Gas Properties as a Function of Temperature.
      Vapour  Data VALID for 0 < t < 100 DegC, Saturation Pressure.
      Dry Air Data VALID for 0 < t < 100 DegC, Atmospheric Pressure.
      DATA for Vapour: "Properties of Water and Steam in SI Units", 1969.
      DATA for Dry Air:  A.J.Chapman, "Fundamentals of Heat Transfer", 1987.

      Calculation of Gas Mixture Properties from Methods Suggested by
      Reid & Sherwood, "The Properties of Gases and Liquids", 1966.
                                                                    =====*/

{
   double    a0, a1, a2, a3, a4, a5;  /* Coeffs of Degree Zero to Five */
   double    Aav;                     /* Factor in Conductivity Equation */
   double    Ava;                     /* Factor in Conductivity Equation */
   double    Tk;                      /* Temperature (K) */
   double    rho;                     /* Density of Mixture (kg/m3) */
   double    Cpvap;                   /* Spec Heat of Vapour (J/kg.DegC) */
   double    Cpair;                   /* Spec Heat of Dry Air (J/kg.DegC) */
   double    muvap;                   /* Dyn Viscosity of Vapour (kg/m.s) */
   double    muair;                   /* Dyn Viscosity of Air (kg/m.s) */
   double    mu;                      /* Dyn Viscosity of Mixture (kg/m.s) */
   double    phi_av;                  /* Coefficient in Viscosity Calc */
   double    phi_va;                  /* Coefficient in Viscosity Calc */
   double    kvap;                    /* Conductivity of Vapour (W/m.DegC) */
   double    kair;                    /* Conductivity of Air (W/m.DegC) */


   Tk = t + 273.15;


   a0 =  1.00569411764706E+03;     a1 = 8.40861099683238E-03;
   a2 =  4.69834087482136E-04;     a3 = 2.09790209787747E-06;
```

```
   a4 = -3.56506238856667E-08;    a5 = 1.50829562593368E-10;
   Cpair = t * (t * (t * (t * (t * a5 + a4) + a3) + a2) + a1) + a0;

   a0 =  1.85407239819005E+03;    a1 = 5.38978472507871E-01;
   a2 =  1.33561291649610E-03;    a3 = 1.30608974358955E-04;
   a4 = -3.62505141916727E-07;    a5 = 1.22549019607782E-09;
   Cpvap = t * (t * (t * (t * (t * a5 + a4) + a3) + a2) + a1) + a0;

   *Cp = Cpair * mafra + Cpvap * mafrv;


   a0 =  1.71994909502262E-05;    a1 = 5.00052704648313E-08;
   a2 = -9.35190422324178E-11;    a3 = 1.32721445221792E-12;
   a4 = -1.18992527081114E-14;    a5 = 3.77073906486929E-17;
   muair = t * (t * (t * (t * (t * a5 + a4) + a3) + a2) + a1) + a0;

   a0 = 8.02E-06;    a1 = 4.00E-08;
   muvap = a0 + a1*t;

   phi_av = sqr(1.0 + sqrt(muair/muvap)*pwr(mmw/mma,0.25)) /
            sqrt(8.0*(1.0+(mma/mmw)));
   phi_va = phi_av*(muvap/muair)*(mma/mmw);

   mu = mofra*muair/(mofra+mofrv*phi_av) +
        mofrv*muvap/(mofrv+mofra*phi_va);

   a0 =  2.40786199095023E-02;    a1 = 8.16837138351862E-05;
   a2 = -2.34763643219648E-07;    a3 = 2.67191142191445E-09;
   a4 = -1.75425065131256E-11;    a5 = 4.52488687783910E-14;
   kair = t * (t * (t * (t * (t * a5 + a4) + a3) + a2) + a1) + a0;

   a0 = 1.82031674208145E-02;    a1 =  5.72360482654547E-05;
   a2 = 2.42372823255551E-07;    a3 = -7.57575757576680E-09;
   a4 = 9.78678184561472E-11;    a5 = -3.77073906486004E-13;
   kvap = t * (t * (t * (t * (t * a5 + a4) + a3) + a2) + a1) + a0;

   Aav = sqr(1+sqrt(muair/muvap*pwr(mmw/mma,3/4.0)*(1+120/Tk)/(1+560/Tk))) *
         0.25 * (1+180/Tk)/(1+120/Tk);
   Ava = sqr(1+sqrt(muvap/muair*pwr(mma/mmw,3/4.0)*(1+560/Tk)/(1+120/Tk))) *
         0.25 * (1+180/Tk)/(1+560/Tk);
   if (mofrv > 0.0)
      *k = kair/(1 + Aav * mofrv / mofra) + kvap / (1 + Ava * mofra / mofrv);
   else
      *k = kair;


   rho = (Pair * mma + Pvap * mmw) / (Ru * Tk);
   *reyn = rho * Vgas * od / mu;
   *pran = *Cp * mu / *k;
}
/*****************************************************************************/
void       GetRi(double  Twater,      /* Bulk Water Temperature (DegC) */
                 double  Twall,       /* Inside Wall Temperature (DegC) */
                 double  *r)          /* Water-Side Resistance (DegC/W) */

/*=====
      Get the Local, Water-Side Thermal Resistance.
                                                    =====*/

{
   double     Re;           /* Reynolds Number for Water */
   double     Pr;           /* Prandtl Number for  Water */
   double     K;            /* Thermal Conductivity of Water (W/m.DegC) */
   double     Vel;          /* Water Velocity (m/s) */
```

```
    double      Nu;             /* Nusselt Number */
    double      mubulk;         /* Dyn Viscosity at Bulk Water Temp (kg/m.s) */
    double      muwall;         /* Dyn Viscosity at Inside Wall Temp (kg/m.s) */

    Water_Prop(Twater,&Re,&Pr,&K,&Vel);

    if (inside_corr == dittus)
        Nu = 0.023 * pwr(Re,0.8) * pwr(Pr,0.4);
    else if (inside_corr == nusselt)
        Nu = 0.036 * pwr(Re,0.8) * pwr(Pr,1/3.0) * pwr(id / l,0.055);
    else if (inside_corr == seider) {
        Water_Prop(Twall,&Re,&Pr,&K,&Vel);
        muwall = Pr * K / Cpw(Twall);
        Water_Prop(Twater,&Re,&Pr,&K,&Vel);
        mubulk = Pr * K / Cpw(Twater);
        Nu = 0.027 * pwr(Re,0.8) * pwr(Pr,1/3.0) * pwr(mubulk / muwall,0.14);
    }

    *r = 1 / (Nu * Pi * K * dl);
}
/*****************************************************************************/
void        GetRo(double  T,        /* Tube Outer Wall Temperature (DegC) */
                  double  Tgas,     /* Gas Temperature (DegC) */
                  double  *r)       /* Gas-Side Thermal Resistance (DegC/W) */


/*=====  Get the Local, Gas-Side Thermal Resistance.
                                                        =====*/

{
    double      Re;       /* Reynolds Number of Mixture */
    double      Pr;       /* Prandtl Number of Mixture */
    double      K;        /* Thermal Conductivity of Mixture (W/m.DegC) */
    double      Cp;       /* Spec Heat @ Const Pressure of Mixture (J/kg.DegC) */
    double      Nu;       /* Nusselt Number */
    double      C;        /* Multiplier in Hilpert Correlation */
    double      enn;      /* Exponent in Hilpert Correlation */

    Gas_Prop((T + Tgas) / 2,&Re,&Pr,&K,&Cp);

    if (outside_corr == hilpert) {
       if (Re < 4000.0) {
          C = 0.683; enn = 0.466;
          }
       else if (Re < 40000.0) {
          C = 0.193; enn = 0.618;
          }
       Nu = C * pwr(Re,enn) * pwr(Pr,1/3.0);
    }

    else if (outside_corr == eckert)
      if (Re <= 1000.0)
         Nu = (0.43 + 0.50 * pwr(Re,0.5)) * pwr(Pr,0.38);
      else
         Nu = 0.25 * pwr(Re,0.6) * pwr(Pr,0.38);

    else if (outside_corr == churchill) {
       Nu = 0.62 * pwr(Re,0.5) * pwr(Pr,1/3.0);
       Nu = Nu * pwr(1 + pwr(Re / 282000.0,0.625),0.8);
       Nu = Nu / pwr(1 + pwr(0.4 / Pr,2/3.0),0.25) + 0.3;
    }

    *r = 1 / (Nu * Pi * K * dl);
}
```

```
/*************************************************************************/
void       Getdql(double  *Tintface, /* Interface Temperature (DegC) */
                  double  Tout,      /* Outside Wall Temperature (DegC) */
                  double  *dqlat)    /* Mass Transfer Coefficient (W/m2.Pa) */

/*=====
     Calculates the Mass Transfer Coefficient.
     Diffusivity Calculated Using Method of Rose in IJHMT V23 pp539-546, 1980.

                                                                    =====*/

{
   double     Tfilm;          /* Gas Film Temperature (DegC) */
   double     TfilmK;         /* Gas Film Absolute Temperature (K) */
   double     diff;           /* Diffusivity of Vapour in Air (m2/s) */
   double     kg;             /* Thermal Conductivity (W/m.DegC) */
   double     Cpg;            /* Spec Heat @ Constant Pressure (J/kg.DegC) */
   double     Reg;            /* Reynolds Number of Mixture */
   double     Prg;            /* Prandtl Number of Mixture */
   double     Sc;             /* Schmidt Number */
   double     mafra_int;      /* Mass Fraction of Air at Interface */
   double     beta;           /* Coefficient Used in Calc of Mass Flux */
   double     rhog;           /* Density of Mixture (kg/m3) */
   double     m;              /* Condensation Mass Flux (kg/m2.s) */
   double     Tint;           /* Interface Temperature (DegC) */
   double     Rec;            /* Reynolds Number of Condensate */
   double     Prc;            /* Prandtl Number of Condensate */
   double     kc;             /* Conductivity of Condensate (W/m.DegC) */
   double     Velc;           /* Velocity of Condensate (m/s) */
   double     rhoc;           /* Density of Condensate (kg/m3) */
   double     muc;            /* Viscosity of Condensate (kg/m.s) */
   double     mug;            /* Viscosity of Gas Mixture (kg/m.s) */
   double     Qlat;           /* Latent Heat Flux (W/m2) */
   double     r;              /* Ratio of Density-Viscosity Products */
   double     a;              /* Factor Used in Equation to Determine Tint */
   double     b;              /* Factor Used in Equation to Determine Tint */
   double     c;              /* Factor Used in Equation to Determine Tint */
   double     check;          /* Updated Value of Tint (DegC) */

   Tint = *Tintface + 10;
   do {
       check = Tint;
       Tfilm = (TG1 + Tint)/2;
       TfilmK = Tfilm + 273.15;
       diff = (7.65E-5/Ptot)*pwr(TfilmK,11/6.0);

       Gas_Prop(Tfilm,&Reg,&Prg,&kg,&Cpg);
       Sc = Vgas * od / (Reg * diff);
       rhog = (Pair*mma + Pvap*mmw) / (Ru * (TfilmK));
       mug = kg*Prg/Cpg;

       mafra_int = (Ptot - Psat(Tint)) / (Ptot - (1-mmw/mma)*Psat(Tint));
       beta = (  sqrt(1.0+2.28*pwr(Sc,1/3.0)*(mafra_int/mafra-1.0)) - 1.0 )
              / (2.0 * Sc);
       if (beta < 0.0) beta = -1.0*beta;
       m = beta * rhog * Vgas / sqrt(Reg);
       Qlat = m * hfg(Tint);

       Water_Prop(Tout+(Tint-Tout)/3,&Rec,&Prc,&kc,&Velc);
       rhoc = Rec*Prc*kc/(Velc*id*Cpw(Tint));
       muc = kc*Prc/Cpw(Tint);

       r = sqrt(rhoc*muc/(rhog*mug));
       a = sqr(Vgas*rhoc*od/muc);
```

```
        b = pwr(1 + muc*hfg(Tint)/(r*kc*(Tint-Tout)),4/3.0);
        c=  0.276*sqr(rhoc)*pwr(od,3.0)*hfg(Tint)*g/(muc*kc*(Tint-Tout));

        Tint = Tout + ( ((Qlat * od)/kc) / pwr(0.656*a*b+c,0.25));

    }  while (!(fabs(Tint-check) < accuracy));

    *dqlat = Qlat * dl * Pi * od;
    *Tintface = Tint;

}
/*****************************************************************************/
void        Show_Prelim_Info(void)

/*=====
     Send the Preliminary Information Either to Screen or to a File.
                                                                    =====*/

{
    double        Regas;     /* Gas-Side Reynolds Number */
    double        Prgas;     /* Gas-Side Prandtl Number */
    double        Rewtr;     /* Water-Side Reynolds Number */
    double        Prwtr;     /* Water-Side Prandtl Number */
    double        kw;        /* Thermal Conductivity of Water (W/m.DegC) */
    double        kg;        /* Thermal Conductivity of Gas (W/m.DegC) */
    double        Vwtr;      /* Mean Water Velocity (m/s) */
    double        Cpg;       /* Gas Specific Heat @ Const Pressure (J/kg.DegC) */

    printf("                          HEAT TRANSFER PREDICTIONS \n");
    printf("\n");
    printf(" Length of Tube, l :              %3.0f mm\n",l * 1000);
    printf(" Tube Outside Diameter, od :      %4.1f mm\n",od * 1000);
    printf(" Outside Surface Area :           %1.7f m2\n",od * Pi * l);
    printf(" Tube Inside Diameter, id :       %4.1f mm\n",id * 1000);
    printf(" Inside Surface Area :            %1.7f m2\n",id * Pi * l);
    printf(" Conductivity of Tube, Kt :       %1.2f W/mDegC\n",Kt);
    printf(" Number of Elements, N :          %ld\n",n);

    printf(" Water-Side Correlation Used :    ");
    switch (inside_corr) {
       case 0:   printf("Dittus-Boelter\n");
                 break;
       case 1:   printf("Seider-Tate\n");
                 break;
       case 2:   printf("Nusselt\n");
                 break;
    }

    printf(" Gas-Side Correlation Used :      ");
    switch (outside_corr) {
       case 0:   printf("Hilpert\n");
                 break;
       case 1:   printf("Eckert-Drake\n");
                 break;
       case 2:   printf("Churchill-Bernstein\n");
                 break;
    }
    printf(" Atmospheric Pressure, Ptot :     %1.0f Pa\n",Ptot);
    printf(" Relative Humidity, phi :         %4.2f %\n",phi * 100);
    printf(" Air Partial Pressure, Pair :     %1.0f Pa\n",Pair);
    printf(" Water Vapour Pressure, Pvap :    %1.0f Pa\n",Pvap);
    printf(" Saturation Temperature, Tsat :   ");
    if (phi > 0.0)
       printf("%5.2f DegC\n",sattemp);
```

```
   else
      printf("-----\n");

   Water_Prop(Tinlet,&Rewtr,&Prwtr,&kw,&Vwtr);
   Gas_Prop((Tinlet + TG1) / 2,&Regas,&Prgas,&kg,&Cpg);

   printf(" Inlet Temperature,Tin (DegC):    %5.2f%11.2f\n",Tinlet,TG1);
   printf(" Mass Flow Rate (kg/s):           %7.5f    -----\n",mfw);
   printf(" Re at inlet :                    %1.0f%11.0f\n",Rewtr,Regas);
   printf(" Pr at inlet :                    %1.3f%11.3f\n",Prwtr,Prgas);
   printf(" Velocity, V (m/s):               %4.3f%11.3f\n",Vwtr,Vgas);
   printf(" Specific Heat, Cp (J/kgDegC):    ");
   printf("%1.2f%11.2f\n",Cpw(Tinlet),Cpg);
   printf(" Conductivity, k (W/mDegC):       %1.4f%11.4f\n",kw,kg);
   printf(" Viscosity, mu (x 10E-5 kg/ms):   %1.3f",kw*Prwtr*1E5/Cpw(Tinlet));
   printf("%10.3f\n",kg * Prgas * 1E5 / Cpg);
   printf(" Density, rho (kg/m3):            ");
   printf("%7.3f",Rewtr * Prwtr * kw / (Vwtr * id * Cpw(Tinlet)));
   printf("%10.4f",Regas * Prgas * kg / (Vgas * od * Cpg));

#ifdef __MSDOS__
   if (file_output == false) {
      fprintf(stderr,"            Press Any Key ");
      getch();
   }
#endif

   printf("\n");
   printf("\n");
   printf(" Element Tw_in   Tinside  ");
   printf("Toutside  Tintfc  dqLatnt   dqTot   hinside  houtside\n");
   printf(" ------------------------------------------");
   printf("-----------------------------------\n");
}
/*****************************************************************************/
void       Show_End_Summary(void)

/*=====
        Send the Summary Information Either to Screen or to a File.
                                                                    =====*/

{
   printf("\n");
   printf(" Total Latent HT Rate:           %10.4f W",qlat);
   printf("      %5.2f % \n",qlat *100.0 / qtot);
   printf(" Total Sensible HT Rate:         %10.4f W",qtot - qlat);
   printf("      %5.2f % \n",(qtot - qlat) *100.0 / qtot);
   printf(" Total Heat Transfer Rate        %10.4f W\n",qtot);
   printf(" Water Exit Temperature:         %10.4f DegC\n",Tex);
   printf(" Water Temperature Rise:         ");
   printf("%10.4f DegC\n",Tex - Tinlet);
   printf(" Overall HT Coefficient:         ");
   printf("%10.4f W/m2DegC\n",qtot*log((TG1-Tinlet)/
                              (TG1-Tex))/((Tex-Tinlet)*od*Pi*l));

#ifdef __MSDOS__
   if (file_output == false) {
      fprintf(stderr,"%10s               Press Any Key To Return To System ");
      getch();
   }
#endif
}
/*****************************************************************************/
                  /********     End of Program     ********/
```

GLASGOW UNIVERSITY LIBRARY